2014

Laboratory of Atmospheric Physics Aristotle University of Thessaloniki

MariLiza Koukouli
Dimitris Balis
Spiros Dimopoulos
Nikos Siomos

For the SACS2-SMASH team

[collaborating institutes in alphabetical order]:

BIRA: Nicolas Theys, Jeroen van Gent, H. Brenot

CGSpace: Lucia Tampellini

DLR: Pascal Hedelt, Pieter Valks

ESA: Claus Zehner

INGV: Stefano Coradini, Claudia Spinetti

KNMI: Ping Wang, Gijs Tilstra, Ronald van der A

ULB: Lieven Clarisse

Univ of Oxford: Elisa Carboni

RAL: Richard Siddans, Caroline Poulsen

[SACS-2/SMASH – VALIDATIONREPORT ON THE EYJAFJALLAJÖKULL & GRIMSVÖTN ERUPTIONS]

TABLE OF CONTENTS

1. OBJECTIVES AND RATIONAL

The main objective of the SACS-2/SMASH project is to create an optimal *End-to-End System for Volcanic Ash Plume Monitoring and Prediction*. This system is based on improved and dedicated satellite-derived ash plume and sulphur dioxide level assessments, as well as an extensive validation using auxiliary satellite, aircraft and ground-based measurements. The focus of the LAP/AUTH satellite data validation activities is to validate SO_2 and ash characteristics products provided by different satellite instruments during the following eruptions:

- 15 to 26 April 2010, Eyjafjallajökull, Iceland.
- 4 to 20 May 2010, Eyjafjallajökull, Iceland.
- 21 to 28 May 2011, Grimsvötn, Iceland.

The validation was performed on two levels, on the total SO_2 column assessment, discussed in length in Section 2, and on the ash plume characteristics, i.e. the aerosol optical depth and, where applicable, the ash plume height, presented in Sections 3, 4 and 5. A short section on satellite-to-satellite inter-comparison is given both in sub-section 2.7 for the SO_2 products as well as in Section 6 for all different ash products.

2. VALIDATION OF TOTAL SO_2 COLUMNS USING BREWER SPECTROPHOTOMETER MEASUREMENTS

The ground-based data that has been used for comparison with the satellite columnar SO_2 products are the daily mean values of total SO_2 columns observed by the global Brewer spectrophotometer network and distributed through the World Ozone and Ultraviolet Data Centre, *WOUDC*, database found in www.woudc.org. The Brewer stations that provide SO_2 for the time period of the Eyjafjallajökull (2010) and Grimsvötn (2011) eruptions are shown in FIGURE 1 and listed in TABLE I, sorted by latitude. The stations have been grouped in three geolocations based on their latitudinal properties and expected SO_2 background loading conditions namely Arctic, rural and urban. The first column denotes this annotation, the second, the station name, the third the latitude, the fourth the longitude and the final column the country of origin.

TABLE I. The 22 ground-based stations that potentially provide daily SO_2 columns within the time frame of Eyjafjallajökull (2010) and Grimsvötn (2011) eruptions and are available online at WOUDC.

Region	Station Name	Latitude	Longitude	Country
Arctic	SODANKYLA	67.37	26.65	Finland
Arctic	SONDRESTROM	67	-50.98	Greenland
Rural	VINDELN	64.25	19.77	Sweden
Urban	OLSO	59.88	10.69	Norway
Urban	CHURCHILL	58.75	-94.07	Canada
Urban	NORKOPING	58.58	16.12	Sweden
Rural	LINDENBERG	52.22	14.12	Germany
Urban	DEBILT	52	5.18	Netherlands
Rural	VALENTIA	51.93	-10.25	Ireland
Urban	READING	51.42	-0.9	GB
Urban	UCCLE	50.8	4.35	Belgium
Rural	HRADEC KRALOVE	50.18	15.83	Czech
Rural	POPRAD-GANOVCE	49.03	20.32	Slovakia
Rural	HOHENPEISSENBERG	47.8	11.02	Germany
Urban	BUDAPEST	47.43	19.18	Hungary
Rural	AROSA	46.77	9.67	Switzerland
Rural	ISPRA	45.8	8.63	Italy
Urban	ROME	41.9	12.52	Italy

Urban	THESSALONIKI	40.52	22.97	Greece
Urban	MADRID	40.45	-3.55	Spain
Urban	MURCIA	38	-1.17	Spain
Rural	EL ARENOSILLO	37.1	-6.73	Spain

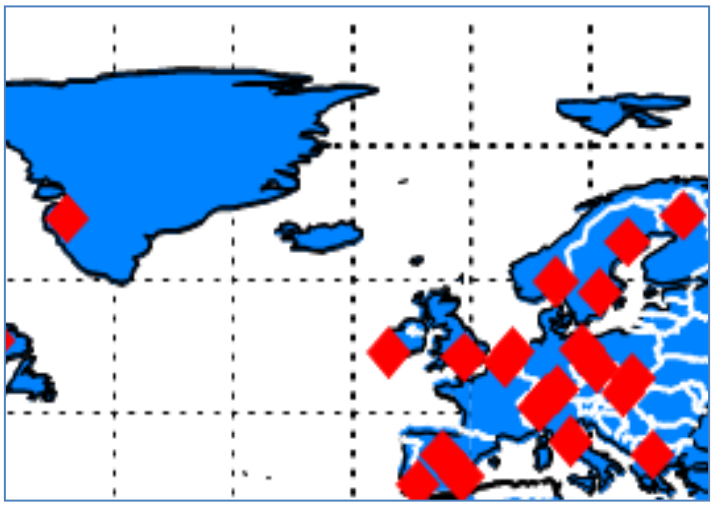

FIGURE 1. The location of the Brewer stations that were possibly affected by the Eyjafjallajökull and Grimvstön (2011) eruptions

The methodology of measuring total SO_2 columns with Brewer instruments is discussed in Kerr et al., 1981. The main premise is that the Brewer spectrophotometer measures the intensity of light in the ultraviolet absorption spectrum of ozone at five wavelengths at 306.3nm, 310.1nm, 313.5nm, 316.8nm and 320.1nm. Once the ozone column is calculated, the total SO_2 column can be determined using a suite of semi-empirical equations that take advantage of the measured light intensity at each of the wavelengths, equivalent extraterrestrial light intensities, the calculated number of atmospheres along the incident light path, the pre-calculated column amount of ozone and the absorption coefficients of the two interfering species, ozone and SO_2.

To summarize,

- SO_2 is a bi-product of the Brewer spectrophotometer measurements, once O_3 is extracted from the data.
- Since the signal-to-noise is quite low, very well-calibrated instruments are required to monitor nominal SO_2 levels.
- In extreme [e.g. volcanic] cases SO_2 levels rise well above instrumental noise.

After imposing a rigorous quality control on the Brewer observations, a total of 16 stations were accepted as possibly being able to show signs of increased SO_2 levels due to the volcanic eruptions.

The satellite data that were provided in order to perform the validation exercise are given in TABLE II. In the first column, the providing institute is labeled, followed in the next column by the satellite instrument/algorithm version used to extract the data. In the third column, the amount of data in days that the validation team received in denoted and in the fourth column, split in half, is the amount of stations for which co-locations were found depending on the eruptive period. In the fifth column the co-location criteria are shown and some comments [where applicable] are shown in column six.

A small comment is necessary on the unphysical negative satellite SO_2 values. The reason that these values appear as an output of the DOAS algorithm that most satellite products are analyzed with, is the small signal of the SO_2 absorption lines in the UV part of the spectrum compared to the O_3 lines. Hence, it often might happen that the algorithm overcompensates for the absorption

observed and reduces the amount of SO_2 required to produce said absorption features, resulting in the negative values. These values also give an indication of the random plus systematic noise levels of the products. It is recommended by the PIs to use these values both in the depiction of the data but also when averaging and in general, performing statistics, since to exclude them would skew the data towards an erroneous outcome. More details on this issue can be found in the ATBD [Theys et al, 2014].

In the following, in a series of sub-sections, example comparisons for all satellite products are provided alongside statistics and discussion. The plots all follow the same nomenclature: the y-axis shows the SO_2 levels and the x-axis the amount of time that has passed since the given date. Red squares denote the daily mean Brewer SO_2 value, blue dots denote the co-located satellite SO_2 data found within 200km of the ground-based station and the green filled circles denote the daily mean satellite SO_2 value. The grey zone depicts the eruptive period, for easy reading of the graph.

TABLE II. The satellite data provided for the validation of columnar SO_2 are summarized in this Table.

Institute	Satellite instrument	Amount of Data	Co-locations found with # of stations		Co-location Criteria	Comments
		# days	EYJA	GRIM		
BIRA	SCIAMACHY/ENVISAT	35	3	1	Same day 200km	3 plume heights provided [1km, 6km & 14km]
BIRA	GOME2/MetopA	7	10	7	Same day 200km	Very few data points , 1 to 3 per station
DLR	GOME2/MetopA	92	12	9	Same day 200km	3 plume heights provided [2.5km, 6km & 15km]
FMI	OMI/Aura	5	---	---	Same day 200km	No co-locations found
OXFORD	IASI/MetopA-Nominal Algorithm	43	10	1	Same day 200km	
OXFORD	IASI/MetopA-Fast Algorithm	24	10	1	Same day 200km	
ULB	IASI/MetopA	37	11	2	Same day 200km	
RAL	MODIS/Terra-IR algorithm	2.5 months ~10 files per day	11	7	Same day, 50 km	Quite high scatter for the satellite values, even two orders of magnitude.
RAL	MODIS/Terra-VIS/NIR algorithm	2.5 months ~5 files per day	11	7	Same day, 50 km	
RAL	MODIS/Aqua-IR algorithm	2.5 months ~10 files per day	11	7	Same day, 50 km	

RAL	MODIS/Aqua-VIS/NIR algorithm	2.5 months ~5 files per day	11	7	Same day, 50 km	

2.1 BIRA SCIAMACHY/Envisat SO_2 column comparisons

As noted from the first row in TABLE II, too few co-locations were found for the BIRA SCIAMACHY/Envisat SO_2 product. We show here two examples for stations that have an agreeable amount of collocations, albeit in Southern Europe which was not as affected by the SO_2 plume as the North. In FIGURE 2 three different satellite estimates are shown for demonstration purposes depending on the a priori plume height, namely, 1km [top row], 6km [middle row] and 14km [bottom row.] As can be noted, with each subsequent increase in plume height, the estimated SO_2 column decreases, leading the daily mean into the noise levels. On the left column, the example shown is from Thessaloniki, Greece, a location with well-known and documented local and regional sources of SO_2 hence the Brewer levels being somewhat elevated compared to the right column, the Mediterranean sea town of Mrsa Mtrouh, Egypt, where the Brewer shows quite low values as well.

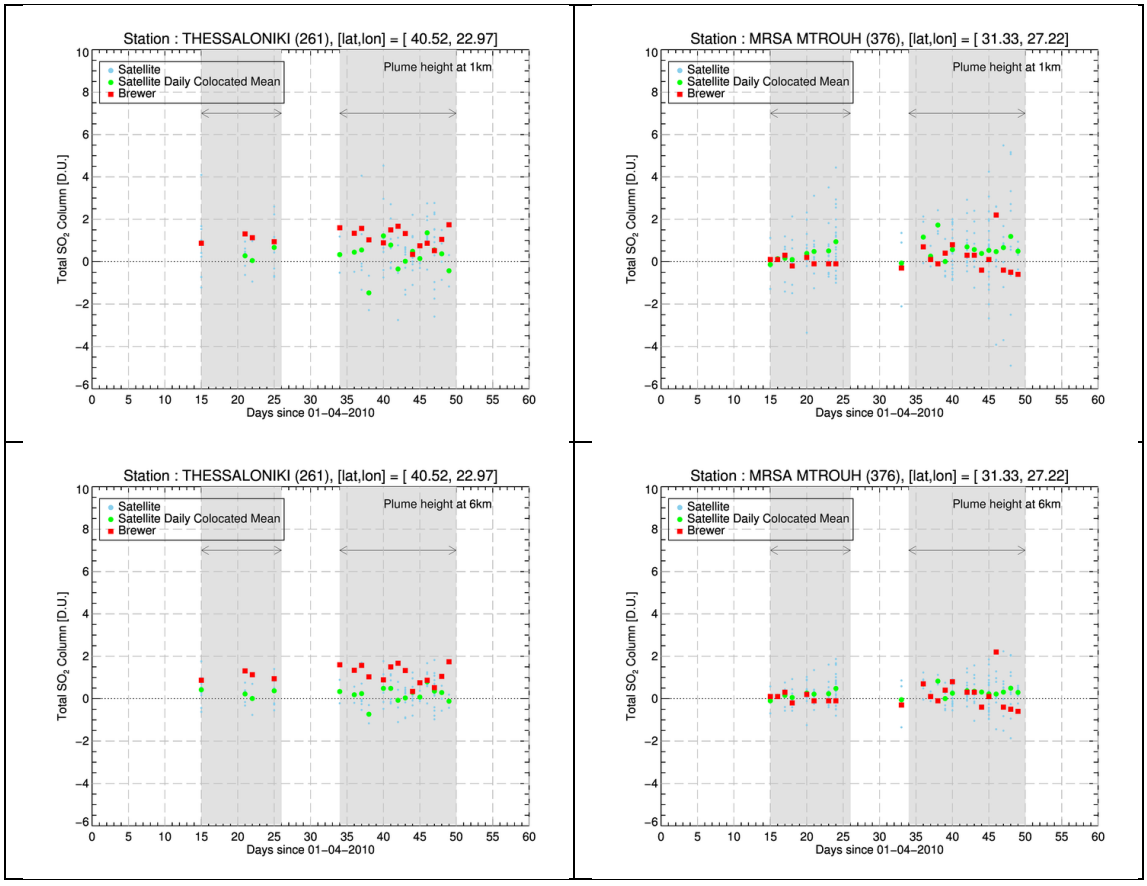

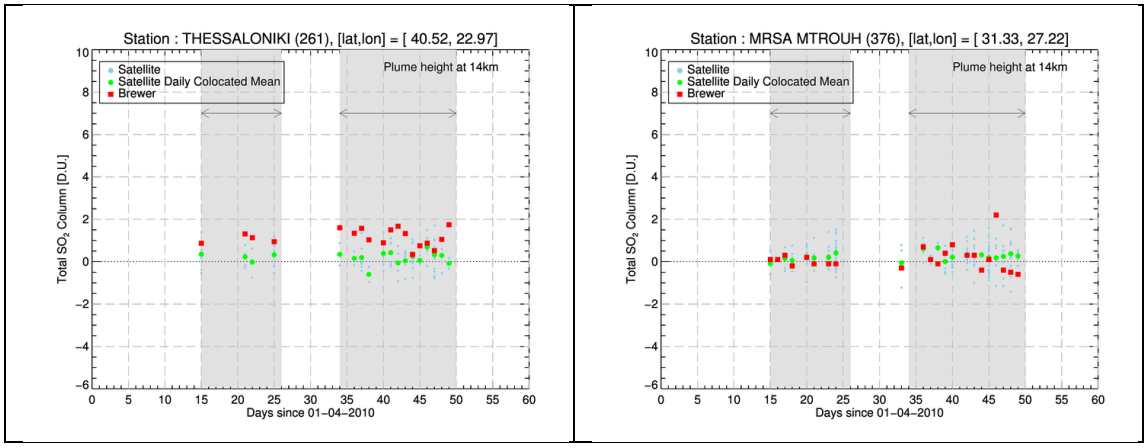

FIGURE 2. Total SO_2 column over Thessaloniki, Greece [left column] and Mrsa Mtrouh, Egypt [right column] for the Eyjafjallajökull eruptions in 2010. Red squares depict the Brewer measurements and the green circles the satellite estimates. From top to bottom: resultant column for the SCIAMACHY overpasses when the plume height is assumed to be 1km, 6km and 14km.

From the above example, we have concluded that the 1km plume product mostly approaches the expected SO_2 levels and the equivalent Brewer estimates, as was also seen for DLR GOME2 products which also employ a plume height as apriori information for the algorithm [not shown in this report.] Hence, from here on, the lowest assumed plume height product will be shown and considered.

2.2 BIRA GOME2/METOPA SO_2 COLUMN COMPARISONS

Two examples only are given for this product and no statistical analysis, since the amount of co-locations found is truly too small for anything significant to be discussed. In FIGURE 3 two locations that are known to have been affected by the Eyjafjallajökull eruptions are shown, namely DeBilt in the Netherlands [left] and Murcia in Spain [right.] Some high values are seen in De Bilt, not so for Murcia. The statistical sample is too small to be able to discuss this comparison further.

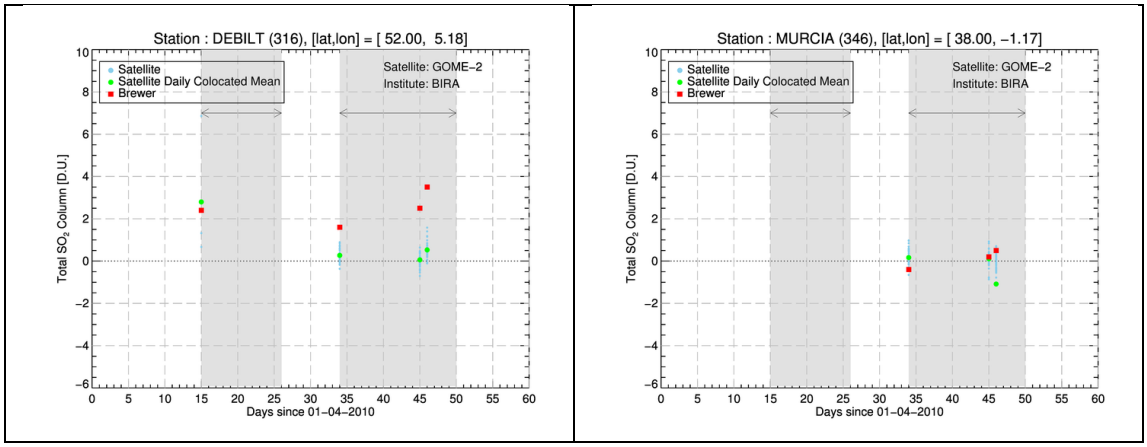

FIGURE 3. Total SO_2 column over DeBilt, The Netherlands [left] and Murcia, Spain, [right] for the Eyjafjallajökull eruptions in 2010. Red squares depict the Brewer measurements and the green circles the satellite estimates.

2.3 DLR GOME2/METOPA SO_2 COLUMN COMPARISONS

The DLR GOME2/MetopA product provides quite long co-located time series for both the Eyjafjallajökull and the Grimsvötn eruptions. As discussed above, the product associated with a plume height of 2,5km is shown for this validation. In FIGURE 4 the SO_2 levels for the

Eyjafjallajökull eruptions [top row] and the Grimsvötn eruptions [bottom row] are given. Over Uccle, Belgium [upper left], during the second eruption the levels show a marked increase in both the ground and the satellite data. Similarly seen for Hohenpeissenberg, Germany [upper right], with elevated columns during and after the second eruption. For the Grimsvötn eruption, the levels are in general lower, with some tentative increase in the eruptive phase. Examples shown are Madrid, Spain [bottom left] and Hohenpeissenberg, Germany [bottom right]. In FIGURE 5 scatter diagrams for selected stations are presented for both Eyjafjallajökull [top row] and Grimsvötn [bottom row.] Correlations between 0.30 and 0.50, based on the totality of the common datasets, demonstrate a promising product to monitor both background and specific SO_2 loading events.

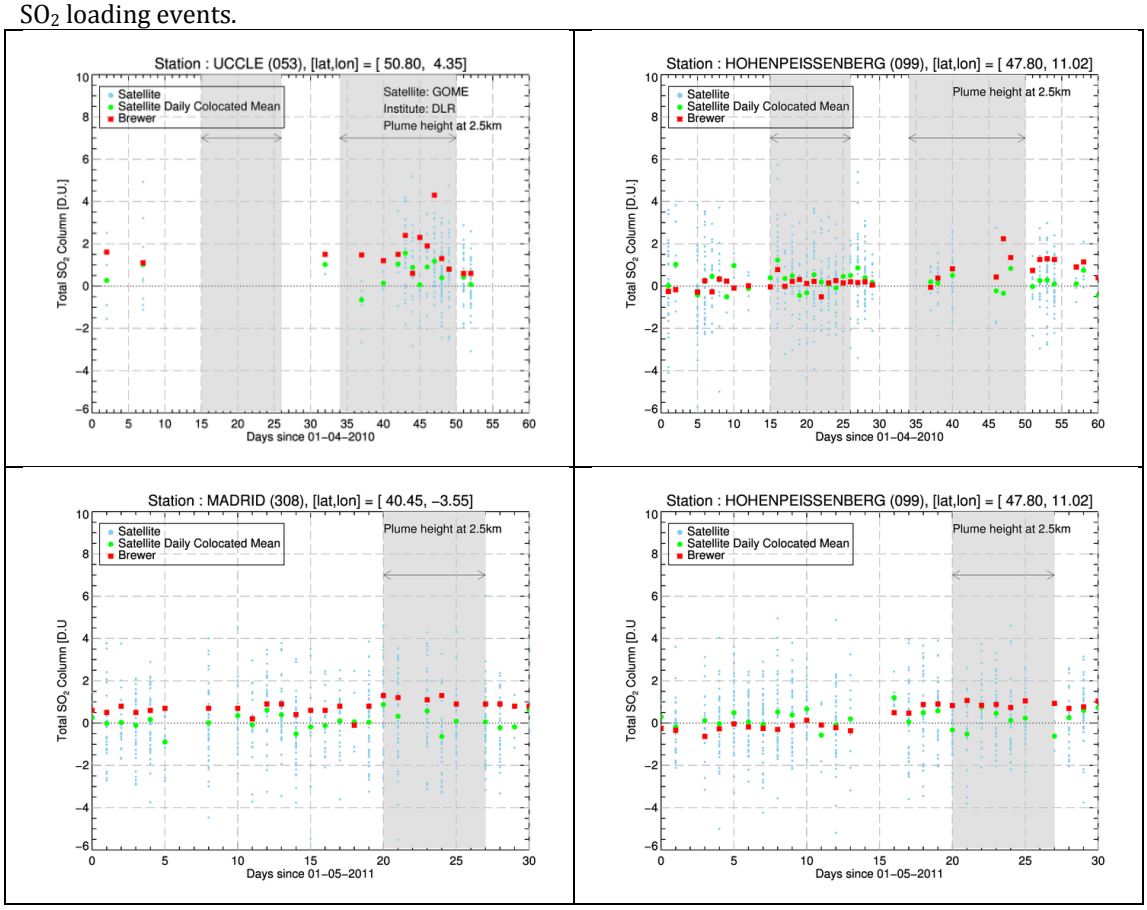

FIGURE 4. Total SO_2 column over Uccle, Belgium [upper left] and Hohenpeissenberg, Germany [upper right] for the Eyjafjallajökull eruptions in 2010 and Madrid, Spain [lower left] and Hohenpeissenberg, Germany [lower right]. Red squares depict the Brewer measurements and the green circles the satellite estimates.

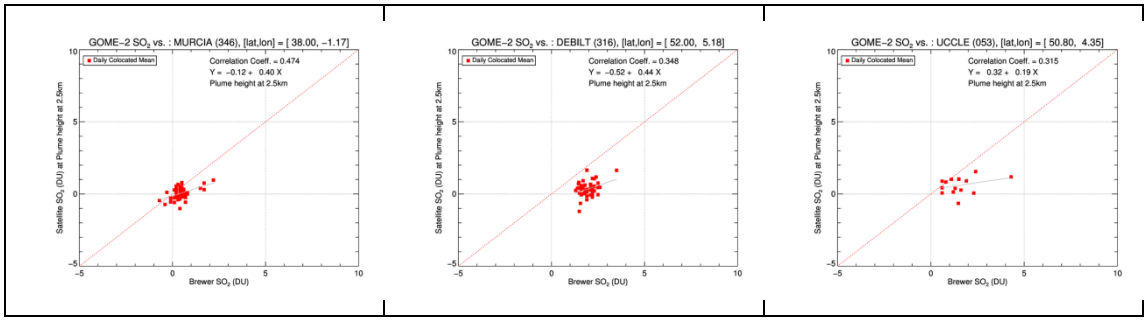

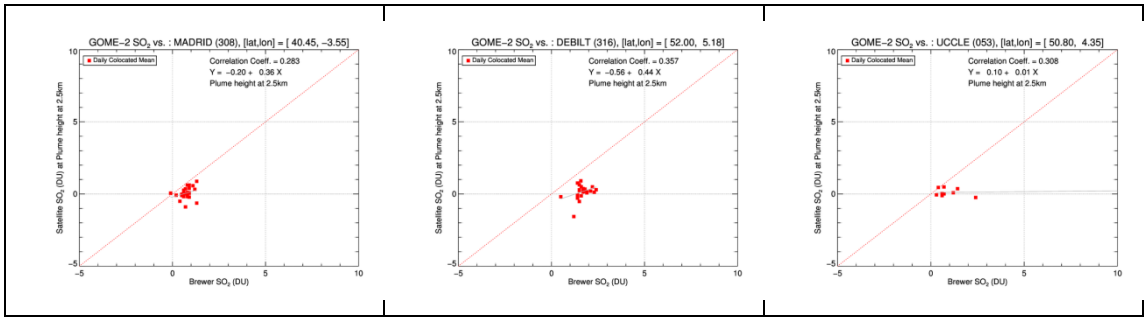

FIGURE 5. Scatter diagrams of the time series for the Eyjafjallajökull eruptions [upper row] and the bottom eruptions [lower row] for two Spanish stations, Murcia [top] and Madrid [bottom], DeBilt in the Netherlands in the middle column and Uccle in the right column. The correlation coefficient, R_2, is also provided.

2.4 OXFORD IASI/METOPA - NOMINAL AND FAST ALGORITHMS SO_2 COLUMN COMPARISONS

The Oxford IASI/MetopA total SO_2 product was extracted using two different algorithms, labeled here forth as *nominal* and *fast algorithms.* For details on the differences between these algorithms, please refer to the ATBD [Theys et al, 2014]. The small amount of co-locations found does not permit a detailed analysis of this product, we do however present a few examples for the Eyjafjallajökull eruptions comparing the two algorithms and products. In FIGURE 6 the nominal algorithm findings are given in the top row and the fast algorithm results in the bottom row for the station of Uccle, Belgium [left column], DeBilt, The Netherlands [middle column] and Madrid, Spain [right column.] The nominal algorithm seems to better capture the increased SO_2 levels for the second Eyjafjallajökull eruption and to follow the Brewer patterns [see top row of FIGURE 6.] For the stations of Uccle and DeBilt things look similar for the Grimsvötn eruption [bottom row, left and middle panels] but not so for the Madrid station. Unfortunately, this qualitative assessment is as far as we can discuss this product.

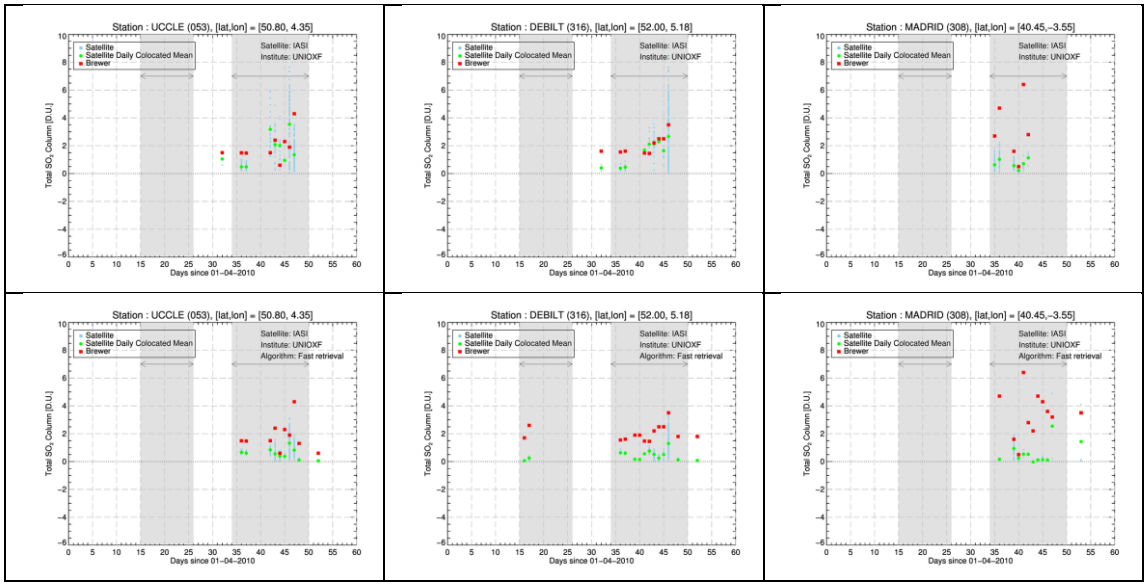

FIGURE 6. Oxford IASI nominal algorithm findings are given in the top row and the fast algorithm results in the bottom row for the station of Uccle, Belgium [left column], DeBilt, The Netherlands [middle column] and Madrid, Spain [right column.]

2.5 ULB IASI/METOPA SO_2 COLUMN COMPARISONS

Even though this product is also lacking in large amount of common data points, the common variability between satellite and ground levels is quite promising and evident from the stations presented in FIGURE 7 and FIGURE 8. In FIGURE 7, as was shown above, the time series for ULB IASI SO_2 columns are compared against the Brewer network for Uccle, Belgium [upper left], DeBilt, The Netherlands [upper right], Madrid, Spain [bottom left] and Hohenpeissenberg, Germany [bottom right.] In FIGURE 8, the scatter diagrams and associated r^2 coefficient is given for top left, Hradec Kralove, Czech Republic; top right, DeBilt, Belgium; bottom left, Murcia; bottom right, Madrid, Spain. The correlations reach 0.65 to 0.7 for the cases of the Spanish station, a very promising result even though the small amount of data does not permit further analysis.

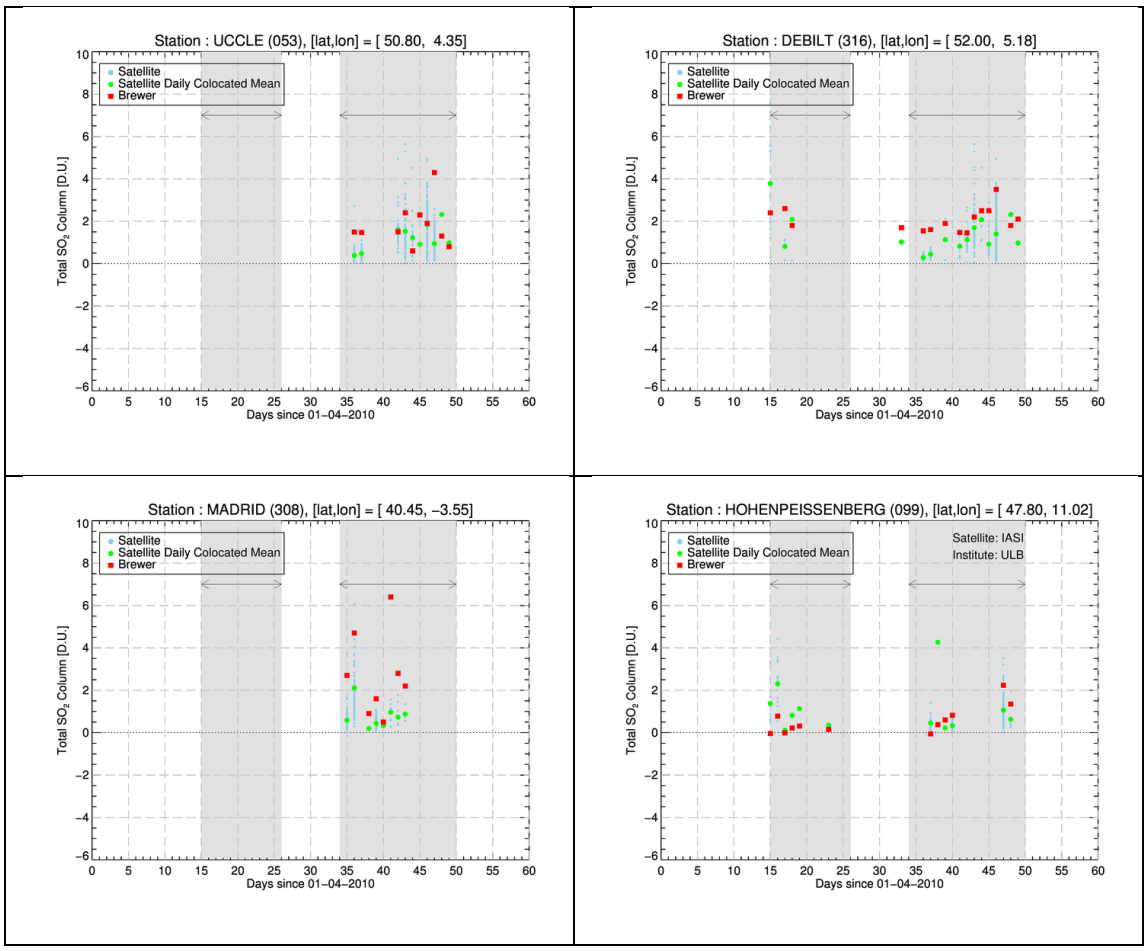

FIGURE 7. ULB IASI SO_2 columns are compared against the Brewer network for Uccle, Belgium [upper left], DeBilt, The Netherlands [upper right], Madrid, Spain [bottom left] and Hohenpeissenberg, Germany [bottom right.]

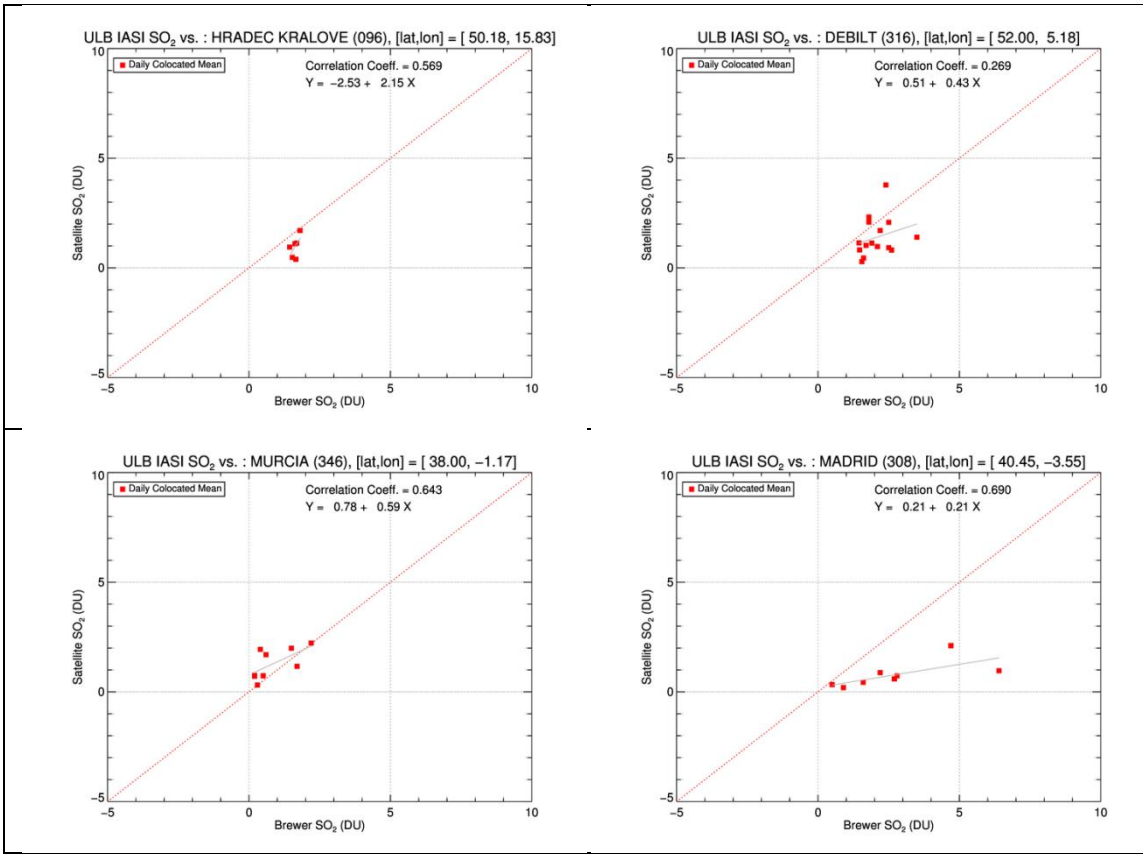

FIGURE 8. Scatter diagrams for four stations during the Eyjafjallajökull eruptive periods between the ULB IASI SO_2 columns and the Brewer SO_2 columns; top left, Hradec Kralove, Czech Republic; top right, DeBilt, Belgium; bottom left, Murcia; bottom right, Madrid, Spain.

2.6 RAL MODIS/TERRA AND MODIS/AQUA SO_2 COLUMNS – IR & VIS/NIR ALGORITHMS

The RAL MODIS/Terra and MODIS/Aqua measurements have been analyzed using two different algorithms, here forth called *IR* and *VIS/NIR algorithms.* The two satellites, Terra and Aqua, both carrying the MODIS sensor, are in sun-synchronous orbits. The Terra overpass time is around 10:30 local solar time at the equator in its descending (daytime) mode and 22:30 local solar time in its ascending (nighttime) mode. The Aqua overpass time is around 13:30 local solar time at the equator in ascending (daytime) mode and 01:30 local solar time in descending (nighttime) mode. For details on the two algorithms and the SO_2 column extraction process refer to the ATBD [Theys et al., 2014]. Due to the smaller instrument field of view, it was possible to obtain a good statistical sample using a narrower spatial filter of 50km, instead of 200km which was used for all the aforementioned satellite products. In FIGURE 9 we give examples for the MODIS/Terra and in FIGURE 10 for the MODIS/Aqua data. Two example stations are shown, namely Uccle and Madrid, which have already been shown for most of the satellite products. The main take away message from these comparisons is that the MODIS SO_2 column is quite high, even during background condition time periods. Note that the y-axis now rises to 16 D.U., levels which are found directly over natural or anthropogenic sources, and definitely not in Western Europe. The MODIS/Aqua levels are somewhat lower, but still exceed expectations. However it should be noted that the estimated random error on SO_2 columns from the RAL scheme MODIS is around 10 D.U. In addition, the data supplied for these comparisons has all very low and negative values are removed. Hence, the current discrepancies found with ground based data are not significant compared to the estimated satellite error bars. It would be necessary to have co-located ground-based observations sampling stronger SO_2 plumes to be able to draw further conclusions about the quality of these retrievals.

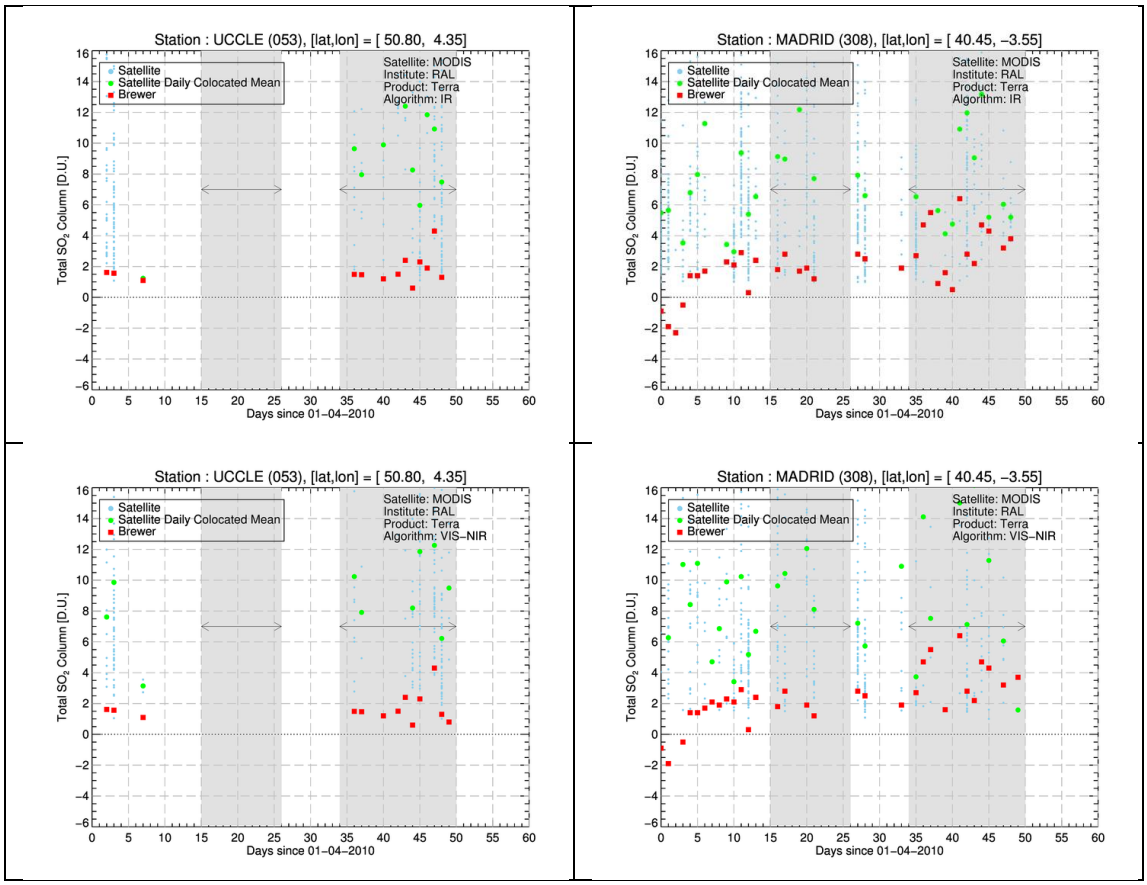

FIGURE 9. RAL MODIS/Terra SO_2 columns for the IR [upper row] and VIS/NIR algorithms [lower row.] Uccle, Belgium [left column] and Madrid, Spain [right column]

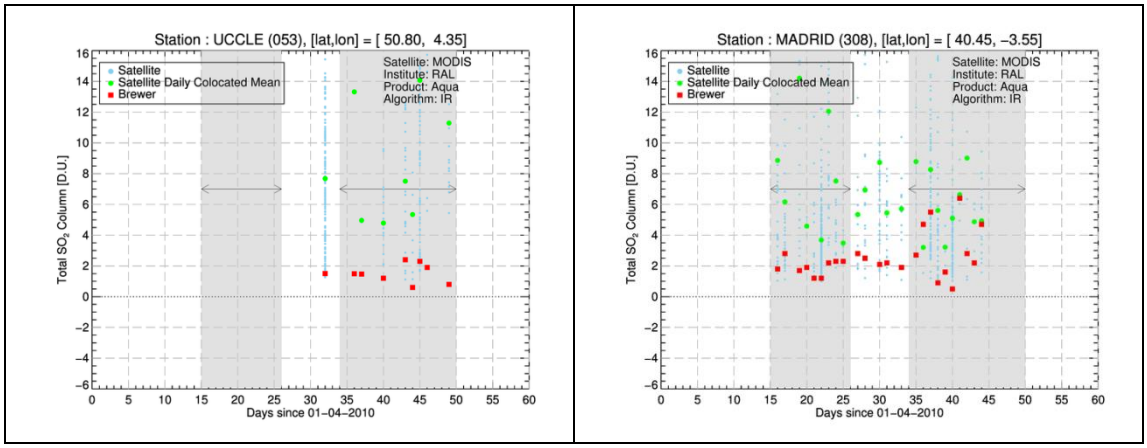

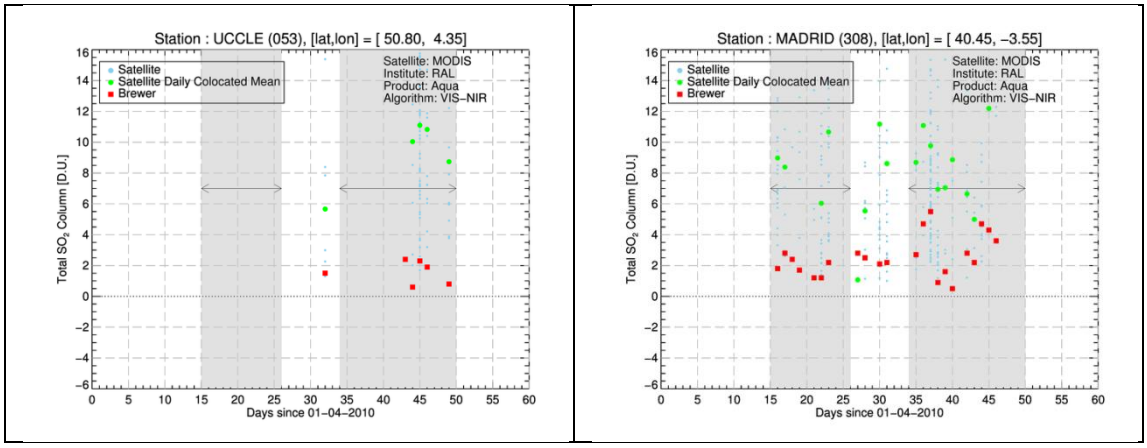

FIGURE 10. RAL MODIS/Terra SO_2 columns for the IR [upper row] and VIS/NIR algorithms [lower row.] Uccle, Belgium [left column] and Madrid, Spain [right column]

2.7 INTER-COMPARISON OF RETRIEVAL SCHEMES FOR THE SO_2 COLUMN AMOUNTS

In the following, algorithm-to-algorithm comparisons for the SO_2 column amounts extracted by the same instrument on the 23rd of May 2011, the Grimsvötn eruption, are presented for the instruments whose observations have been analyzed by more than one algorithm, namely, GOME2/MetopA [sub-section 2.7.1], MODIS/Terra & /Aqua [sub-section 2.7.2] and IASI/MetopA [sub-section 2.7.3]. The data have been gridded into a level-3 type product for ease of comparison, depending on the original instrument footprint. The values range from 1x1° to 0.5x0.5° boxes.

2.7.1 COMPARISON BETWEEN BIRA AND DLR GOME2/MetopA SO_2 COLUMN AMOUNTS

In order to attempt as close a comparison as possible between the two GOME2/MetopA SO_2 total columns as extracted by the BIRA and the DLR algorithms we have to carefully select which of the three DLR products to choose from; the one associated with a 2.5km plume height, with a 6km plume height or a 14km plume height. The dependability of the BIRA algorithm depends on the concurrent retrieval of a dependable effective plume height. In Figure 11 we show the BIRA plume height and associated error. Since the apriori height error was set to 5km, any value that approaches the apriori error levels signifies data where the SO_2 amounts were too low for dependable detection. From Figure 11 we hence discern that during the Grimsvötn eruption on the 23rd of May 2011, the average plume height revolved between 6 and 8 km for most pixels considered. We should hence investigate the comparison between the BIRA SO_2 column and the DLR one extracted for the 6km plume height apriori.

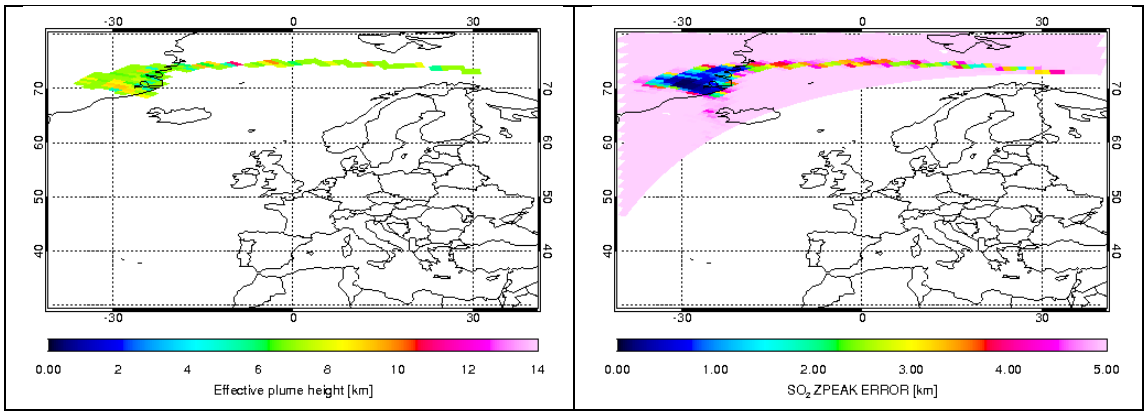

Figure 11. The GOME2 SO_2 plume height associated with the BIRA SO_2 concentration retrievals [left] and corresponding error [right.] [courtesy of Jeroen van Gent, BIRA.]

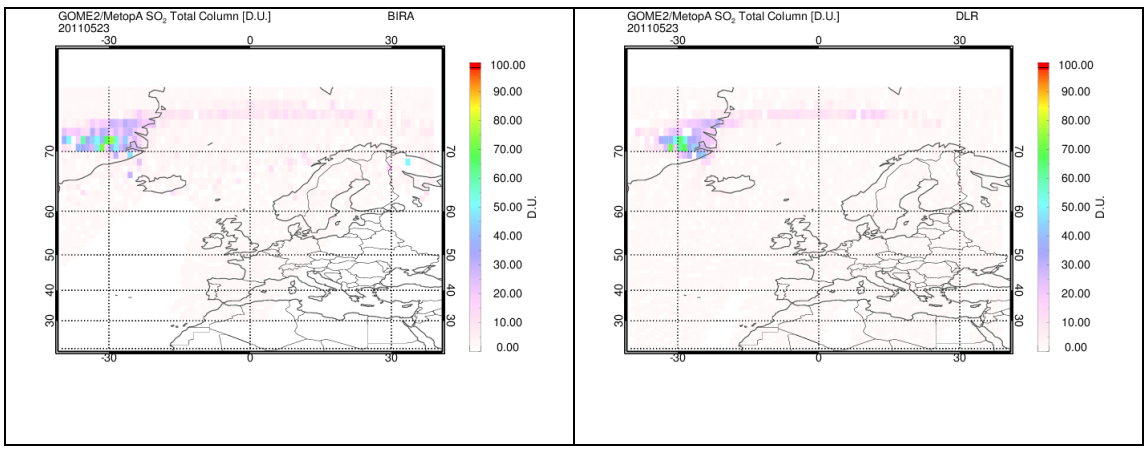

Figure 12. GOME2/MetopA SO2 levels as extracted for the Grimsvötn eruption on May 23rd, 2011, by the BIRA algorithm [left] and the DLR algorithm [right.]

In Figure 12 the BIRA SO_2 field is shown on the left and the DLR SO_2 field for the 6km plume height on the right. No restrictions/cut-offs were used in the plotting. The colour scale ranges from 0 to 100 D.U. The SO_2 plume is very well described in both cases, with the maximum of the loading over the South-East coast of Greenland and a plume, like an arm, travelling the North Sea with loadings between 20 and 30 D.U. A small reminder is paramount here, that the morning equatorial crossing time of the MetopA satellite is around 09:30 in L.T.

2.7.2 COMPARISON BETWEEN RAL AND INGV MODIS/TERRA AND /AQUA SO_2 COLUMN AMOUNTS

The MODIS/Terra and MODIS/Aqua SO_2 amounts have been extracted by both the RAL and the INGV algorithms. Due to the ability of the MODIS instrument to observe the atmosphere at night-time also, the data are separated in the daytime and night-time overpasses in order to examine the movement of the SO_2 plume during that day. The 23rd of May 2011 was also chosen as example for this comparison. In Figure 13, upper row, the morning MODIS/Terra [around 10:30 equatorial crossing time in L.T.] is shown and in the lower row, the evening MODIS/Terra [around 22:30 equatorial crossing time in L.T.]. The left column shows the INGV algorithm and the right column shows the RAL algorithm. Exactly the same type of plots but for the MODIS/Aqua instrument is shown in Figure 14. MODIS/Aqua overpasses around 13:30 and 01:30 equatorial crossing time in L.T., around three hours after the MODIS/Terra overpass. This provides a nice way with which to monitor the direction and magnitude of the volcanic plume during the day in question.
In general, the location of the SO_2 loading maxima seen in Figure 13 are found to be in accordance in both datasets for the morning overpasses [not so for the evening overpasses] however note that the colour scale rises to 200 D.U. for the INGV SO_2 columns and to 100 D.U. for the RAL SO_2 columns.

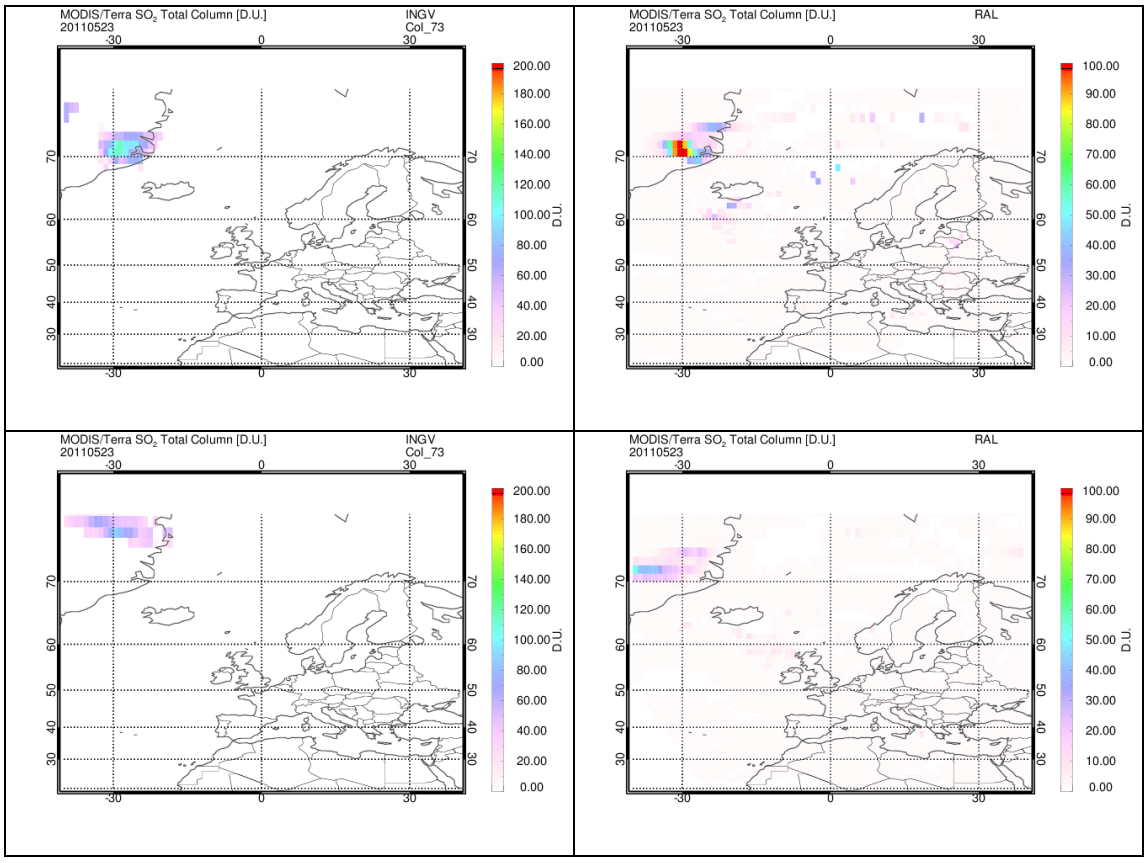

Figure 13. The MODIS/Terra SO_2 fields for the morning overpass [upper row] and the evening overpass [lower row] for May 23rd 2011. In the left column the INGV algorithm and in the right column the RAL algorithm.

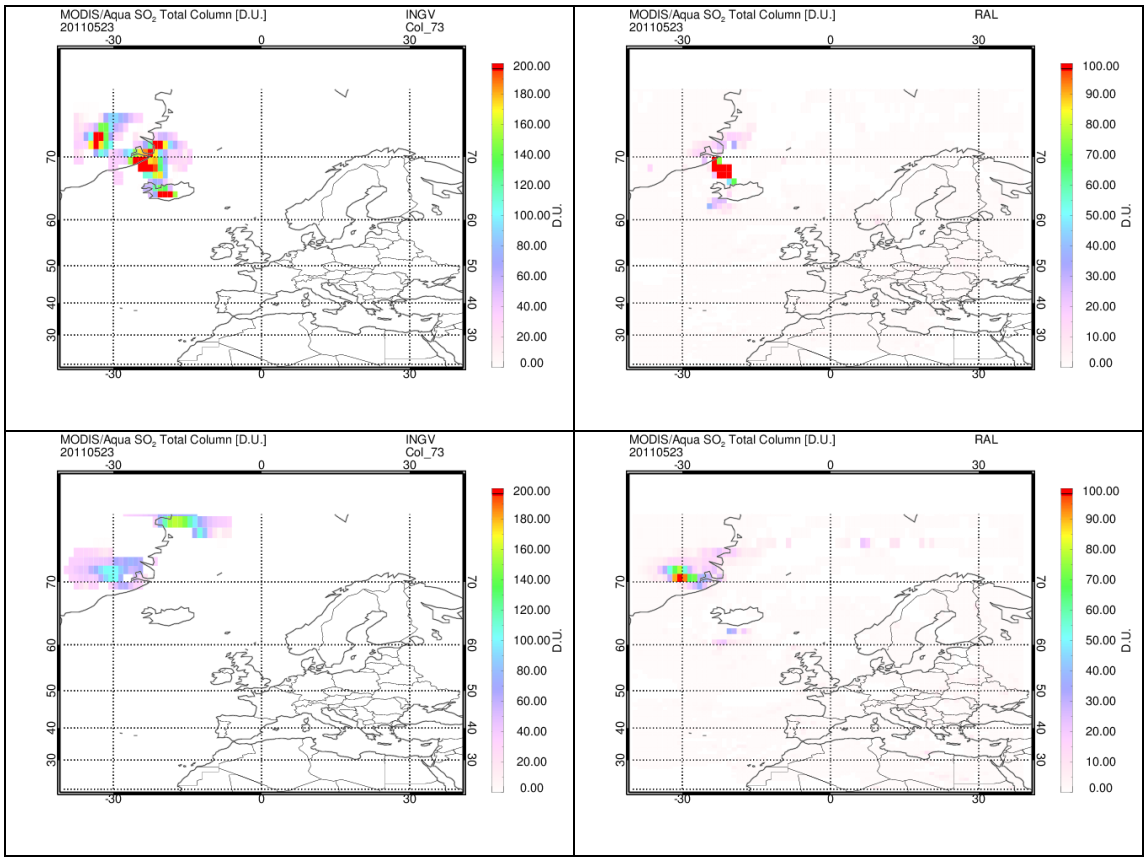

Figure 14. The MODIS/Aqua SO_2 fields for the morning overpass [upper row] and the evening overpass [lower row] for May 23rd 2011. In the left column the INGV algorithm and in the right column the RAL algorithm.

In the case of the MODIS/Aqua comparisons [Figure 14], the two algorithms show greater deviation both in the location of the SO_2 loading as well as the absolute amount and the individual features of the two overpasses.

2.7.3 COMPARISON BETWEEN OXFORD AND ULB IASI/METOPA SO_2 COLUMN AMOUNTS

The IASI/MetopA SO_2 columns have in effect been analysed using three different algorithms: the Oxford nominal algorithm, the Oxford fast algorithm and the ULB algorithm. Further to the SO_2 column, the ULB and the Oxford nominal algorithm also provide an estimate for the SO_2 plume height, which will also be used in these comparisons. In Figure 15 the results of the three algorithms are compared for May 23rd 2011; the ULB data on the left column, the Oxford nominal data in the middle and the Oxford fast algorithm in the right column. In the upper row, the morning overpass is shown and in the lower, the evening overpass, some 12 hours later. Note that, unavoidably, the colour scale is not the same for all graphs, even though we kept all scales forming part of multiples of 40. In particular, for the ULB results [left] the column rises to 80 D.U., for the Oxford nominal algorithm [middle], to 40 D.U. and for the Oxford fast algorithm [right] to 480 D.U. The ULB result is the one best in accordance with the GOME2/DLR and /BIRA findings shown in Figure 12 as well.

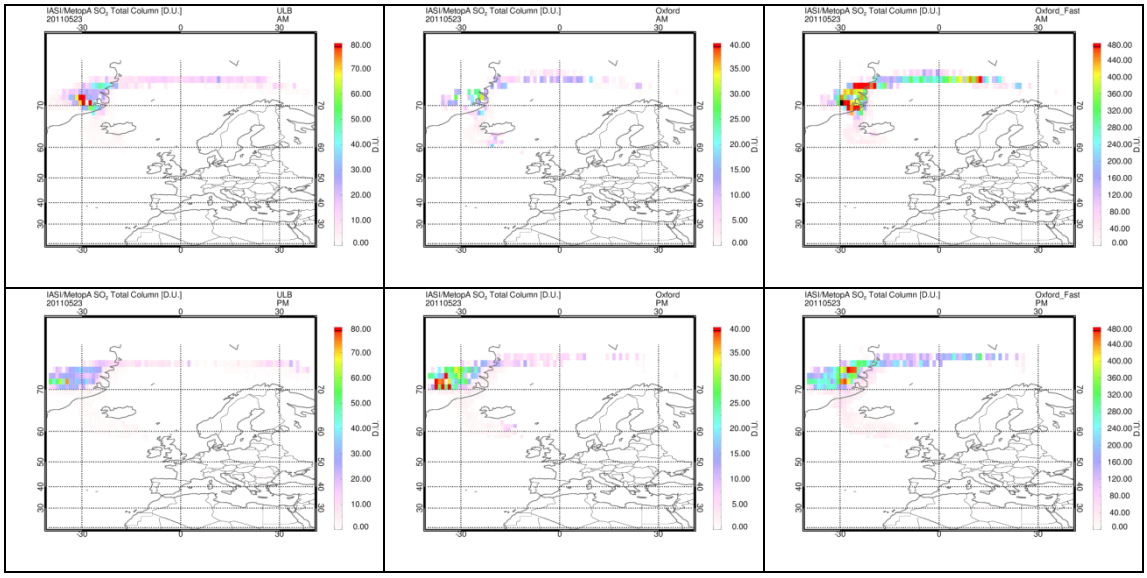

Figure 15. The IASI/MetopA SO_2 columns as extracted by the ULB algorithm [left column], the Oxford nominal algorithm [middle column] and the Oxford fast algorithm [right column] for the 23rd of May 2011. In the upper row, the morning overpass and in the lower row, the evening overpass is shown.

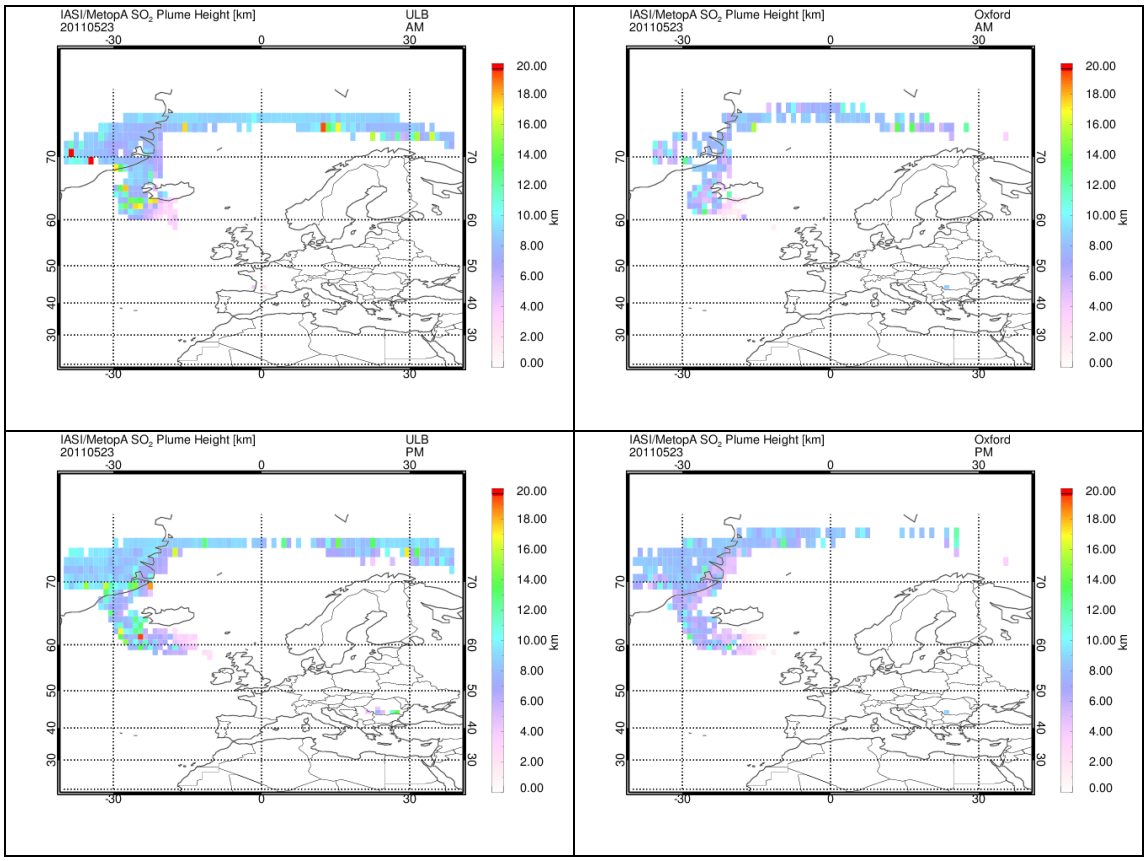

Figure 16. The estimated SO_2 plume height as extracted from the IASI/MetopA morning [upper row] and evening [lower row] overpasses. Left column, the ULB algorithm and right column, the Oxford nominal algorithm are shown.

In FIGURE 16 the estimated SO_2 plume height as extracted from the IASI/MetopA morning [upper row] and evening [lower row] overpasses. In the left column, the ULB algorithm results are

shown and in the right column, the Oxford nominal algorithm. The comparative picture is quite impressive with the mean height for the main plume as well as the arm around the Northern Sea rising to between 7 and 9km, approximately the height given by the BIRA algorithm applied to the GOME2/MetopA data as well. However, the absolute SO_2 amounts differ by a substantial amount between the three algorithms, a far that merits further investigation by the respective P.I.s.

2.8 CONCLUSIONS AND FUTURE OUTLOOK

Table III. Statistics of the SO_2 levels viewed by a selection of the instruments presented in sub-sections 2.1 to 2.6 .

Institute	Instrument & algorithm	Mean Satellite SO_2 levels	Mean Brewer SO_2 Levels	Mean difference	Number of common obs
DLR	GOME2/MetopA	0.18±1.53	1.22±1.07	1.06±1.83	493
Oxford	IASI/MetopA Nominal Algorithm	1.57±1.53	1.78±1.25	0.80±1.85	44
Oxford	IASI/MetopA Fast Algorithm	0.62±0.55	1.58±1.28	1.22±1.19	87
ULB	IASI/MetopA	1.09±0.95	1.50±1.09	1.13±1.41	80

As far as the comparison between satellite and ground-based total SO_2 columns is concerned, a number of main points may be listed here;

- The BIRA/SCIAMACHY and BIRA/GOME-2 data set had too few co-locations with the Brewer network to be able to analyse further.
- The DLR/GOME-2 total SO_2 column is promising for the 2.5km plume height, with an acceptable signal during the main eruptive period and noise levels otherwise. A moderate correlation, R^2, was found for some of the ground-based stations, with values between 0.3 and 0.5.
- The Oxford_Fast/IASI algorithm, for the full days of data processed, provides a higher total SO_2 column compared to the nominal algorithm by around by 2-4 DU, with an acceptable signal during the main eruptive period. However, too few co-locations with the Brewers were found making further analysis difficult.
- The Oxford_nominal/IASI algorithm total SO_2 columns are quite promising when there is a strong signal. However, too few co-locations were found making further analysis difficult.
- The ULB/IASI ULB total SO_2 columns are very promising when there is a strong signal with correlations, R^2, for some of the ground-based stations, 0.3 and 0.7.
- The levels of SO2 in co-locations were too small (compared to the estimated retrieval noise) to enable a meaningful evaluation of the RAL MODIS/Terra & MODIS/Aqua IR & VIS/NIR algorithms.

Some numerical findings, following the comments above, are given in Table III.

As far as the comparison between algorithm and algorithm for the same satellite instruments is concerned, a number of main points may be listed here;

- The BIRA and DLR GOME2/MetopA algorithms produce very similar patterns for the SO_2 loading as well as very similar absolute SO_2 column levels providing the SO_2 signal is high enough, i.e. the SO_2 loading is high enough.
- The ULB and Oxford IASI/MetopA algorithms produce very similar patterns for the SO_2 plume height [where given] however the absolute SO_2 levels vary dramatically. There is an order of magnitude difference between the two Oxford algorithms, with the nominal algorithm providing absolute SO_2 columns within the same order of magnitude to the ULB findings and the GOME2 findings. The SO_2 loading patterns are the same for the three IASI algorithms pointing to a very promising future for these algorithms.

- The INGV and RAL MODIS/Terra & /Aqua algorithms deviate quite a bit, both in the magnitude of the estimates SO_2 column but also in the geographical extend of the loading, which bares further investigation.

In order to continue with this line of validation activities, a suggestion to be made for future works is to:

- Include other eruptions with strong SO_2 plumes since from the Eyjafjallajökull and Grimsvötn 2010/2011 eruptions we had too few co-locations for most satellite products.

3. VALIDATION OF ASH OPTICAL DEPTH AND HEIGHT USING EARLINET LIDAR MEASUREMENTS

For the validation of the ash plume height as well as the optical depth of the ash plume, LIDAR data from the EARLINET network will be used in this section [http://www.earlinet.org/]. EARLINET is the first aerosol LIDAR network on a continental scale with the main goal to provide data for the aerosol distribution over Europe at 25 participating stations [see FIGURE 17]. Aerosol extinction and backscatter profiles are the standard products of LIDAR measurements and are stored in a standardized data format in a centralized database which allows for an easy access to the complete data set for further scientific studies. At most EARLINET stations, products include Raman extinction profiles that are obtained without using critical assumptions from which ash plume height and optical thickness can be derived. A relational database, containing the output of the 4-D analysis of EARLINET data related to the volcanic eruption of 2010, has been set up [Pappalardo et al., 2013]. A MySQL-type server has been used as it is based on open-source software and allows platform-independent access. The full Eyja2010 MySQL database is freely available on request at http://www.earlinet.org.

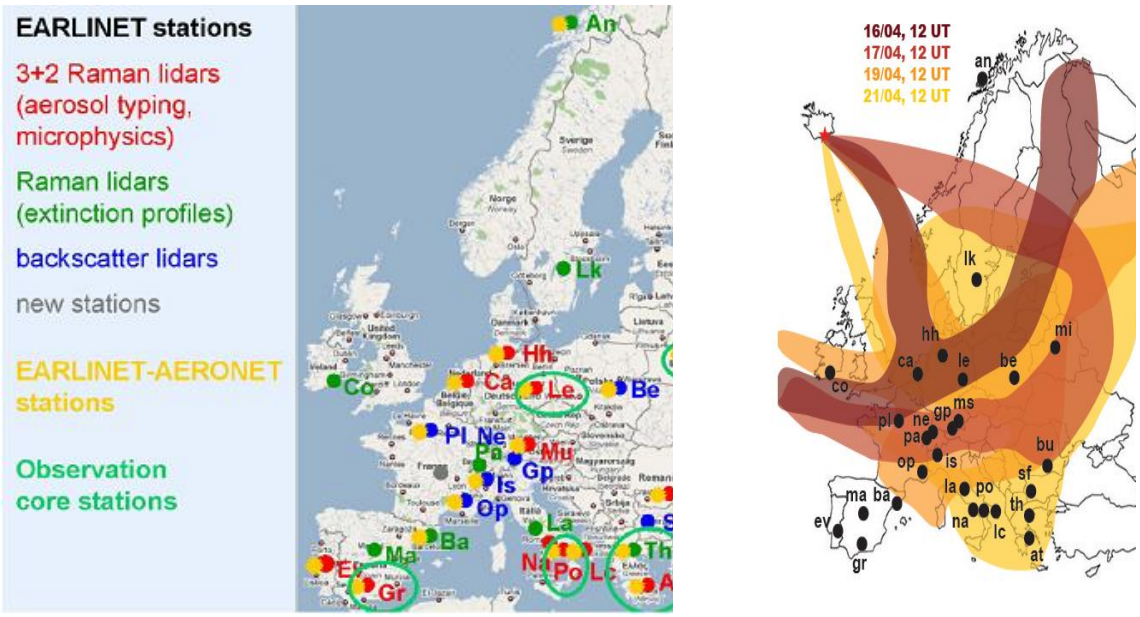

FIGURE 17. EARLINET stations that performed measurements during the Eyjafjallajökull eruption [left panel].EARLINET stations affected by the 1st phase of the eruption (from Pappalardo et al., 2013) [right panel.]

The list of the stations that will be considered for the validation of the satellite products is shown in Table IV. In the first four columns the location of the stations is given, including altitude and geographical co-ordinates. In the last column, the quantities that are measured directly by the lidar instrument at each station are shown and the available the advanced products that can be [or already have been] retrieved from these. LAP/AUTH, as part of the EARLINET network, can freely access EARLINET data.

Table IV. Locations of EARLINET lidar stations, their geographical coordinates as well as relative measurable aerosol parameters.

Site	Altitude a.s.l. (m)	Lat. (N)	Long. (E)	Data products available
Andøya, Norway	380	69.28	16.01	aerosol height/thickness, β(355), τ(355), σ(355), S(355), β(532), τ(532), σ(532), S (532), β(1064)

Athens, Greece	200	37.96	23.78	aerosol height/thickness, β(355), τ(355), σ(355), S(355), β(532), τ(532), σ(532), S (532), β(1064)
Barcelona, Spain	115	41.39	2.11	aerosol height/thickness, β(532), τ(532), σ(532), S(532), β(1064)
Belsk, Poland	180	51.84	20.79	aerosol height/thickness β(532), β(1064)
Bucharest-Magurele Romania	93	44.45	26.03	aerosol height/thickness, β(355), τ(355), σ(355), S(355), β(532), τ(532), σ(532), S (532), β(1064), β'(R, 532nm) $_{\|\|}$/β'(R, 532nm)$_{\perp}$
Cabauw, The Netherlands	1	51.97	4.93	aerosol height/thickness, β(355), τ(355), σ(355), S (355), β(532), τ(532), σ(532), S (532), β(1064)
Evora, Portugal				aerosol height/thickness, β(355), τ(355), σ(355), S (355), β(532), τ(532), σ(532), S (532), β(1064), β'(R, 532nm)$_{\|\|}$/β'(R, 532nm)$_{\perp}$,
Garmisch-Partenkirchen, Germany	730	47.48	11.06	aerosol height/thickness, β(532), τ(532), σ(532), S(532), β(355), β(1064), extinction 532 at daytime
Granada, Spain	680	37.16	-3.61	aerosol height/thickness, β(532), τ(532), σ(532), S(532),β(1064), β(355), τ(355), σ(355), S(355), β'(R, 532nm) $_{\|\|}$/β'(R, 532nm)$_{\perp}$
Hamburg, Germany	25	53.57	9.97	aerosol height/thickness, β(355), τ(355), σ(355), S (355), β(532), τ(532), σ(532), S (532), β(1064), β'(R, 532nm) $_{\|\|}$/β'(R, 532nm)$_{\perp}$
Ispra, Italy	209	45.82	8.63	aerosol height/thickness, β(532)
L'Aquila, Italy	683	42.38	13.32	aerosol height/thickness, β(355), τ(355), σ(355), S(355), β'(R, 355nm) $_{\|\|}$/β'(R, 355nm)$_{\perp}$
Lecce, Italy	30	40.30	18.10	aerosol height/thickness, β(355), τ(355), σ(355), S (355), β'(R, 355nm) $_{\|\|}$/β'(R, 355nm)$_{\perp}$
Leipzig, Germany	100	51.35	12.44	aerosol height/thickness, τ(355), σ(355), β(355), S(355), τ(532), σ(532), β(532), S(532), β'(R, 532nm) $_{\|\|}$/β'(R, 532nm)$_{\perp}$, β(1064)
Linköping, Sweden	80	58.39	15.57	aerosol height/thickness, τ(355), σ(355), β(355), S(355), τ(532), σ(532), β(532), S(532),
Madrid, Spain	669	40.45	-3.73	aerosol height/thickness, τ(532), σ(532), β(532), S(532),
Maisach, Germany	515	48.21	11.26	aerosol height/thickness, β(532), τ(532), σ(532), S (532), β(1064), β(355), τ(355), σ(355), S(355), β'(R, 532nm) $_{\|\|}$/β'(R, 532nm)$_{\perp}$
Minsk, Belarus	200	53.92	27.60	aerosol height/thickness, β(532), β(1064), β(355), τ(355), σ(355), S(355), β'(R, 532nm)$_{\|\|}$/β'(R, 532nm)$_{\perp}$
Napoli, Italy	118	40.84	14.18	aerosol height/thickness, β(532), τ(532), σ(532), S (532), β(355), τ(355), σ(355), S (355)
Neuchâtel, Switzerland	487	47.00	6.96	aerosol height/thickness, β(532), β'(R, 532nm)$_{\|\|}$/β'(R, 532nm)$_{\perp}$

OHP, France	683	43.96	5.71	aerosol height/thickness, β(532)
Palaiseau, France	162	48.70	2.20	aerosol height/thickness, β(532), β(1064), $\beta'(R, 532nm)_{||}/\beta'(R, 532nm)_{\perp}$
Payerne, Switzerland	456	46.81	6.94	aerosol height/thickness, τ(355), σ(355), β(355), S(355), water vapor mixing ratio
Potenza, Italy	760	40.60	15.72	aerosol height/thickness, β(355), τ(355), σ(355), S (355), β(532), τ(532), σ(532), S (532), β(1064), $\beta'(R, 532nm)_{||}/\beta'(R, 532nm)_{\perp}$, water vapor mixing ratio
Sofia, Bulgaria	550	42.67	23.33	aerosol height/thickness, β(511)
Thessaloniki, Greece	60	40.63	22.95	aerosol height/thickness, β(355), τ(355), σ(355), S (355), β(532), τ(532), σ(532), S(532)

β: backscatter coefficient profile; σ: extinction coefficient profile; τ: optical depth (columnar quantity) from AERONET; S: lidar ratio profile; $\beta'_{||}$ and $\beta'_{\perp}$: parallel polarized and cross polarized components of radiation respectively.

We requested the EARLINET LIDAR network measurements related to the volcanic eruption of 2010 from the EARLINET website. Data was received as a relational MySQL database file which was loaded in our Database server. Information pertinent to this work included in the database involves backscatter profiles for each of the ground-based stations, as well as the presence of both volcanic and mixing layers. The station-related information provided is: its incremental ID, Location, Latitude and Longitude in degree and Altitude above the sea level in meters. The backscatter profiles provide information about each backscatter file analysis for the 4D volcanic cloud distribution study. The volcanic layers information contains the geolocations layers identified as volcanic layers whereas the mixed layers information relates to and aerosol layer in which a mixing between volcanic and other aerosol types is observed. Database information was combined and extracted in CSV file appropriate for comparison with the satellite data. The resulting final measurement data for volcanic layers for each ground station were archived. Mixed layers information was rejected as a tool for the comparisons due to the inherent inability to identify between volcanic ash and other aerosol types. Hence only the pure volcanic cases have been used in the following work.

TABLE V. The satellite data provided for the validation of the ash plume characteristics are summarized in this Table.

Institute	Satellite instrument	Overpass time	Amount of Data	Co-location Criteria	Comments
			In days		
KNMI	SCIAMACHY/ENVISAT	10:00 LT	12	---	No co-locations found
KNMI	GOME2/MetopA	09:30 LT	14	3h & 300km 5h & 500km	
OXFORD	IASI/MetopA-Nominal Algorithm	09:30 LT 21:30 LT	18	1h & 100km 3h & 300km	
OXFORD	IASI/MetopA-Fast Algorithm	09:30 LT 21:30 LT	19	1h & 100km 1h & 300km 3h & 100km 3h & 300km	3 fixed heights provided, 400mbar, 600mbar &

					800mbar
ULB	IASI/MetopA-Eyja Algorithm	09:30 LT 21:30 LT	48	1h & 100km 1h & 300km 3h & 100km 3h & 300km	
ULB	IASI/MetopA-Pollock Algorithm	09:30 LT 21:30 LT	53	1h & 100km 1h & 300km 3h & 100km 3h & 300km	
RAL	MODIS/Terra	10:30 L.T.	2.5 months ~10 files/day	1h & 50km 2h & 100km	
RAL	MODIS/Aqua	13:30 L.T.	2.5 months ~10 files/day	1h & 50km 2h & 100km	

Satellite data processed by four different scientific institutes was provided for the comparison with the EARLINET data. Data from the satellites SCIAMACHY/Envisat and GOME-2/MetopA has been provided by the KNMI. Their algorithmic processing resulted in three different output types depending on the assumed *apriori* refractive index of volcanic ash. Data from IASI/MetopA has been provided by both the ULB and Oxford scientific institutes. The algorithmic processing of the ULB institute resulted in two different output types depending on the assumed volcanic ash characteristics whereas the algorithmic processing of the OXF institute resulted in four different output types, three of which assumed a fixed volcanic ash layer height analysis. Data from the instruments MODIS/TERRA and MODIS/AQUA has been provided by the RAL scientific institute. The algorithmic processing resulted in two different output types for each satellite depending on the detection wavelength used to extract the AOD and plume height information. Further details can be seen in TABLE V.

The values of each satellite product mentioned above have been algorithmically restricted within an area of variable radius, dependent of the satellite, around each EARLINET station. Out of those values the closest spatially and chronically to each station has been selected and has been compared with the respective EARLINET layer for each day. The spatial filtering is applied before the time filtering. Values satisfying the spatial criteria with a time difference between the satellite and the EARLINET measurement time exceeding a specific time limit were excluded from the analysis. In the rare cases when two different points of an EARLINET station had the same measurement time (double layer) the worse correlated point was excluded. For all the satellite products a comparison of the Aerosol Optical Depth (AOD) has taken place. For the few satellite products that provided volcanic ash layer height information a comparison of volcanic ash layer height also took place. The AOD of the EARLINET layers was derived by the layers' integrated backscatter coefficient multiplied by a constant conversion factor (lidar ratio) with a value of 50 sr. An estimated 20% uncertainty on the EARLINET AOD was employed due to the uncertainty on the lidar ratio [typically between 40 and 60 sr]. Please refer to Pappalardo et al., 2004; Sawamura et al., Environ. Res. Lett. 2012, and references therein for further details. As far as the layer height comparison is considered, the height of the center of the layers' mass was used and as estimated uncertainty, the distance between the mass center from the top and base of the later was employed.

As far as the wavelength from which the AOD values were extracted is concerned; all the satellite AOD products were calculated using a wavelength of 550nm apart from the KNMI/GOME2 and KNMI/SCIAMACHY products which were calculated using a wavelength of 380 nm however a table of conversion factors was provided and hence, those findings were also converted to a 550nm-extracted AOD. Correspondingly, only the 532nm AOD LIDAR measurements were used in the following comparisons.

3.1 KNMI GOME2/METOPA ASH AOD AND ASH PLUME HEIGHT COMPARISONS

After the conversion of the KNMI/GOME2 AOD data to 550 nm was performed, as discussed in the ATBD [Theys et al, 2014], the co-locations with the European LIDAR measurements were found and plotted in FIGURE 18 for the "Dust" algorithm and in FIGURE 19 for the "Volz" algorithm for different spatiotemporal patterns [given in the bottom right corner in each plot]. Even though the amount of co-located data is quite small, from around 8 to maybe 18 for the entire Eyjafjallajökull eruptive period in 2010, the *Volz* algorithm seems to be faring better, considering the correlation coefficients calculated. In general, we may note that the spread of AOD values extracted by the satellite measurements is larger than those observed by the ground-based LIDAR systems, by quite a substantial amount in some cases.

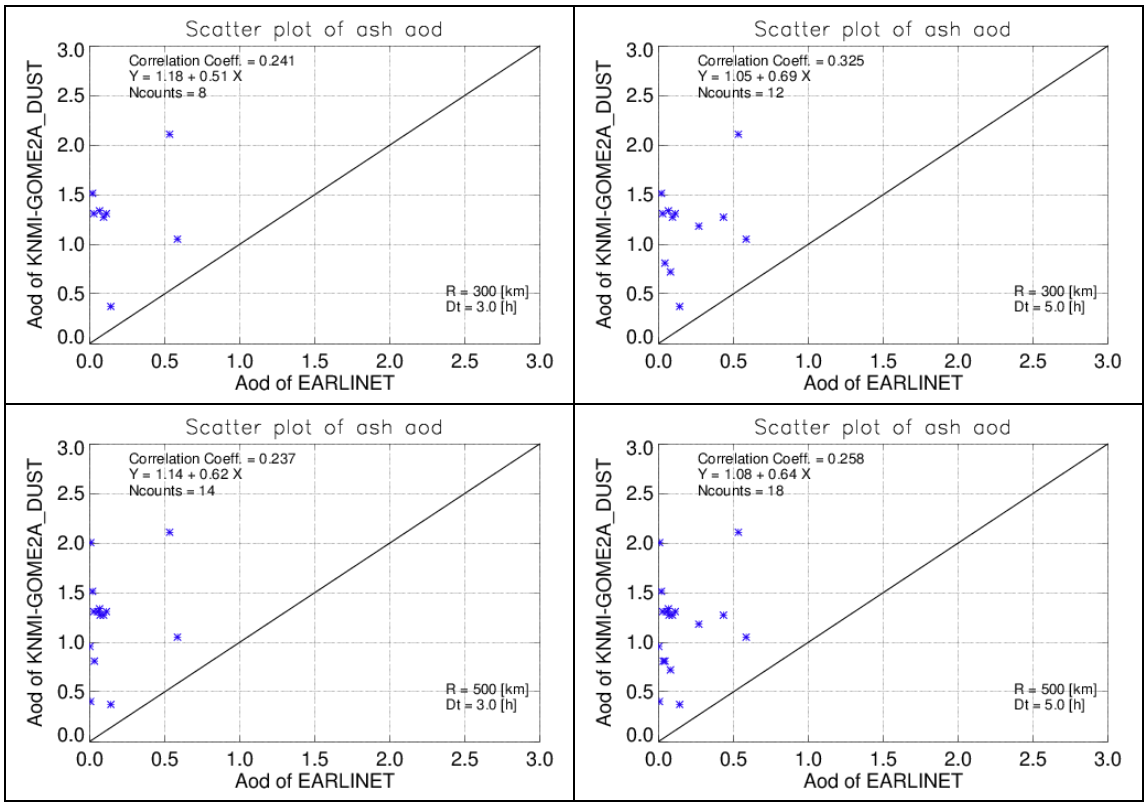

FIGURE 18. Scatter diagrams between the KNMI GOME2 *DUST* algorithm AOD and the co-located EARLINET stations for the Eyjafjallajökull eruptions in 2010. Top left, coincidences within 300km and 3h; top right, within 300km and 5h; bottom left, within 500km and 3h and bottom right, within 500km and 5h.

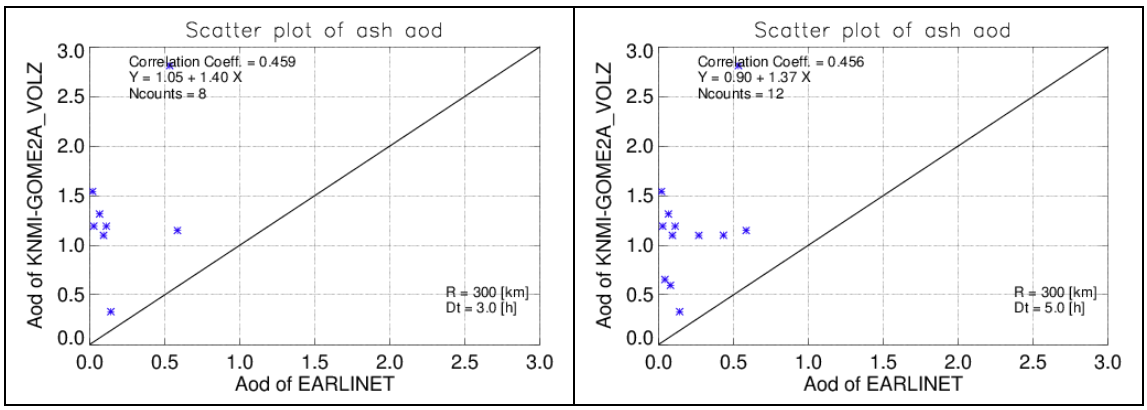

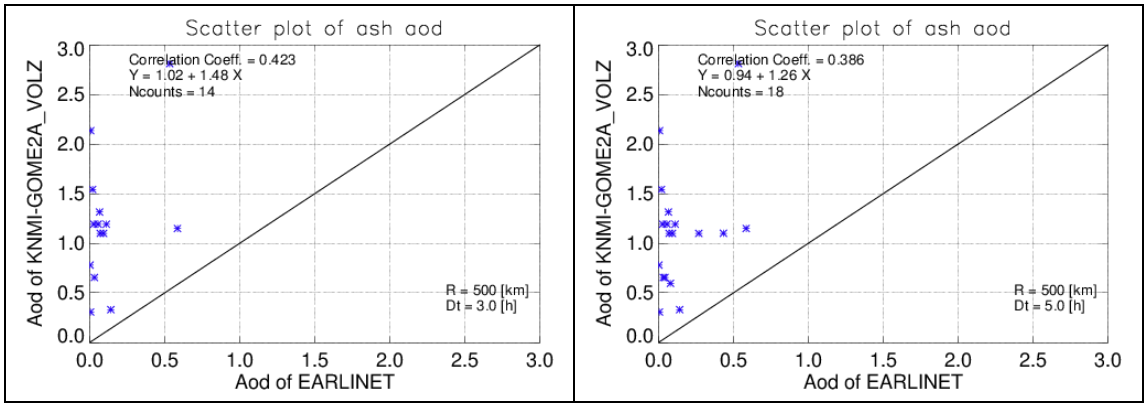

FIGURE 19. Scatter diagrams between the KNMI GOME2 *VOLZ* algorithm AOD and the co-located EARLINET stations for the Eyjafjallajökull eruptions in 2010. Top left, coincidences within 300km and 3h; top right, within 300km and 5h; bottom left, within 500km and 3h and bottom right, within 500km and 5h.

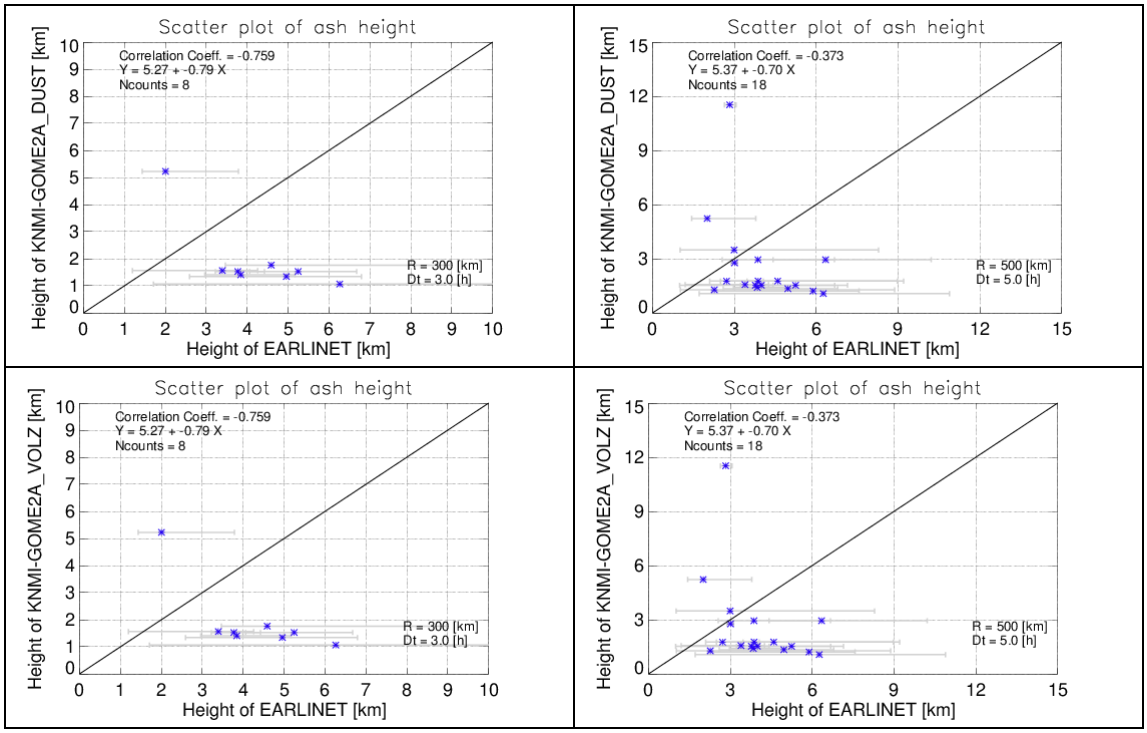

Figure 20. Scatter diagrams between the KNMI GOME2 *DUST* [upper row] and *VOLZ* [lower row] algorithm ash plume height and the co-located EARLINET stations for the Eyjafjallajökull eruptions in 2010. Left column: coincidences within 300km and 3h. Right column: within 500km and 5h.

In Figure 20, the ash plume height estimated by the KNMI/GOME2 algorithms and the EARLINET network is compared for two extreme cases of co-locations. Irrespective of the search radius the comparison is not satisfactory for either one of the two algorithms, since the satellite height seems to under-estimate the ground-based values with a very narrow range of values between 1 and 2km, whereas the ground instruments show a spread between 3 and 6km.

3.2 OXFORD IASI/METOPA ASH AOD AND ASH PLUME HEIGHT COMPARISONS

The ash characteristics extracted by the IASI/MetopA instrument by the Oxford team have a double providence, since the team operates two different algorithms; one, henceforth called "nominal" applied to an optimal estimation technique which permits also the retrieval of ash plume height however is a lot more cost/time effective, and a second one, henceforth called "fast", is less time effective however requires a fixed plume height as input. As a result, in the following sections, four Oxford results will be presented, one from the nominal algorithm and three from the fast algorithm, one each for the three fixed heights provided.

3.2.1 NOMINAL ALGORITHM

As can quickly be verified by FIGURE 21, the ash AOD extracted from the IASI/MetopA Oxford nominal algorithm is quite low, with values rarely rising above the 0.2 limit. Depending on the spatiotemporal choices imposed, the common points rise from 18 to 36, with little effect on the accordance with the ground-based AOD assessment. This accordance provides quite promising correlation coefficients between 0.6 and 0.85 depending on the restrictions on the correlative dataset. Great care is needed though when interpreting these findings, due to the small amount of data points.

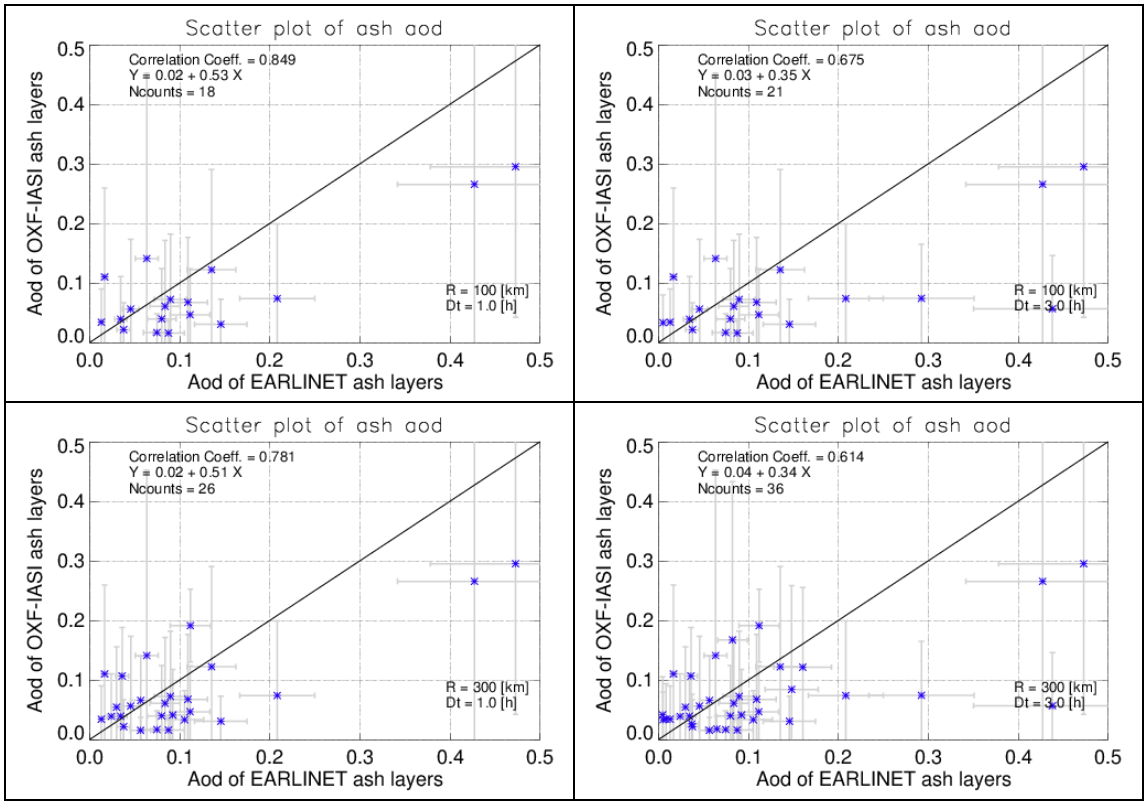

FIGURE 21. Scatter diagrams between the Oxford IASI nominal algorithm ash AOD and the co-located EARLINET stations for the Eyjafjallajökull eruptions in 2010. Top left, coincidences within 100km and 1h; top right, within 100km and 3h; bottom left, within 300km and 1h and bottom right, within 300km and 3h.

In FIGURE 22, the comparison of the ash plume height extracted from the IASI/MetopA Oxford nominal algorithm and the one observed by the EARLINET network is shown, in a format similar to FIGURE 21. In all four cases we note than the spread of plume heights found by the EARLINET network is higher than those found by the Oxford nominal IASI algorithm leading to rather poor correlations. The scatter bars provide an indication of the amount of uncertainty inherent in both sets of observations.

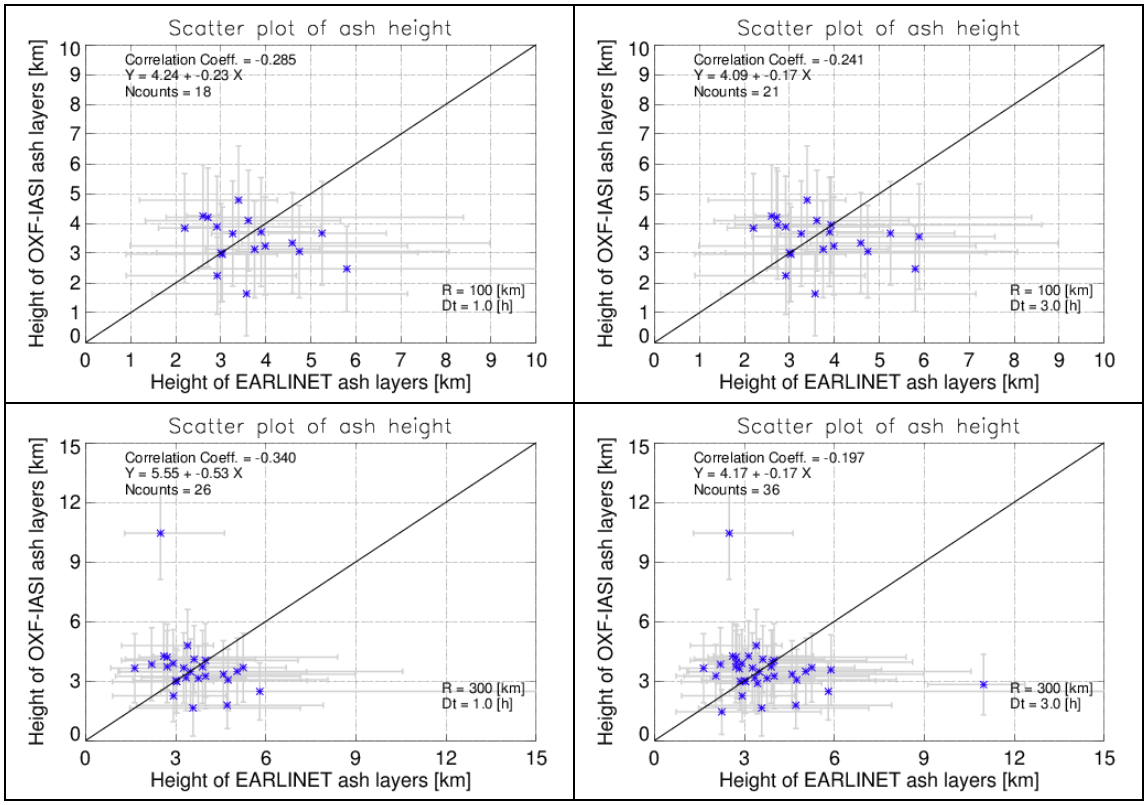

FIGURE 22. Scatter diagrams between the Oxford IASI nominal algorithm ash plume height and the co-located EARLINET stations for the Eyjafjallajökull eruptions in 2010. Top left, coincidences within 100km and 1h; top right, within 100km and 3h; bottom left, within 300km and 1h and bottom right, within 300km and 3h.

3.2.2 FAST ALGORITHM

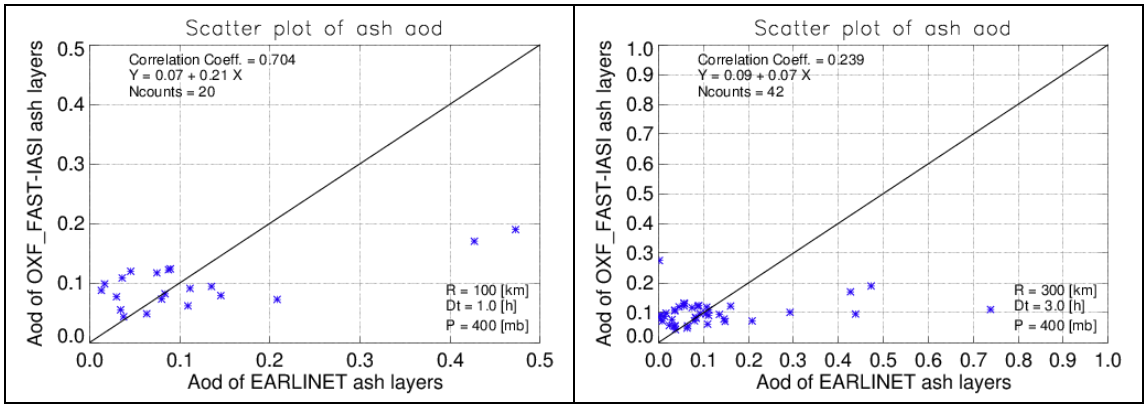

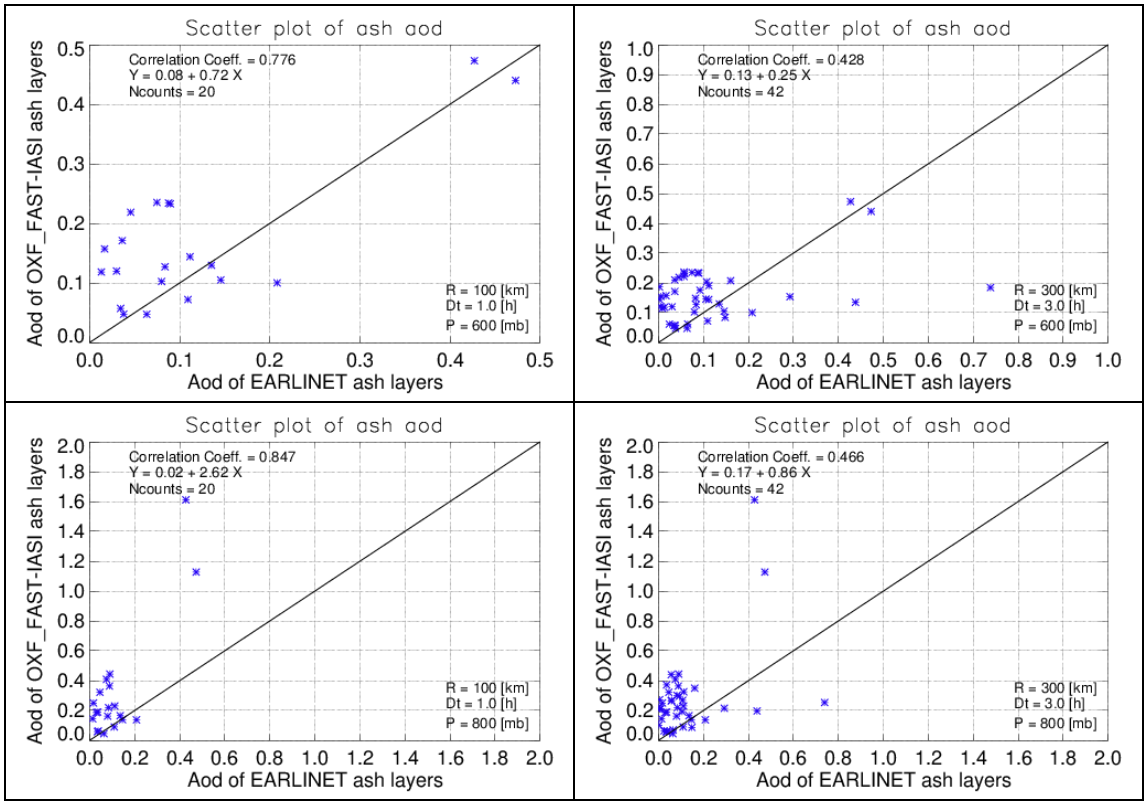

FIGURE 23. Scatter diagrams between the Oxford IASI fast algorithm ash AOD and the co-located EARLINET stations for the Eyjafjallajökull eruptions in 2010. Top row, assumed ash cloud at 400mbars; middle row, at 600 mbars; bottom row, at 800 mbars. Left column, coincidences within 100km and 1h; right column, within 300km and 3h.

Even though all four spatiotemporal choices were also studied during the analysis of the Oxford IASI fast algorithm results, as for the nominal algorithm [see FIGURE 21], only the two extreme cases are shown in FIGURE 23 for space reasons. In the top row, the AOD associated with an apriori plume height of 400 mbar is given, in the middle row, for 600mbar and in the lower row, for 800 mbar. First issue to note is that the amount of co-locations doubles when tripling the spatiotemporal criteria, i.e. moving from 100km and 1h [left column] to 300km and 3h [right column]. It appears as though the lowest assumed plume height provides the closest AODs to the ones observed by the ground-based LIDAR systems, with correlation coefficients between 0.46 for the wider spatiotemporal criterion and 0.85 for the narrower spatiotemporal criterion.

3.3 ULB IASI/METOPA ASH AOD COMPARISONS

Two different refractive indices were used as input to the direct fitting ULB IASI algorithm, resulting in two very similar ash AOD datasets. Examples of both are presented in FIGURE 24 and FIGURE 25. The comparisons when using the refractive index according to the Eyjafjallajökull ash [FIGURE 24] perform better with correlations, r^2, at 0.94 for the narrower spatiotemporal choice [upper left] and 0.74 for the wider choice [lower right.] For the case of the Pollack ash refractive index [FIGURE 25] the equivalent coefficient rises to 0.8 for the narrow case and 0.44 for the wider choice. Even though the sampling is poor, this product shows very promising results and further on, only results using the Eyjafjallajökull ash refractive index will be shown.

To avoid confusion with the rest of the text, note that the ULB Eyjafjallajökull ash product is also identified as simply "ULB ash" in other parts of this report and the ULB Pollack ash product as "ULB Basalt".

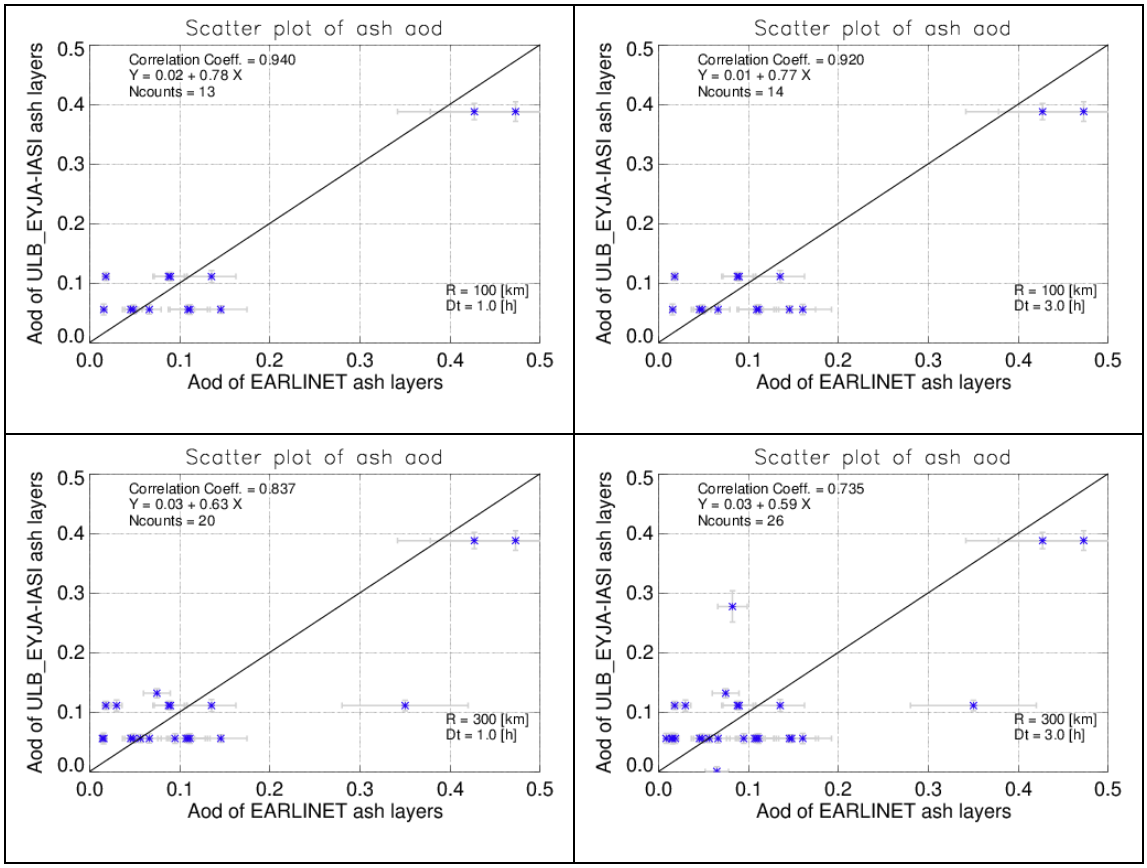

FIGURE 24. Scatter diagrams between the ULB IASI algorithm ash AOD and the co-located EARLINET stations for the Eyjafjallajökull eruptions in 2010 with assumed refractive indices according to Eyjafjallajökull ash. Top left, coincidences within 100km and 1h; top right, 100km and 3h; bottom left, 300km and 1h and bottom right, 300km and 2h.

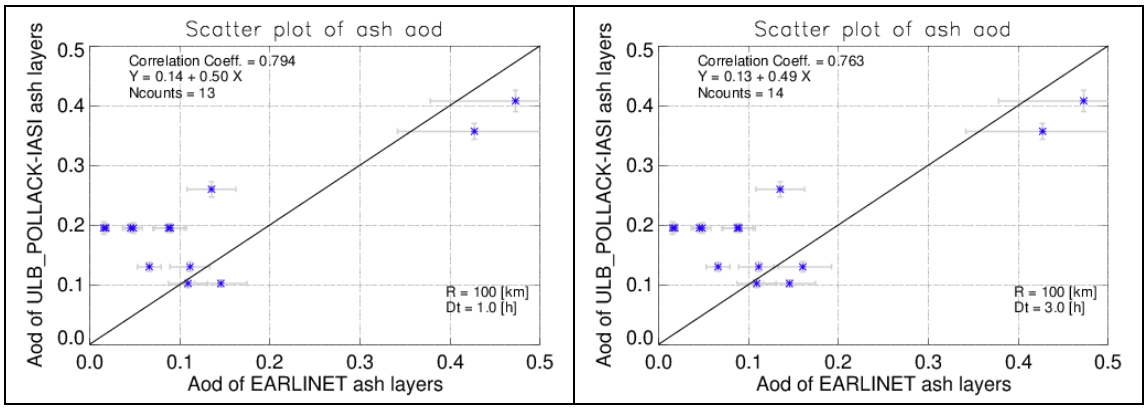

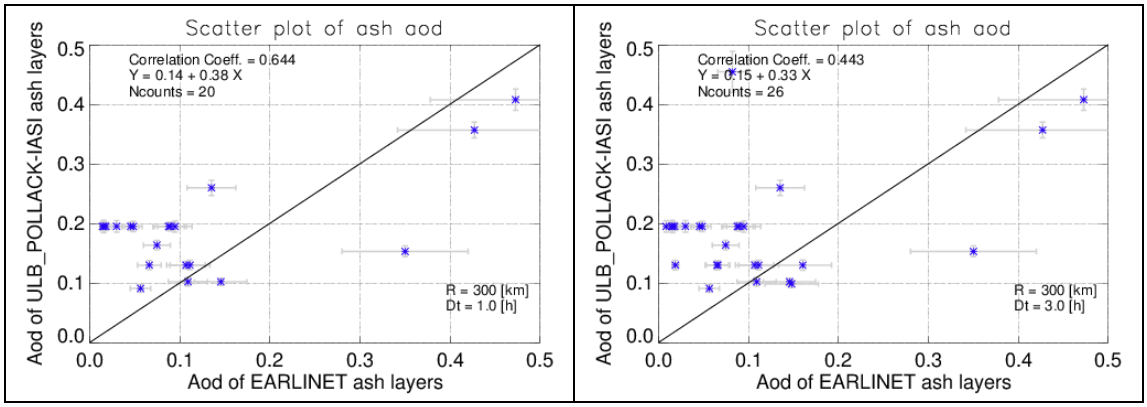

FIGURE 25. Scatter diagrams between the ULB IASI algorithm ash AOD and the co-located EARLINET stations for the Eyjafjallajökull eruptions in 2010 with assumed refractive indices according to Pollock ash. Top left, coincidences within 100km and 1h; top right, 100km and 3h; bottom left, 300km and 1h and bottom right, 300km and 2h.

3.4 RAL MODIS/TERRA AND MODIS/AQUA ASH AOD AND PLUME HEIGHT

In FIGURE 26, the AOD coincidences within 50km and 1h [left column] and 100km and 2h [right column] are given for the RAL MODIS/Terra data [upper row] and the MODIS/Aqua data [lower row]. Note the different axes ranges between the Terra and Aqua instruments. In general, the agreement is not satisfactory, with quite high values for the Terra instrument compared to the ground-based LIDAR and moderate over-estimation for the Aqua instrument as well.

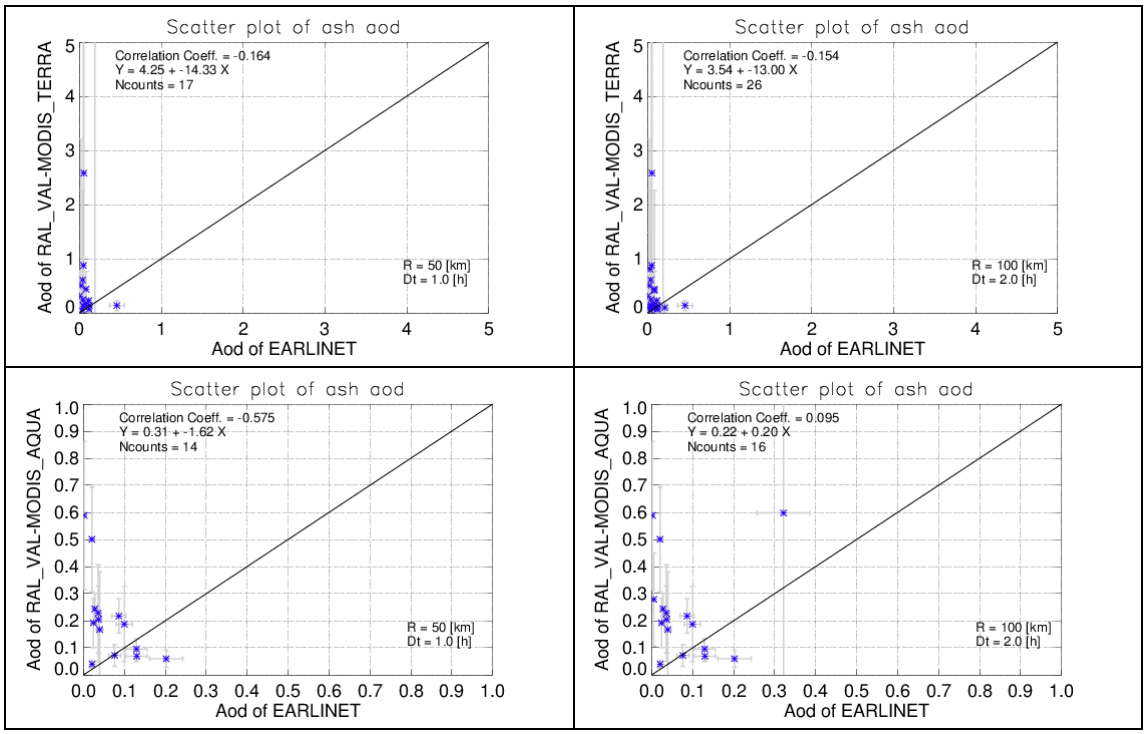

FIGURE 26. Scatter diagrams between the RAL MODIS/Terra [upper row] and MODIS/Aqua [bottom row] for ash AOD and the co-located EARLINET stations for the Eyjafjallajökull eruptions in 2010. Left column, collocations within 50km and 1h and right column, 100km and 2h.

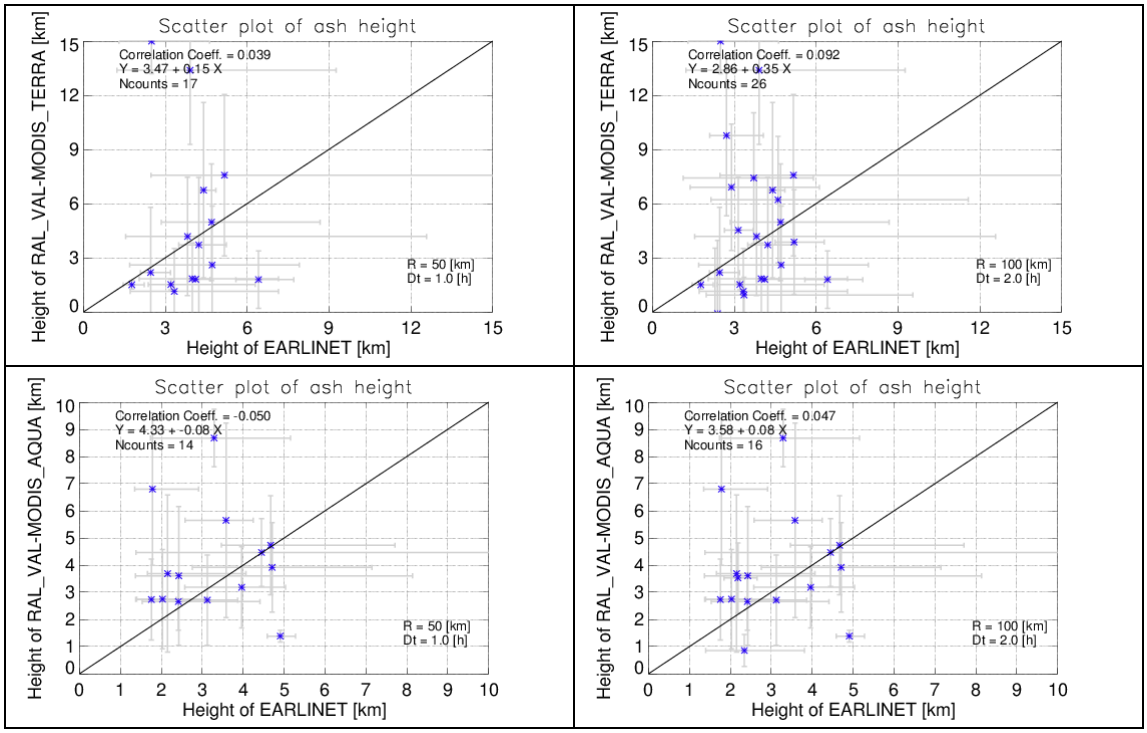

FIGURE 27. Scatter diagrams between the RAL MODIS/Terra [upper row] and MODIS/Aqua [bottom row] for ash plume height and the co-located EARLINET stations for the Eyjafjallajökull eruptions in 2010. Left column, collocations within 50km and 1h and right column, 100km and 2h.

In FIGURE 27, the ash plume height coincidences within 50km and 1h [left column] and 100km and 2h [right column] are given for the RAL MODIS/Terra data [upper row] and the MODIS/Aqua data [lower row]. Note the different axes ranges between the Terra and Aqua instruments. In general, the agreement is not satisfactory, with the MODIS instrument showing a greater range in values than the ground-based LIDAR observations. As an example, in the left column of the Figure, the satellite height ranges between 1 and 8km whereas the ground-based height estimates fall mostly within the 3 to 6km range. It is noted however the reported retrieval errors on height are not taken into account in these comparisons. For thin plumes retrieval errors will be large, so these discrepancies may not be significant.

3.5 CONCLUSIONS AND FUTURE OUTLOOK

In general the comparisons with the ground-based EARLINET LIDAR network suffered from the number of co-locations found between satellite observations and ground-based measurements. A short summary of the mean AOD and ash plume height values encountered in the Figures shown in this Section is given by Table VI and Table VII.

As far as the ash AOD is concerned:

- The KNMI GOME2 AOD over-estimates the ground-based values, showing quite high values for cases where the LIDAR see a low AOD range. As a result, the *dust* algorithm shows relatively low correlation coefficients between 0.25 and 0.3 depending on the spatiotemporal search radius, whereas the *volz* algorithms performs slightly better with r^2 values ranging between 0.4 and 0.5.
- The Oxford nominal IASI algorithm shows an acceptable correlation with the ground values, with coefficients ranging between 0.6 and 0.85, and, even though it provides rather low values, these are of the same order of magnitude as the LIDAR ones.
- The Oxford fast IASI algorithm also provides same order of magnitude AOD estimates as the ground, with the narrower spatiotemporal choice providing the most promising results, with

a correlation ranging between 0.7 for the 400 mbars product to 0.8 for the 800 mbars product.

- The ULB Eyjafjallajökull refractive index AOD estimates are also quite promising, with correlations ranging between 0.74 and 0.94, the highest yet.
- The RAL MODIS/Terra & /Aqua AOD show high values for the Terra instrument compared to the ground-based LIDAR and moderate over-estimation for the Aqua instrument as well. Further investigation into the reasons for these discrepancies is required, though it seems that the Terra results are likely to be subject to more cloud-contamination than was the case for Aqua.

As far as the ash plume height is concerned:

- The KNMI GOME2 ash plume height comparisons are not satisfactory, irrespective of the search radius, for either one of the two algorithms. The satellite height seems to under-estimate the ground-based values with a very narrow range of values between 1 and 2km, whereas the ground instruments show a spread between 3 and 6km.
- The Oxford nominal IASI algorithm ash plume height comparisons are not satisfactory; the satellite estimates have no spread in values compared to the LIDAR assessments.
- The RAL MODIS/Terra & /Aqua ash plume height estimates are not satisfactory, with the MODIS instrument showing a greater range in values than the ground-based LIDAR observations. It is not clear whether these discrepancies are significant within the estimated measurement / co-location related errors. It should be noted that the mean and standard deviation heights reported in table VII are in much better agreement, indicating that indeed the scatter in the figures is dominated by random effects

In order to continue with this line of validation activities, a suggestion to be made for future works is to:

- Include other eruptions with strong ash plumes since from the Eyjafjallajökull and Grimsvötn 2010/2011 eruptions we had too few co-locations for most satellite products.

Table VI. Statistical mean values and associated standard deviation for the EARLINET and the satellite AOD estimates presented in the figures above.

Product	**Spatiotemporal criteria**	**EARLINET mean and standard deviation**	**Satellite mean and standard deviation**
Oxford nominal	100km & 1h	0.12±0.12	0.08±0.08
Oxford fast 400mbars	100km & 1h	0.12±0.12	0.10±0.04
Oxford fast 600mbars	100km & 1h	0.12±0.12	0.17±0.12
Oxford fast 800 mbars	100km & 1h	0.12±0.12	0.32±0.38
KNMI *dust*	300km & 3h	0.19±0.22	1.29±0.48
KNMI *volz*	300km & 3h	0.19±0.22	1.32±0.69
RAL MODIS/Terra	50km & 1h	0.09±0.11	3.0±9.3
RAL MODIS/Aqua	50km & 1h	0.06±0.06	0.20±0.16
ULB Eyja	100km & 1h	0.14±0.14	0.12±0.12

Table VII. Statistical mean values and associated standard deviation for the EARLINET and the satellite ash plume height estimates presented in the figures above.

Product	**Spatiotemporal criteria**	**EARLINET mean and standard deviation [km]**	**Satellite mean and standard deviation [km]**
Oxford nominal	100km & 1h	3.63±0.95	3.4±0.78
RAL MODIS/Terra	50km & 1h	3.81±1.15	4.01±4.42
RAL MODIS/Aqua	50km & 1h	3.23±1.16	4.01±1.91

4. AIRCRAFT LIDAR DATA FOR ASH OPTICAL DEPTH AND ASH HEIGHT

Several European research aircraft measurements were carried out during the Eyjafjallajökull eruption. We will seek for the measurements form 12 flights from UK's BAe-146-301 Atmospheric Research Aircraft managed by the Facility for Airborne Atmospheric Measurements (FAAM, Johnson et al., 2011). Marenco et al. (2011) also reported on the measurements obtained during 6 flights of the Facility for Airborne Atmospheric Measurements BAe-146 research aircraft over the United Kingdom and the surrounding seas in May 2010. Most of these data have already been published in the literature. The lidar measurements include aerosol extinction and backscatter profiles, which result in plume height and layer optical depth as well as in certain cases effective radius of the particles. Apart from the Lidar systems, other probes on the aircraft provided in situ observations. An example of the AOD estimated during the aircraft flight is given in FIGURE 28 for visual purposes.

The research flights, over the United Kingdom and surrounding sea regions, were conducted during the Eyjafjallajokull May 2010 eruption from the UK's Bae-146-301 Atmospheric Research Aircraft managed by the Facility for Airborne Atmospheric Measurements. The most relevant ones correspond to the second period of the 2010 eruption. More specifically the following dates were found of interest for comparison: flight B526 at 4 May, flight B527 at 5 May, flight B528 at 14 May, flight B529 at 16 May, flight B530 at 17 May, flight B531 at 18 May. Data was available on a per flight basis and included lidar measurement variables: aerosol extinction and backscatter profiles that result in Plume height and Layer optical depth. The values of these variables were compared with the satellite product values of aerosol Optical Depth and aerosol Layer Height (where given) over a cross-section of variable radius from 50km to 200km. The closest point value in terms of spatial proximity for every path location was also found and presented. Since most of the satellite data overpass around 10:00 L.T., in order to have co-locations, only spatial criteria where used. Details on the satellite data validated against the flight measurements can be found in TABLE VIII. In the following section one day per satellite instrument/algorithm will be presented for demonstration purposes.

All products presented in FIGURE 29 to FIGURE 31 have been extracted using a 50km radius of search apart from KNMI/GOME2 where the search of radius for co-locations is 200km.

TABLE VIII. The satellite data provided for the validation of the ash plume characteristics with the aircraft data are summarized in this Table.

Institute	Satellite instrument	Overpass time	Amount of Data	Co-location # of days found	Co-location Criteria	Comments
			In days	Max # 5	No time constraint	
KNMI	SCIAMACHY/ENVISAT	10:00 LT	12	---		No co-locations found
KNMI	GOME2/MetopA	09:30 LT	14	1	100km/200km	
OXFORD	IASI/MetopA-Nominal Algorithm	09:30 LT 21:30 LT	18	4	50/100/200km	
OXFORD	IASI/MetopA-Fast Algorithm	09:30 LT 21:30 LT	19	4	50/100/200km	3 fixed heights provided, 400, 600 &

						800mbar
ULB	IASI/MetopA-Ash Algorithm	09:30 LT 21:30 LT	48	5		
ULB	IASI/MetopA-Basalt Algorithm	09:30 LT 21:30 LT	53	4		
RAL	MODIS/Terra-IR algorithm	10:30 L.T.	2.5 months ~10 files/day	3	50/100/200km	
RAL	MODIS/Terra-VIS/NIR algorithm	10:30 L.T.	2.5 months ~5 files/day	3	50/100/200km	
RAL	MODIS/Aqua-IR algorithm	13:30 L.T.	2.5 months ~10 files/day	4	50/100/200km	
RAL	MODIS/Aqua-VIS/NIR algorithm	13:30 L.T.	2.5 months ~5 files/day	4	50/100/200km	

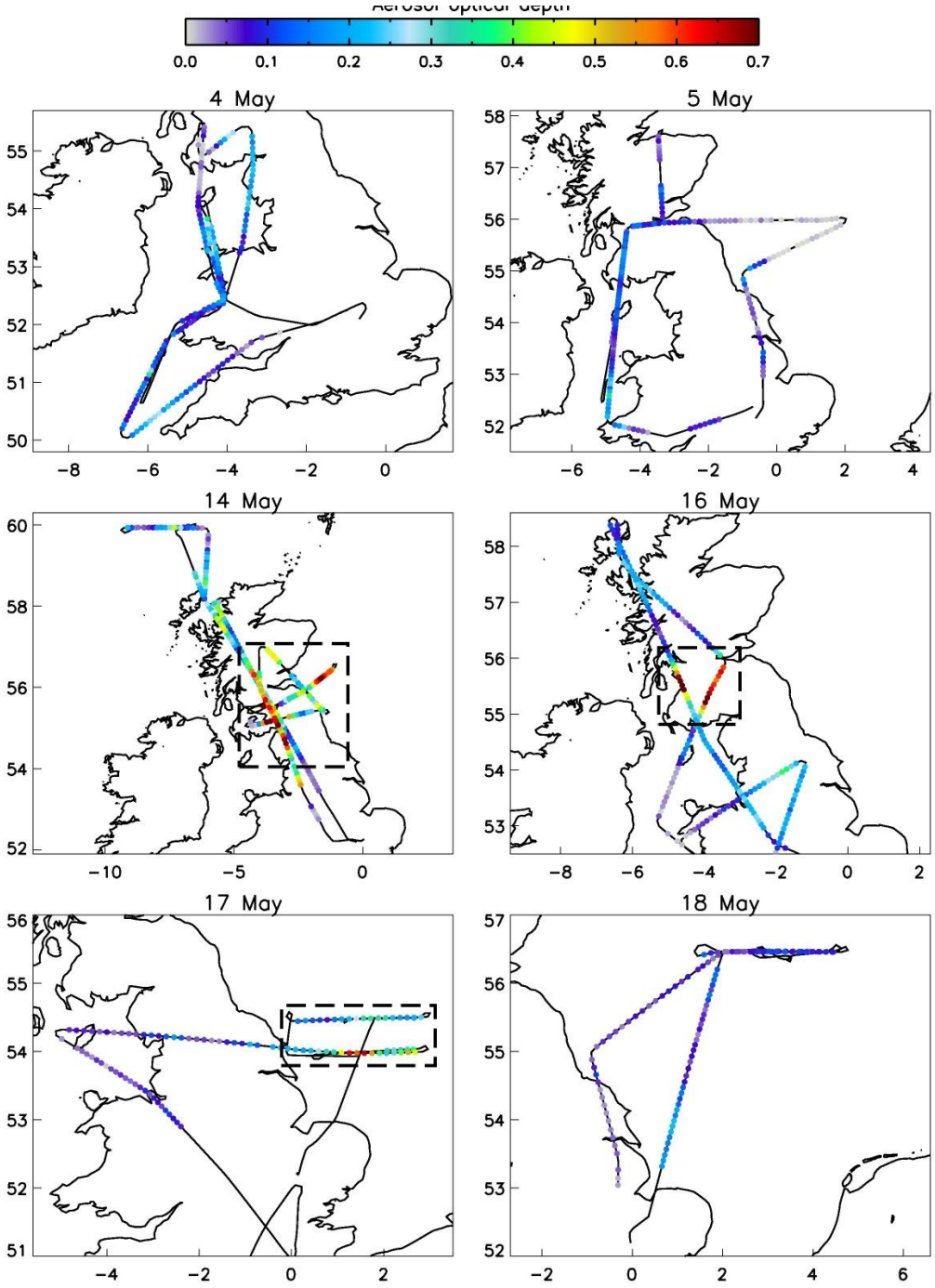

FIGURE 28. The aerosol optical depth [in colour] of six Falcon aircraft flights between the 4th and the 18th of May during the 2010 Eyjafjallajökull eruption periods, courtesy of Franco Marenco and the UK Met Office.

4.1 KNMI/GOME2, OXFORD IASI-NOMINAL ALGORITHM, RAL MODIS/AQUA IR ALGORITHM AND RAL MODIS/AQUA VIS-NIR ALGORITHM COMPARISONS.

In Figure 29 four different comparisons between satellite and aircraft lidar measurements are presented. In the first row, the KNMI/GOME2 estimates for the 17th of May 2010; in the second row, the Oxford/IASI nominal algorithm for the 16th of May 2010; in the third row, the MODIS/Aqua IR algorithm for the 14th of May 2010 and in the fourth row, the MODIS/Aqua Vis-NIR algorithm for the 14th of May.

The KNMI products [upper row] seem to suffer from the GOME-2 pixel size, compared to the instantaneous aircraft measurement, however the same order of magnitude estimates as for the aircraft, both for AOD and for height, are found. The Oxford/IASI nominal products show quite good agreement for the AOD [second left] and a rather high scatter for the ash plume height [second right], which amounts to a promising finding indeed. The RAL IR algorithm [third left] for the AOD product seems to have the best agreement, especially around 13:00-14:00 UT. The RAL VIS/NIR algorithm [fourth row] provides either too high [for AOD] or too low [for height] estimates. This would be consistent with the scheme being affected by the presence of cloud under the ash plume, which will affect the VIS/NIR scheme much more than the IR scheme.

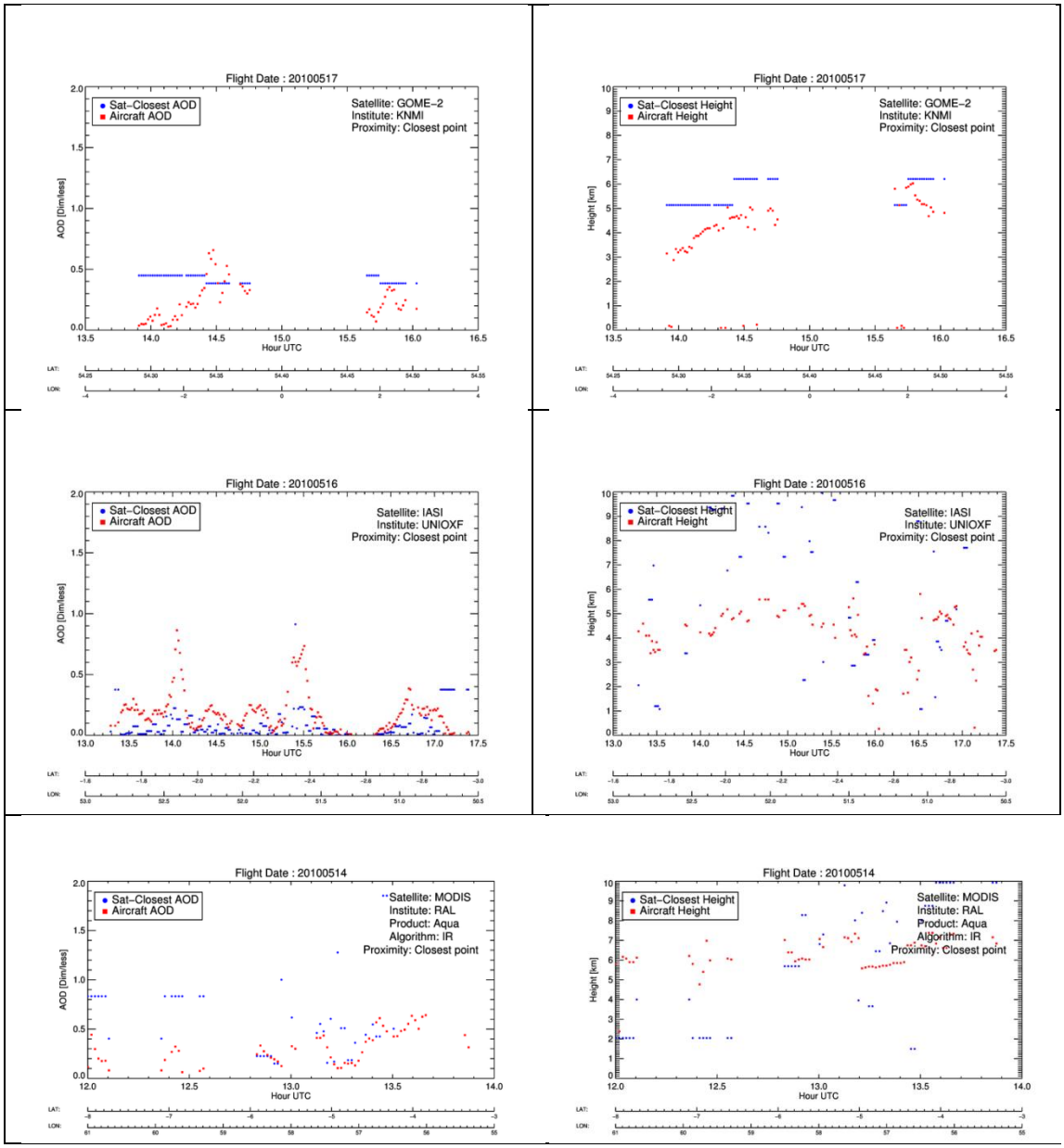

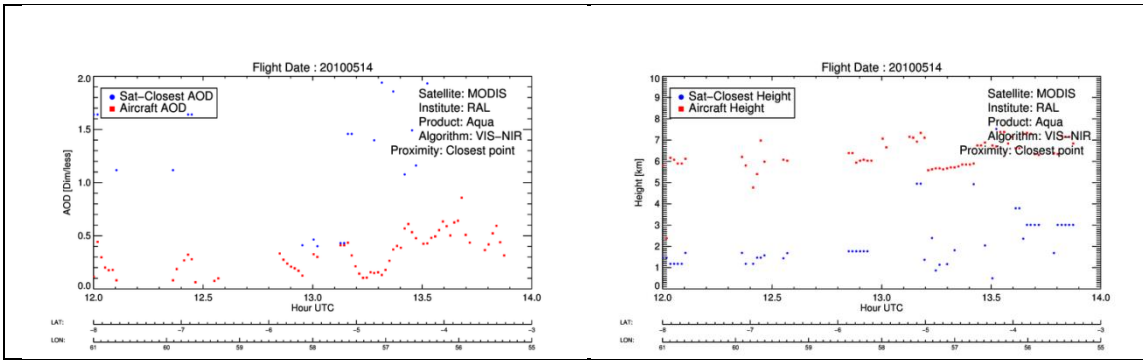

FIGURE 29. Comparisons between the AOD [left column] and plume height [right column] estimated by the aircraft instruments [red dots] and different satellite products [blue dots]: KNMI/GOME2 [first row], Oxford IASI-nominal algorithm [second row], RAL MODIS/Aqua IR algorithm [third row] and RAL MODIS/AQUA VIS-NIR algorithm [fourth row]. For KNMI/GOME2 the search of radius for co-locations is 200km and for the rest of the satellites, 50km.

4.2 OXFORD IASI FAST ALGORITHM AND ULB IASI ALGORITHMS COMPARISONS

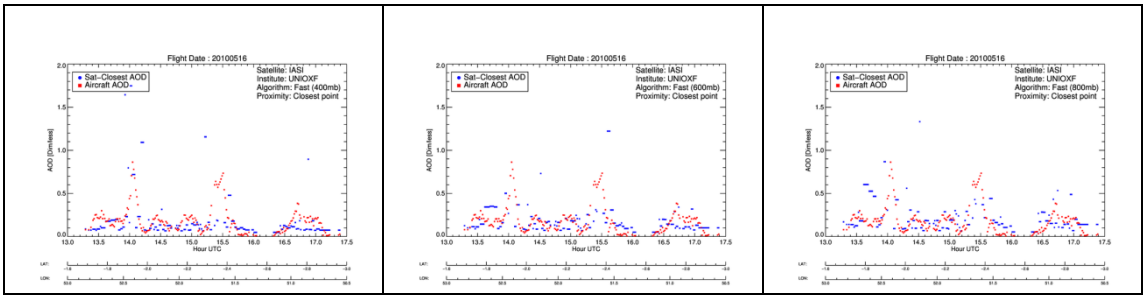

FIGURE 30. Comparisons between the AOD estimated by the aircraft instruments [red dots] and different Oxford IASI-Fast algorithm products [blue dots]: 400mbars [left], 600 mbars [middle] and 800 mbars [right.] Search of radius for co-locations: 50km.

In Figure 30 the three AOD estimates extracted by the Oxford/IASI Fast algorithm depending on the assumed plume height are shown for 400mbars [left] 600 mbars [middle] and 800 mbars [right.] All three products show a very good agreement with the collocated aircraft AOD estimates. In Figure 31 the comparisons for the two ULB/IASI products is shown, on the left, the Eyjafjallajokull-type refractive index and on the right, the Basalt-type refractive index. Also an excellent agreement with the Eyjafjallajokull-type refractive index producing slightly better comparisons than the other type.

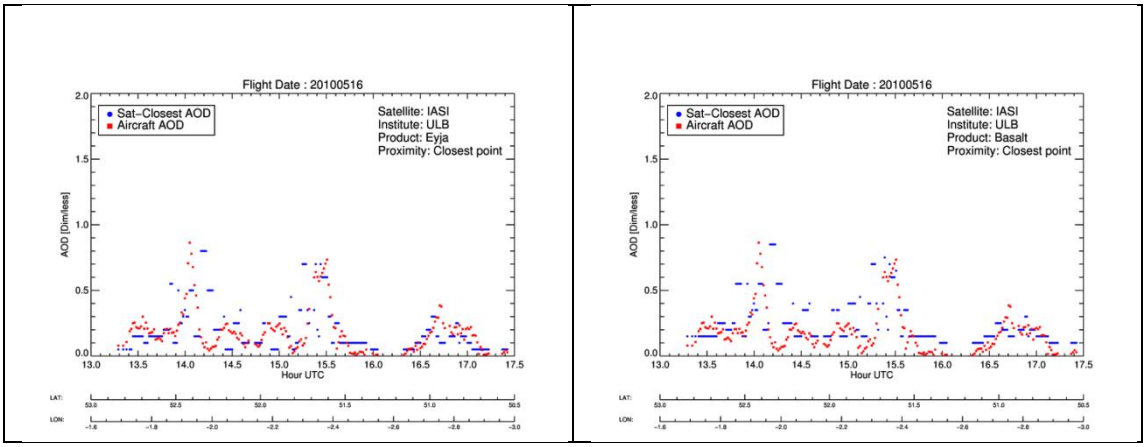

FIGURE 31. Comparisons between the AOD estimated by the aircraft instruments [red dots] and different ULB IASI algorithm products [blue dots]: Eyjafjallajokull-type refractive index [left] and Basalt-type refractive index [right.] Search of radius for co-locations: 50km.

4.3 CONCLUSIONS AND FUTURE OUTLOOK

Some statistical values to accompany the findings shown in the Figures of this Section are presented in Table IX.

As far as each individual satellite estimate comparison to the aircraft instrument is concerned:

- The KNMI/GOME2 data seem to suffer from the spatial resolution of the satellite data which made the spatial criterion rather large, at 200km, precluding any conclusive comparisons between the two datasets.
- The Oxford nominal IASI algorithm presents quite good comparisons for the AOD patterns observed during the course of the flight shown in the Figures, a promising result. Not so for the height estimate.
- The RAL MODIS/Aqua IR algorithm, shows an excellent agreement between 13:00 and 14:00 UTC both for the AOD, the ash height and the features observed at those hours, a promising result. Not so for the RAL MODIS/Aqua VIS-NIR algorithm, which is presumably affected by the presence of a water cloud under the ash layer.
- The Oxford fast IASI algorithm shows an excellent agreement, with the 800mbar product appearing to perform best.
- The ULB IASI algorithm shows an excellent agreement, both with respect to the absolute AOD values as well as AOD features during the flight shown. The actual absolute AOD maxima are also represented best by this product.

Table IX. Statistics of the AOD levels viewed by a selection of the instruments presented above.

Institute	Instrument & algorithm	Mean Satellite AOD levels	Mean Aircraft AOD Levels	Mean difference	Number of common observations
KNMI	GOME2/MetopA	0.42±0.03	0.231±0.15	-0.19±0.18	64
Oxford	IASI/MetopA Nominal Algorithm	0.09±0.09	0.22±0.18	0.13±0.17	600
Oxford	IASI/MetopA Fast Algorithm 400mbars	0.24±0.33	0.22±0.17	-0.03±0.32	586
Oxford	IASI/MetopA Fast Algorithm 600mbars	0.29±0.32	0.21±0.17	-0.08±0.28	550
Oxford	IASI/MetopA Fast Algorithm 800mbars	0.38±0.44	0.21±0.17	-0.17±0.39	542
ULB	IASI/MetopA Eyjafjallajökull Algorithm	0.22±0.15	0.25±0.17	0.03±0.22	463
ULB	IASI/MetopA Basalt Algorithm	0.29±0.15	0.25±0.177	-0.04±0.22	462

5. CALIOP/CALIPSO ASH HEIGHT AND ASH OPTICAL DEPTH ESTIMATES

As an independent satellite source for the validation of the ash plume height the Cloud-Aerosol Lidar with Orthogonal Polarization (CALIOP) instrument onboard the CALIPSO mission will be used. CALISPO is the first polarization lidar to provide global atmospheric measurements. Calipso is quite able to identify volcanic eruption plumes and data from its instruments have been used in numerous publications. An example of the volcanic plume over Northern Europe during one of Eyjafjallajökull's 2010 eruptions is shown in FIGURE 32.

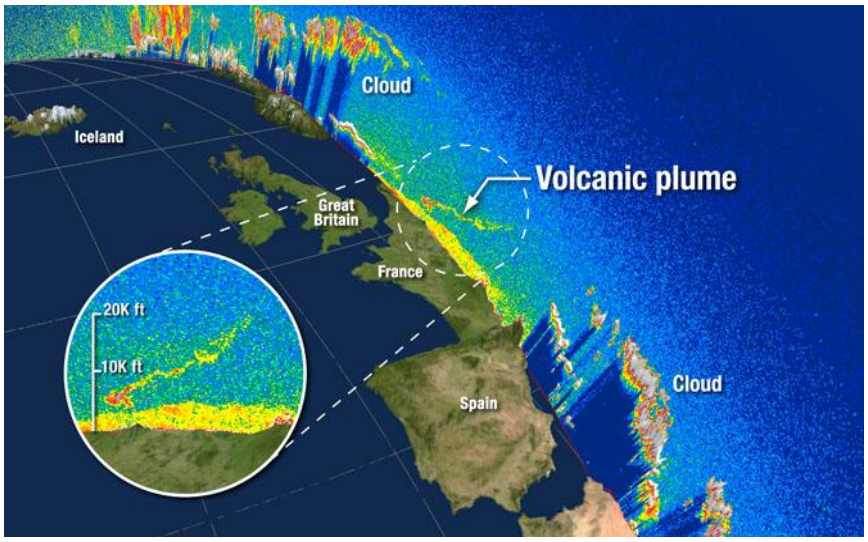

FIGURE 32. NASA's Cloud-Aerosol Lidar and Infrared Pathfinder Satellite Observations (CALIPSO) satellite watches Eyjafjallajökull's plume drift over northern Europe. Credit: NASA/Kurt Severance and Tim Marvel.

For the validation of the SMASH/SACS2 products level 2 data products CALPSO products will be used. These consist of three basic types of information: layer products, profile products, and the vertical feature mask (VFM). Layer products provide layer-integrated or layer-averaged properties of detected aerosol and cloud layers. Profile products provide retrieved extinction and backscatter profiles within these layers. Because information on the spatial locations of cloud and aerosol layers is of fundamental importance, the VFM was developed to provide information on cloud and aerosol locations and types. The methodology described in Winker et al, 2012 will be applied in the comparisons, which will be based on the scenes presented in this paper and cover the period 15-20 April 2010 [see Figure 33]. CALIPSO categorizes in its operational algorithm ash as dust or polluted dust, so its identification and distinction is not always straightforward, especially when dust and ash coexist. Such conditions were more frequent during the 4-20 May 2010 events, so for these cases a careful identification of ash in the CALISPO data should be performed before these data could be used for validation purposes. All data products are freely available from the Atmospheric Sciences Data Center at NASA Langley Research Center (available online at http://eosweb.larc.nasa.gov).

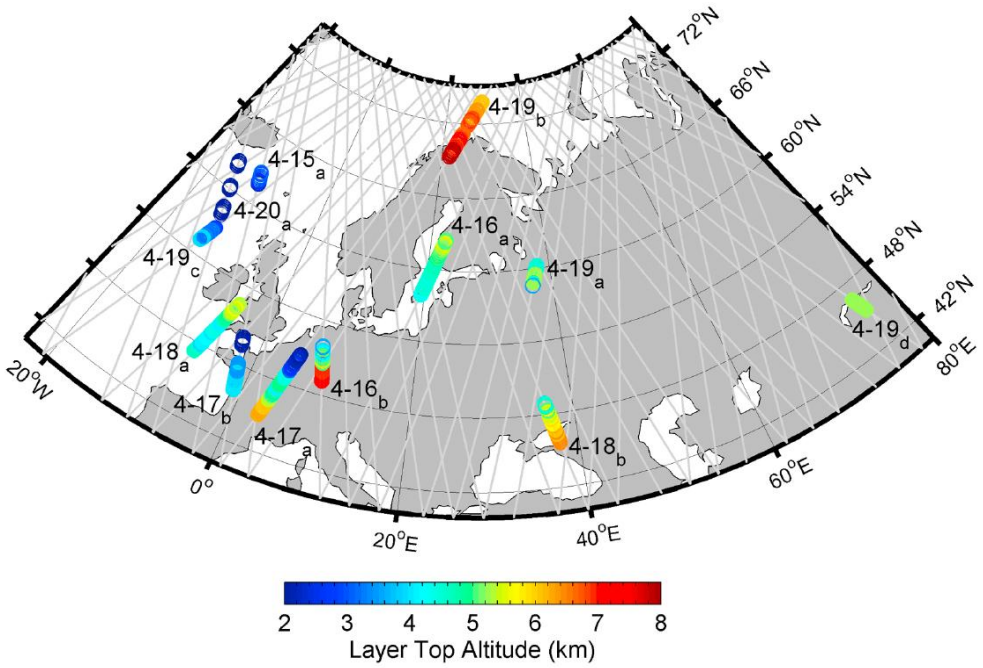

Figure 33. Summary of locations where CALIPSO observed the volcanic plume during 15–20 April 2010. Color coding indicates observed altitude of the layer top. (From Winker et al., 2012)

CALIPSO NASA mission data was requested using the online data ordering tool of Atmospheric Sciences Data Center at NASA Langley Research Center [https://www-calipso.larc.nasa.gov/search/]. Requested data covered the two periods of interest during the Eyjafjallajökull volcanic eruption over the European domain, between April 15 to 26 and May 04 to 20 of year 2010. The following level-2 data products were used: vertical feature mask and aerosol layer products. The Vertical Feature Mask describes the vertical and horizontal distribution of layers, including both cloud and aerosol. A 16-bit integer value describes the data bin of each level-0 data, with every bit range describing a characteristic[http://www-calipso.larc.nasa.gov/resources/calipso_users_guide/data_summaries/layer/index.php]. Initially, the data was decoded and utilized to find the date and time ranges that aerosol layers were detected. In the next step the Aerosol Layer Product data was processed and aerosol layer variables were extracted for comparison with other satellite products. The Feature Optical Depth at 532 nm was extracted. Additionally, using the Layer Top Altitude and Layer Base Altitude, the Aerosol Layer Height was estimated and used in the comparison process. Only layers that were found consisting of dust and polluted dust aerosol subtypes were selected for comparison. Dust is mostly mineral soil and polluted dust is a mixture of desert dust and smoke or urban pollution. The Calipso AOD was compared with other satellite orbit AOD values in various cross-section regions that were dependent on a variable radius between 50km and 200km and a time window variable from 1 hour to 2 hours. The closest point value in terms of spatial proximity was also found and presented. The same process was done for the Aerosol Layer Height variable, only if it was available in the other satellite products.

Slightly different than what was presented in the Sections above, the actual co-locations between Calipso and satellite overpasses are not at all satisfactory and we have hence opted to present full day comparisons between the space-born lidar and the satellite instruments. The days 24th of April 2010 and 8th of May 2010 where chosen as days where the plumes reached the UK and Spain respectively and a prominent feature may be seen in the Calipso maps.

5.1 THE ULB/IASI, THE OXFORD/IASI AND THE INGV/MODIS AOD ESTIMATES

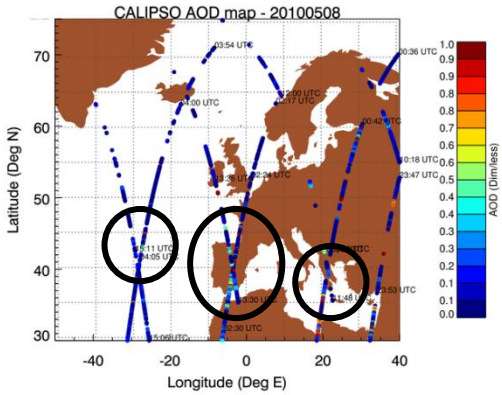
CALIPSO AOD map - 20100508
Latitude (Deg N)
Longitude (Deg E)
AOD (Dimless)

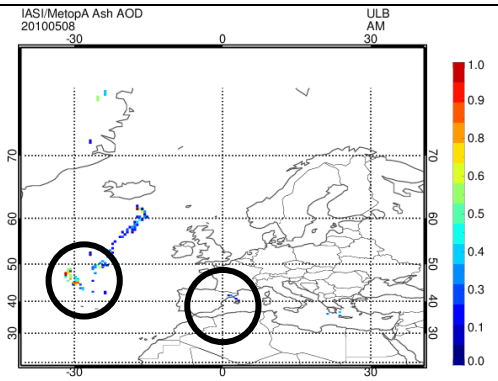
IASI/MetopA Ash AOD
20100508
ULB
AM

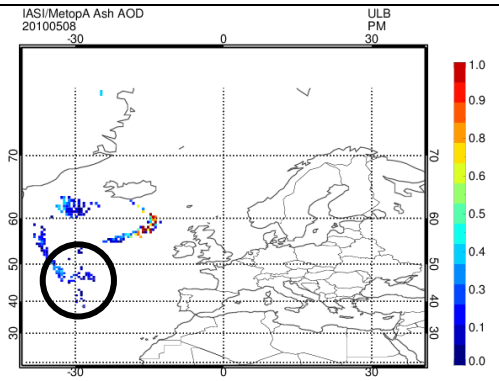
IASI/MetopA Ash AOD
20100508
ULB
PM

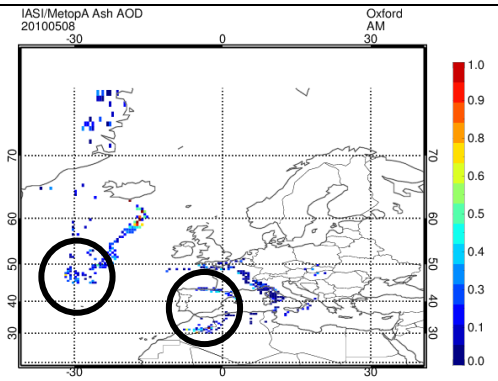
IASI/MetopA Ash AOD
20100508
Oxford
AM

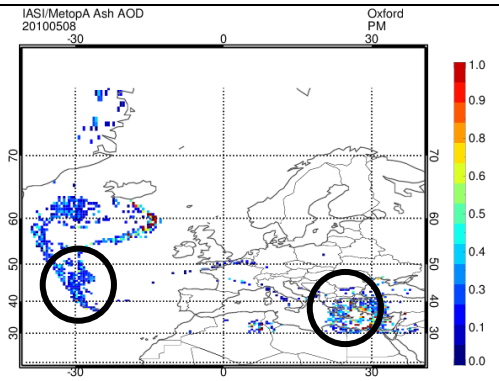
IASI/MetopA Ash AOD
20100508
Oxford
PM

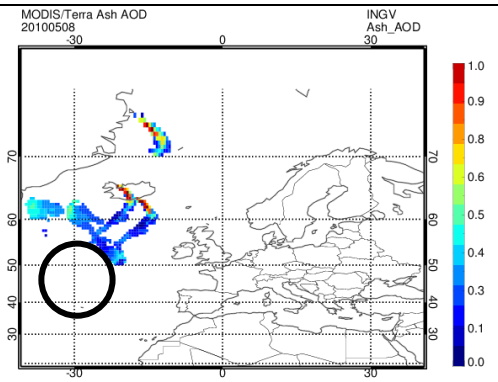
MODIS/Terra Ash AOD
20100508
INGV
Ash_AOD

n/a

Figure 34. The CALIPSO overpasses over Europe on the 8th of May 2010 [upper row] as seen through the AOD estimates for dust aerosols in all layers found. In the second row, the ULB/IASI AM [left] and PM overpasses [right]. In the third row, the Oxford/IASI nominal algorithm AM [left] and PM [right] overpasses. In the fourth row, the INGV MODIS/Terra AM overpass.

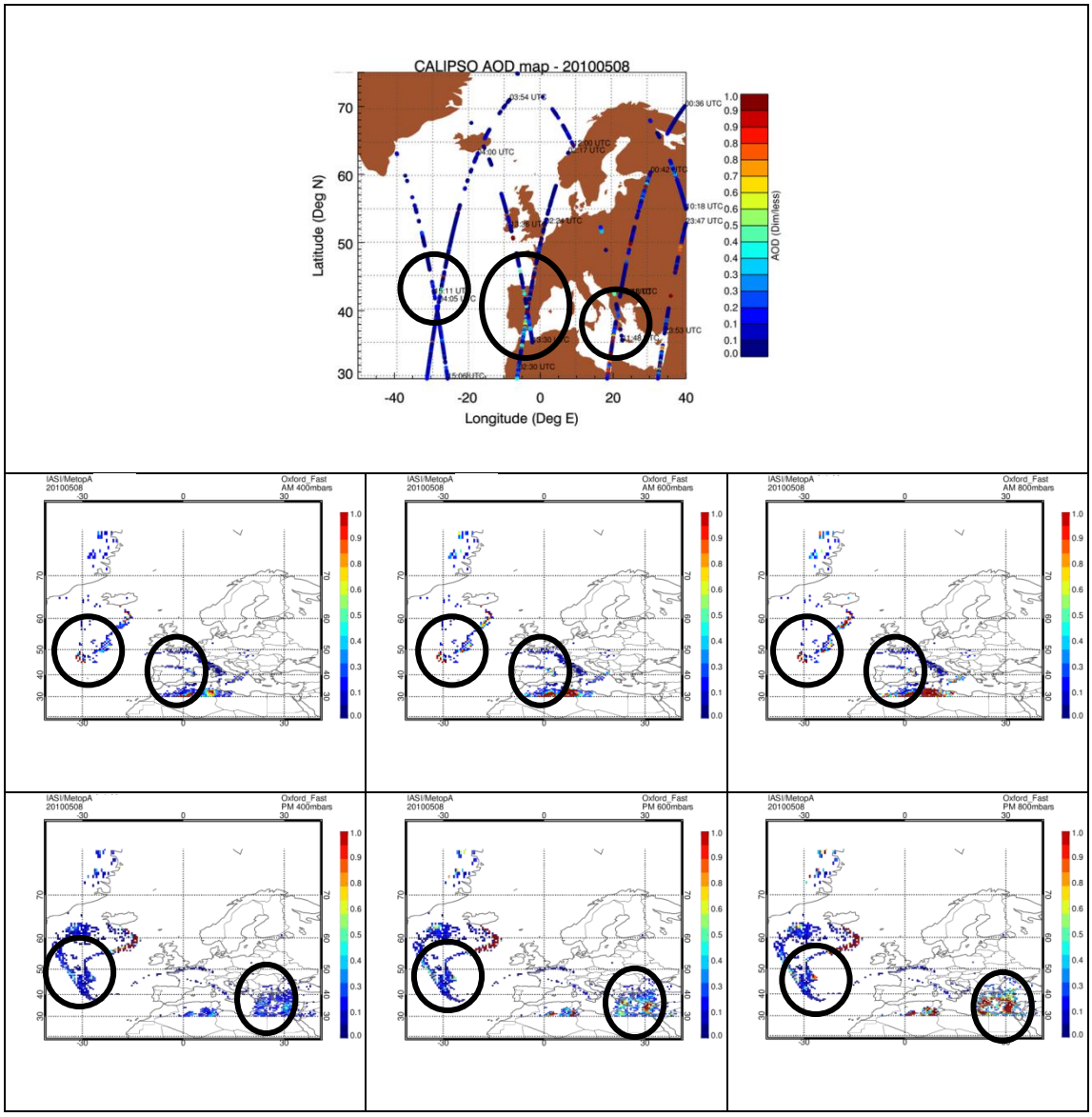

Figure 35. The CALIPSO overpasses over Europe on the 8th of May 2010 [upper row] as seen through the AOD estimates for dust aerosols in all layers found. In the second row, the Oxford fast algorithm AOD for the morning overpass and in the third row, the evening overpass is shown From left to right columns; the AOD with assumed plume height at 400mbars, at 600mbars and at 800mbars respectively.

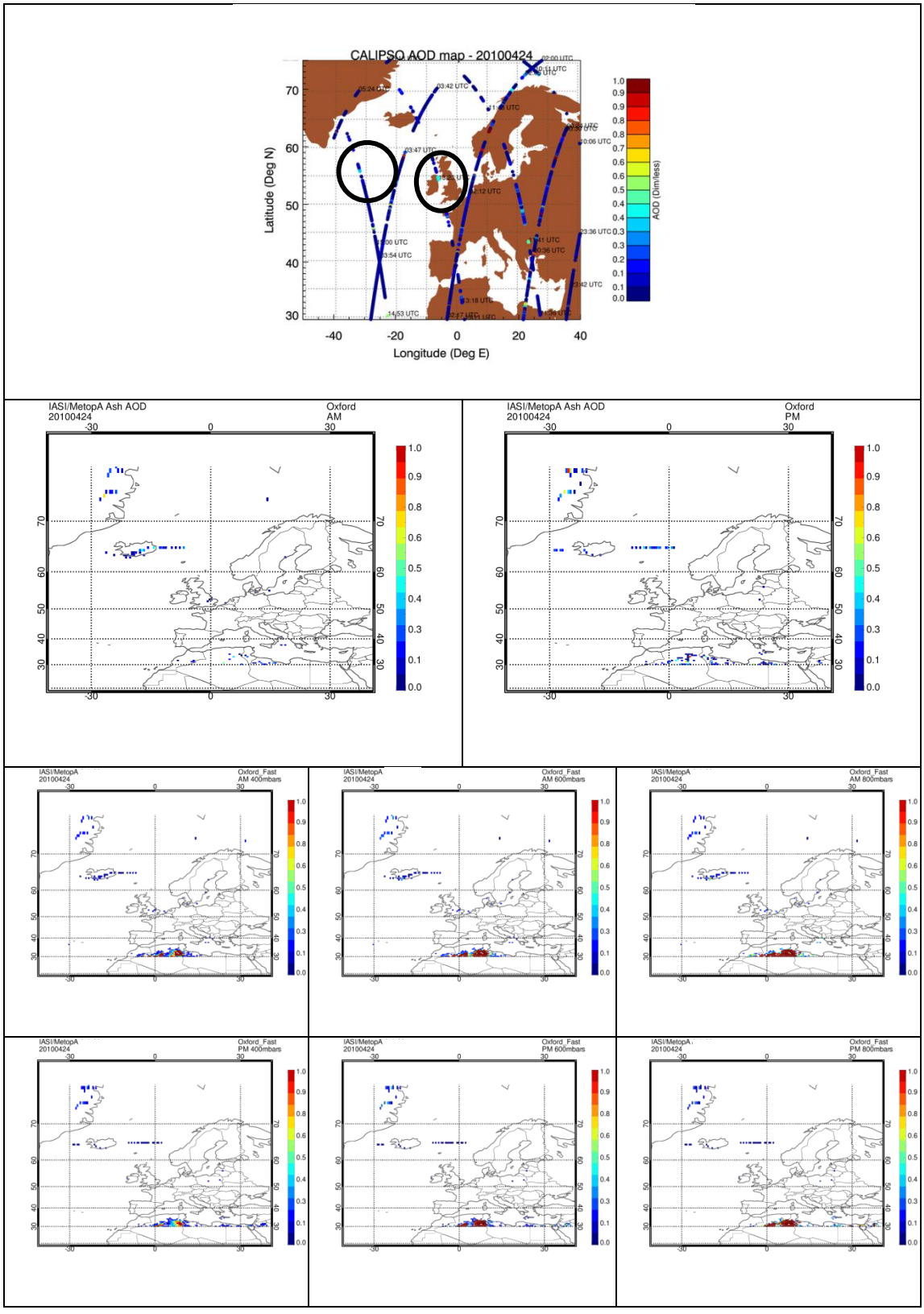

Figure 36. The CALIPSO overpasses over Europe on the 24th of April 2010 [upper row] as seen through the AOD estimates for dust aerosols in all layers found. In the second row, the Oxford nominal algorithm AOD for the morning overpass [left] and the evening overpass [right]. In the third and fourth row, the Oxford fast algorithm AODs for the morning and the evening overpass respectively. From left to right columns; the AOD with assumed plume height at 400mbars, at 600mbars and at 800mbars respectively.

In Figure 34 the CALIPSO overpasses over Europe on the 8th of May 2010 [upper row] as seen through the AOD estimates for dust aerosols in all layers found are shown. In the second row, the ULB/IASI AM [left] and PM overpasses [right]. In the third row, the Oxford/IASI nominal algorithm AM [left] and PM [right] overpasses. In the fourth row, the MODIS/Terra AM overpass. The satellite data are shown in the same colour scale and range as the CALIPSO estimates to facilitate easy reading between the graphs. Where no figure appears this signifies that the algorithm did not reach a satisfactory retrieval result for the day. Black circles have been added over the figures in order to pin-point the location of the signal as seen by CALIPSO. Even though it is hard to make an estimate, the North Atlantic loading seems to be depicted well from both the spectrometers and the LIDAR evaluations for most of the products considered. The Iberian and Greek peninsula loadings are not usually seen by the satellite data, apart from the Oxford/IASI nominal algorithm maps [third row.] In Figure 35 the same Calipso map, for the 8th of May 2010 [upper row], is compared to the findings of the Oxford/IASI fast algorithm [middle and bottom rows.] For the morning overpass, the Oxford/IASI maps seems to have captured both the N. Atlantic loading as well as the Iberian loading, whereas for the evening overpass, some loading over the Balkan peninsula seems to be depicted well. However, examining the days previously to the one shown, it is evident that there is no such strong ash plume headed towards Greece, but a sand plume originating in North Western Africa, Morocco, and headed west [a typical feature of the spring months in the area.] Hence, one might say that the Oxford/IASI fast algorithm is also sensitive to sand or other aerosol sources as well as volcanic ash and great care should be taken when evaluating such complicated AOD maps. In general, from both these figures, we may deduce that the approximate ash loading over the region due to the volcanic eruption is estimated well by most algorithms, and was found to be of the same order to magnitude as that of the satellite LIDAR measurements. A different picture for the Oxford/IASI algorithms as was seen in Figure 35 can be found in Figure 36 where both Oxford nominal and fast algorithm results are shown. The loading observed by Calipso over the UK and the N. Atlantic is not depicted by the IASI algorithms, possible due to the small loading and detection limit. The high values at the Southernmost edge of the IASI domain for the Oxford fast algorithm [third and fourth rows] maybe be either algorithm artifacts or Saharan dust misidentified by the algorithm as volcanic ash, as discussed above.

5.2 CONCLUSIONS AND FUTURE OUTLOOK

The comparisons between satellite and CALIPSO overpasses are in a preliminary stage, mainly due to the fact that different validation strategies than those followed so far is required in order to increase the amount of coincidences and hence the statistical value of the validation. Nevertheless, the mean AOD loading of the region following the main eruptive days is common between CALIPSO and individual satellite findings, with similar increasing tendencies in the cases of high loading. As a future recommendation, a period of dates with suspected aerosol loading should be carefully chosen and used in average in order to be able to statistically analyze the coincidences.

6. INTER-COMPARISON OF RETRIEVAL SCHEMES FOR ASH AOD AND ASH PLUME HEIGHT.

In the following section, we have opted to compare ash optical depth and plume height, where applicable, as extracted by different algorithms on the same satellite measurements. Hence, in Section 6.1 the RAL and INGV estimates from the MODIS/Terra and /Aqua instruments is shown side by side whereas in Section 6.2 the ULB and Oxford estimates from the IASI/MetopA instruments is presented in a similar fashion. Two dates will be discussed, the 23rd of May 2011 [Grimsvötn eruption] and the 9th of May 2010 [Eyjafjallajökull eruption].

6.1 RAL AND INGV MODIS/TERRA AND MODIS/AQUA ASH AOD AND ASH PLUME HEIGHT

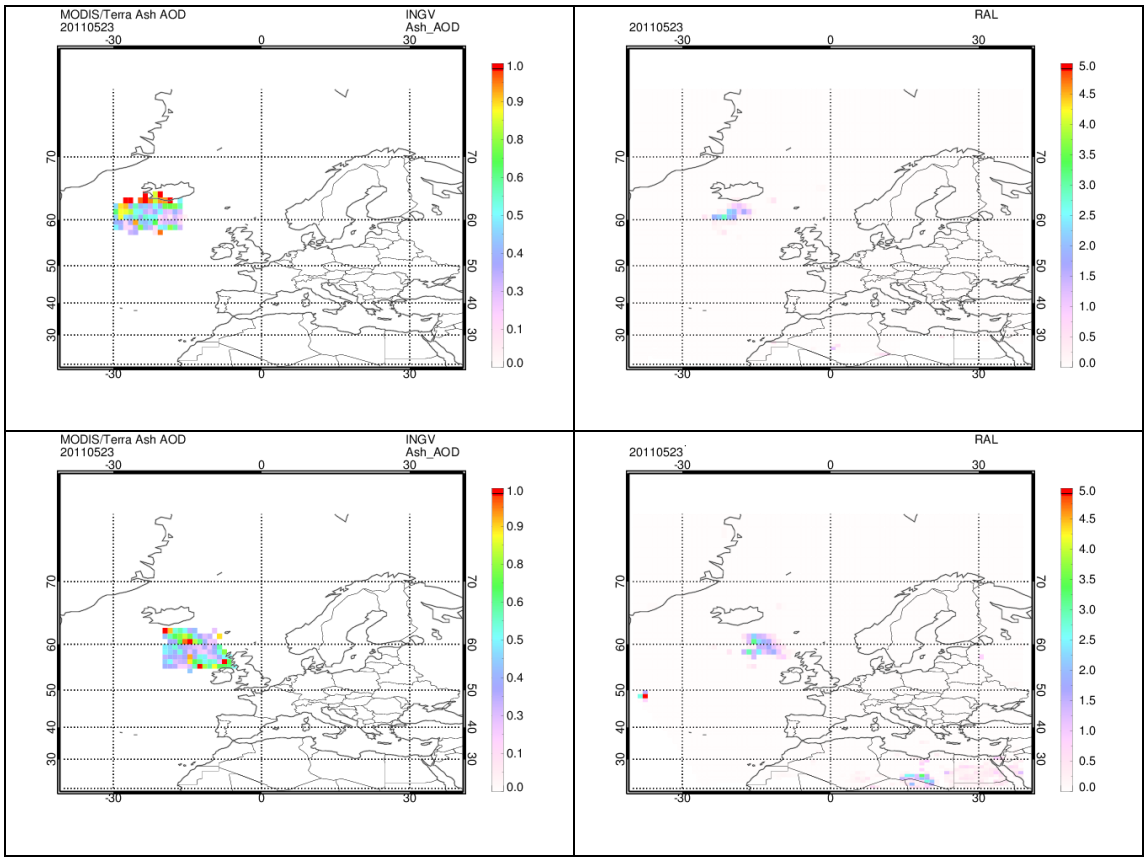

Figure 37. The INGV [left column] and RAL [right column] MODIS/Terra AOD for the morning overpass [upper row] and the evening overpass [lower row] for the 23rd of May 2011.

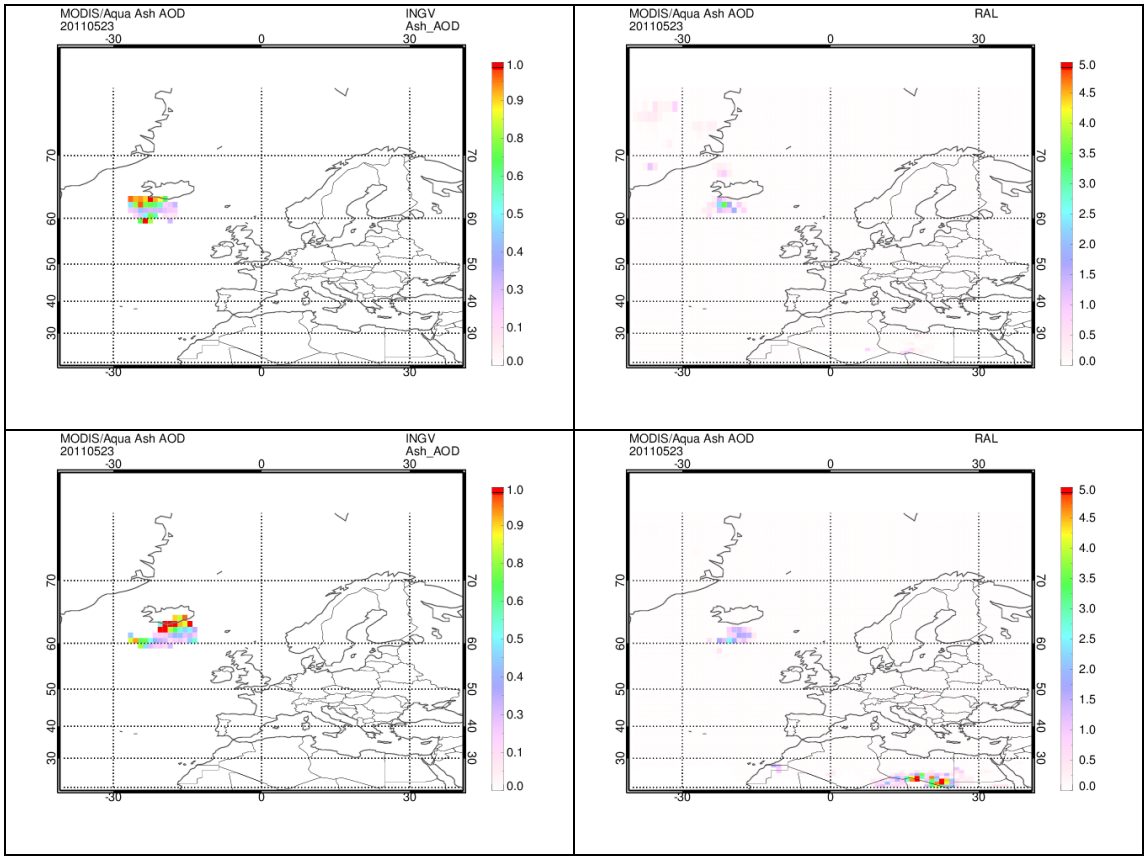

Figure 38. The INGV [left column] and RAL [right column] MODIS/Aqua AOD for the morning overpass [upper row] and the evening overpass [lower row] for the 23rd of May 2011.

The INGV and RAL MODIS/Terra and /Aqua AOD estimates are depicted for the 23rd of May 2010 in Figure 37 and Figure 38 respectively. The morning overpass is shown in the upper row and the evening overpass in the lower row. Note that the colour scale is different between the products, a necessity. In general, one might note that the INGV product identifies more pixels as leaden with ash, and hence assign an AOD value, than the RAL algorithm.

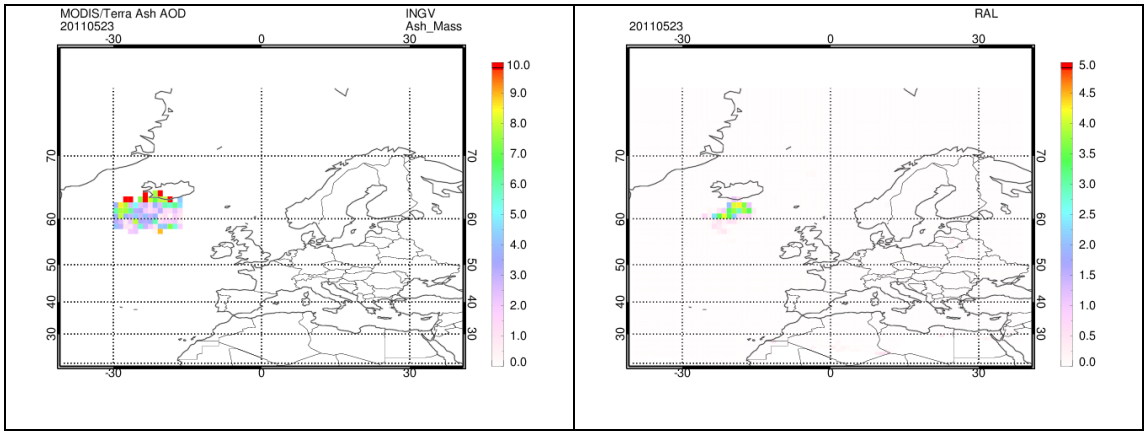

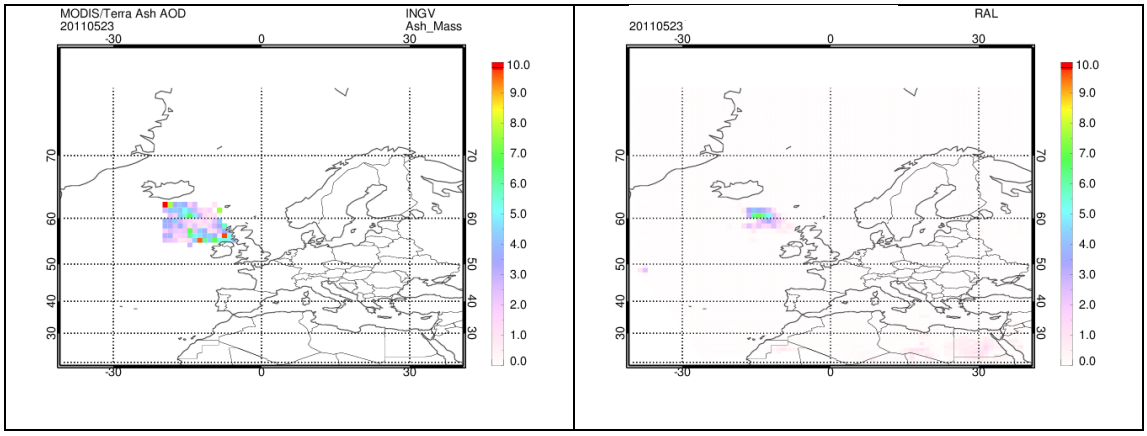

Figure 39. The INGV [left column] and RAL [right column] MODIS/Terra Ash Mass [tons/km] for the morning [upper row] and the evening overpass [lower row] for the 23rd of May 2011.

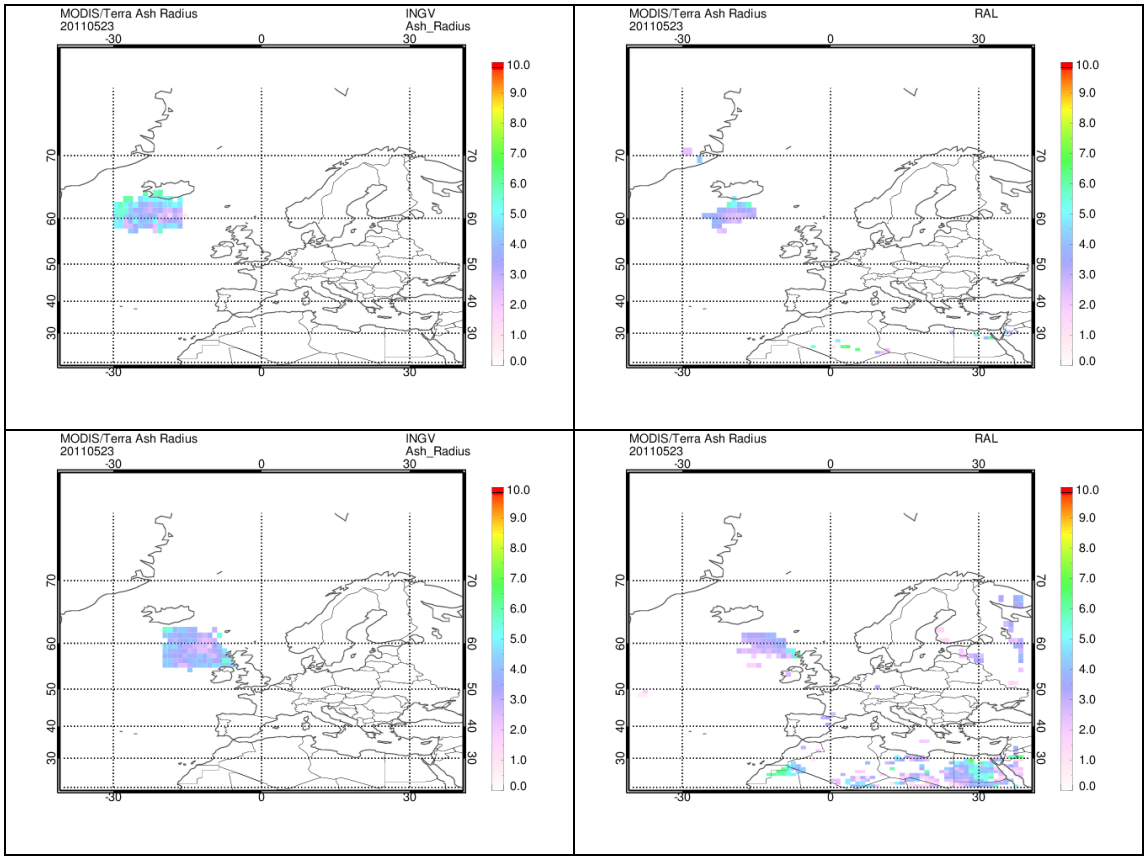

Figure 40. The INGV [left column] and RAL [right column] MODIS/Terra Ash Radius [μm] for the morning [upper row] and the evening overpass [lower row] for the 23rd of May 2011.

6.2 IASI/METOPA ASH AOD, ASS MASS AND ASH PLUME HEIGHT

For the comparisons of the different IASI ash products we chose to grid the data into a grid of 0.5x0.5 bins in latitude/longitude since the ash plume is thinner than the SO_2 plume and the high spatial resolution of 12by12km of IASI in the nadir permits this type of gridding. Furthermore, two of the eruptive days will be shown as examples, the 9th of May 2010 as the Eyjafjallajökull eruption over-flowed over the Atlantic Sea and the 23rd of May 2011 as the Grimsvötn eruption over-flowed over the North Atlantic and Europe.

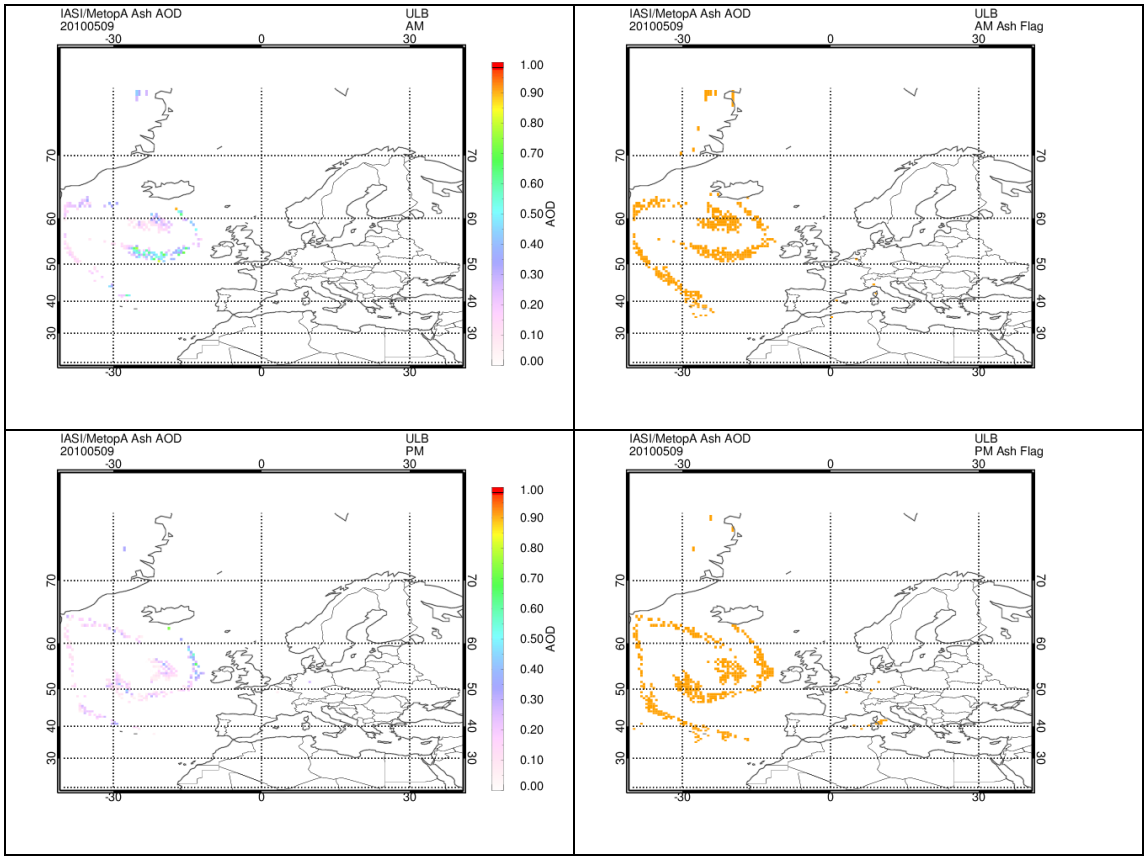

Figure 41. The ULB IASI ash AOD and ash flag estimates for the 9th of May 2010. Upper row the IASI AM overpass and in the lower row, the IASI PM overpass. On the left column, the ash AOD and on the right column, the ash flag.

In Figure 41 the ULB IASI ash AOD [left column] and ash flag estimates [right column] for the 9th of May 2010 are shown, in the upper row the IASI AM overpass and in the lower row for the IASI PM overpass. The ash plume on that day seems to be following the anticyclonic meteorological system over the North Atlantic, with the evening overpass showing the slight dispersion and thinning of the plume. These plots can be directly contrasted to Figure 42 where the Oxford IASI ash AOD estimates for the AM overpass by the nominal [upper left] and fast [upper right and bottom row] algorithms are given for the 9th of May 2010. The Fast algorithm provides three estimates depending on the apriori ash plume height: upper right, plume at 400mbars; lower left, plume at 600mbars and lower right, plume at 800mbars. All three IASI products seem to coincide well for the ash AOD estimate over the sea with the ULB algorithm, however also showing a signal on the South-East coast of Greenland which is not quite depicted by the ULB product. A very similar comment may be also made for Figure 43 where the Oxford IASI ash AOD estimates are shown for the PM overpass. It is almost certain that this ash detected over Greenland is not in fact ash but due to the high surface emissivity features over the ice and depending on the algorithm these affect the result in a small or in a larger manner.

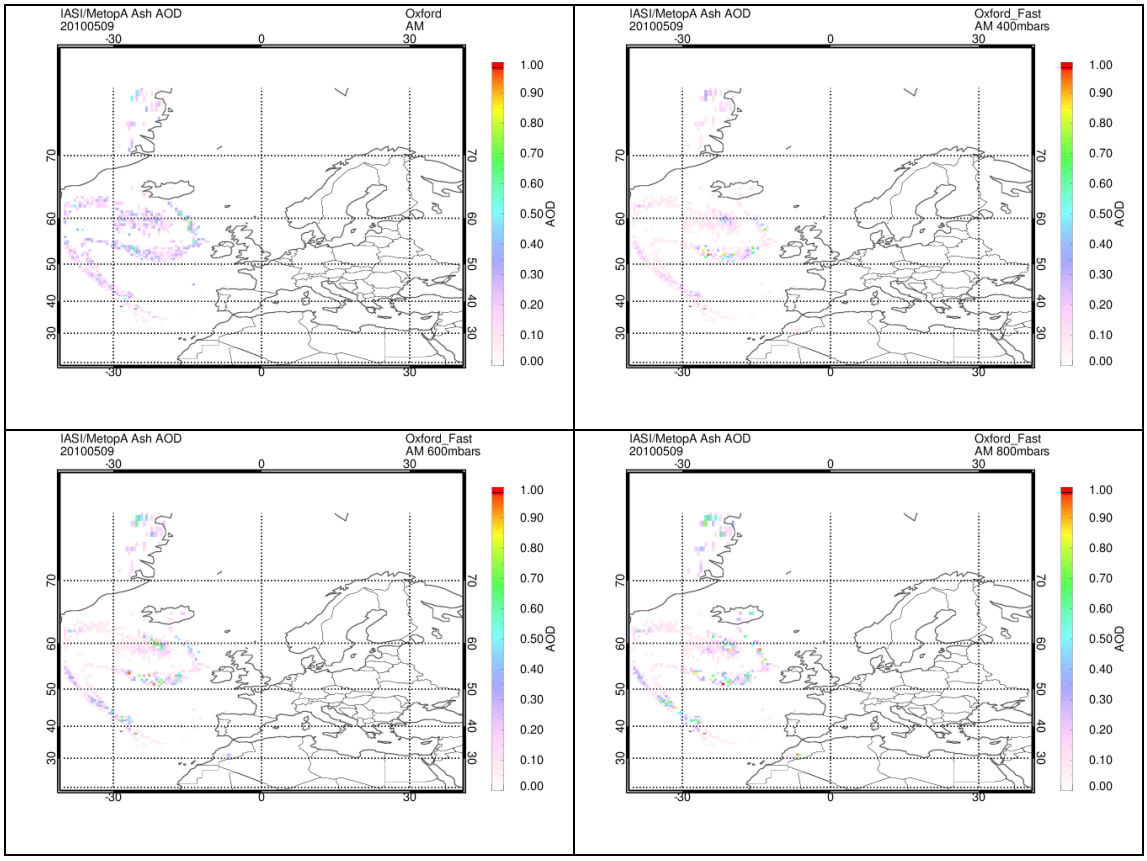

Figure 42. The Oxford IASI ash AOD estimates for the AM overpass by the nominal [upper left] and fast [upper right and bottom row] algorithms for the 9th of May 2010. The Fast algorithm provides three estimates depending on the apriori ash plume height: upper right, plume at 400mbars; lower left, plume at 600mbars and lower right, plume at 800mbars.

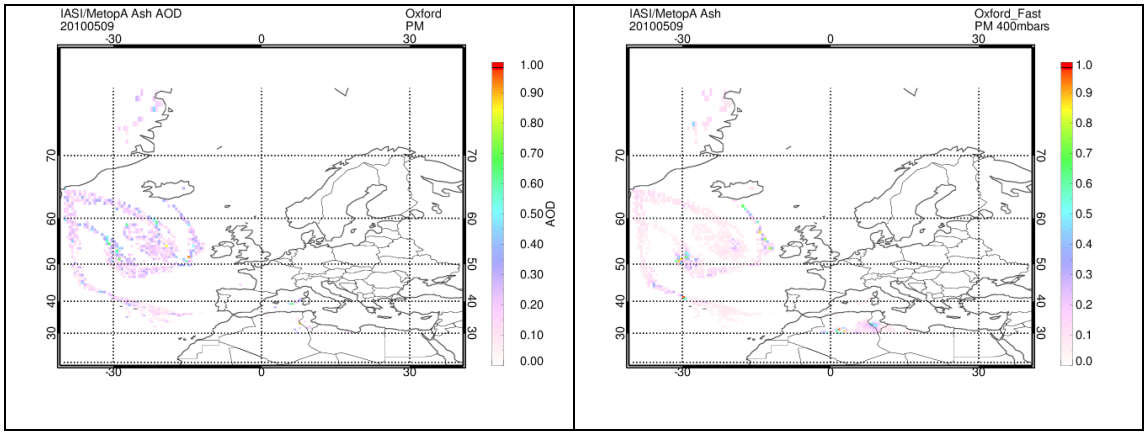

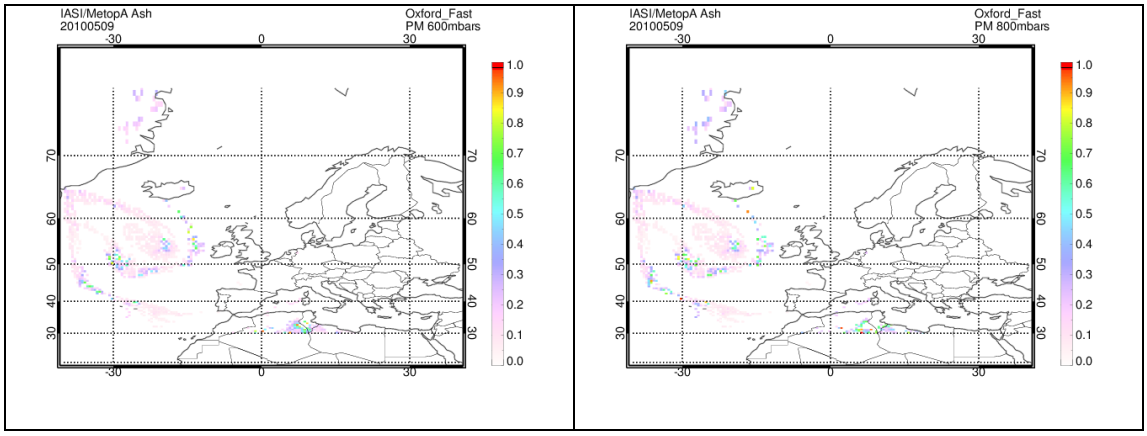

Figure 43. The Oxford IASI ash AOD estimates for the PM overpass by the nominal [upper left] and fast [upper right and bottom row] algorithms for the 9th of May 2010. The Fast algorithm provides three estimates depending on the apriori ash plume height: upper right, plume at 400mbars; lower left, plume at 600mbars and lower right, plume at 800mbars.

As far as the 23rd of May 2011 is concerned, a similar suite of figures is presented below. For the ULB algorithm, from Figure 44, we note that the ash AOD signal is not so strong [left column] even though the ash flag algorithm has identified more pixels as containing ash as the algorithm was able to retrieve the AOD for. This finding differs from the plots shown in Section 2.7.3 where the IASI SO_2 plume is investigated for the same day. This may either mean that the ash plume and the SO_2 plume were completely separated that day, or that the ash loading of the plume was quite low. In Figure 45 and Figure 46 the Oxford IASI ash AOD estimates for the AM & the PM overpasses by the nominal [upper left] and fast [upper right and bottom row] algorithms for the 23rd of May 2011 are shown. Here the picture follows the findings of Section 2.7.3 when the SO_2 plume, after a southwards trajectory, follows a North-Eastern direction, like an arm over Europe. Of particular interest is the apparent increase in ash AOD for the evening overpass, both over the plume but also over the coast of Greenland, which is almost certainly an artifact of the high surface emissivity over ice and not actual ash detection.

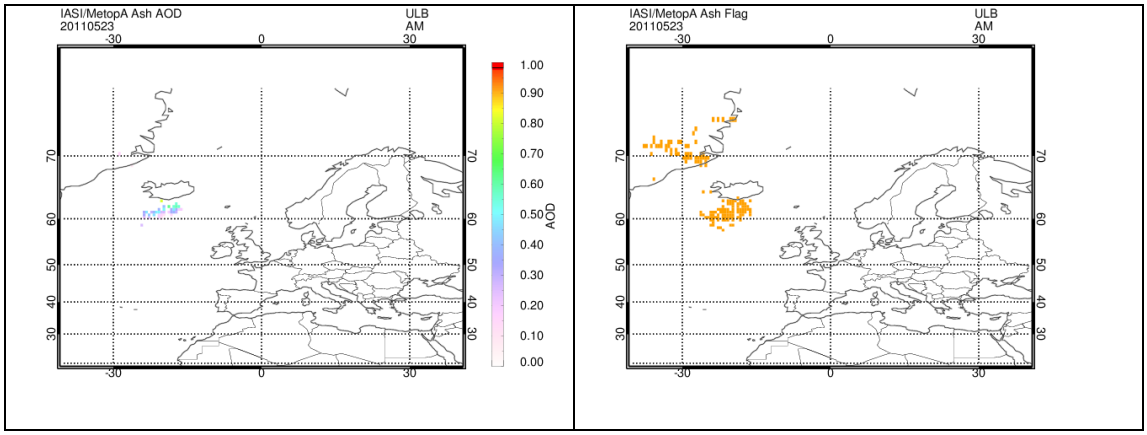

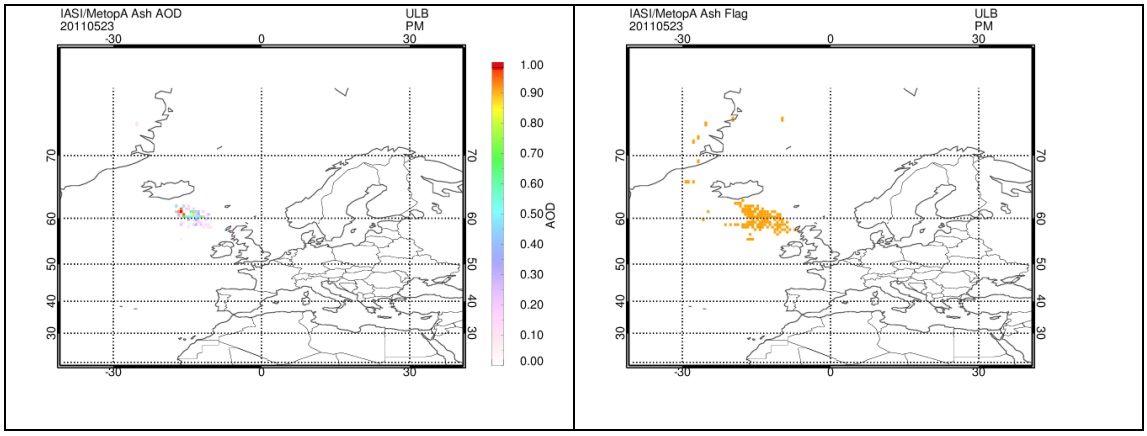

Figure 44. The ULB IASI ash AOD and ash flag estimates for the 23rd of May 2011. Upper row the IASI AM overpass and in the lower row, the IASI PM overpass. On the left column, the ash AOD and on the right column, the ash flag.

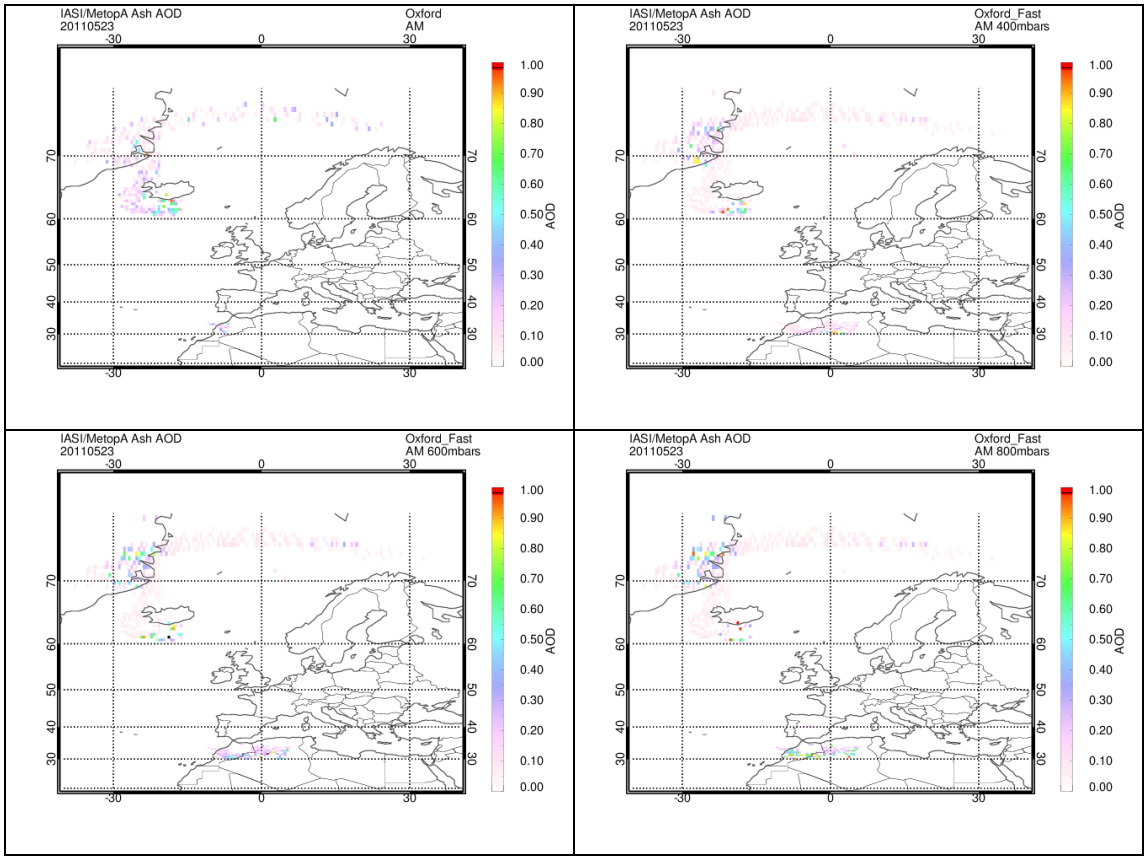

Figure 45. The Oxford IASI ash AOD estimates for the AM overpass by the nominal [upper left] and fast [upper right and bottom row] algorithms for the 23rd of May 2011. The Fast algorithm provides three estimates depending on the apriori ash plume height: upper right, plume at 400mbars; lower left, plume at 600mbars and lower right, plume at 800mbars.

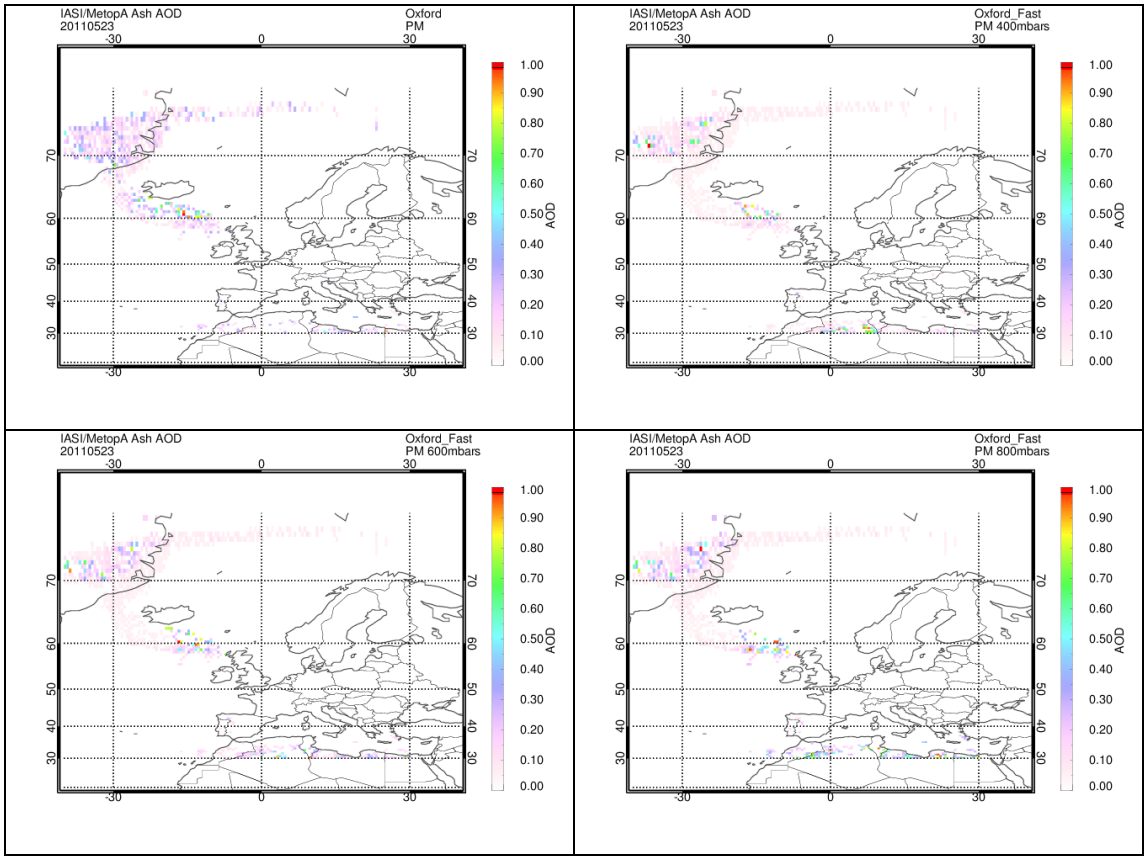

Figure 46. The Oxford IASI ash AOD estimates for the PM overpass by the nominal [upper left] and fast [upper right and bottom row] algorithms for the 23rd of May 2010. The Fast algorithm provides three estimates depending on the apriori ash plume height: upper right, plume at 400mbars; lower left, plume at 600mbars and lower right, plume at 800mbars.

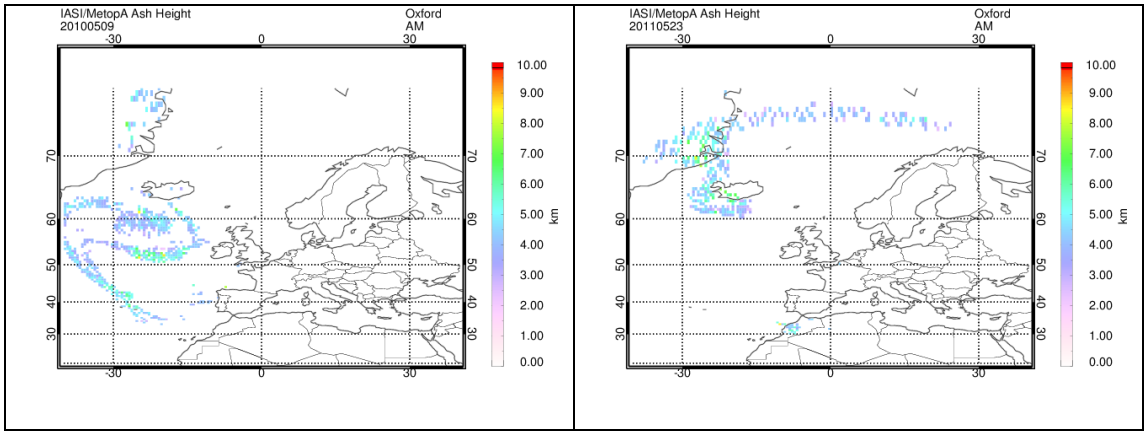

Figure 47. The Oxford nominal algorithm IASI ash height estimate for the 9th of May 2010 [left] and the 23rd of May 2011 [right].

The ash plume height estimate is provided by the Oxford nominal algorithm in km. In Figure 47 the plume height for the 9th of May 2010 [left] and the 23rd of May 2011 [right] are shown as examples. For the Eyjafjallajökull eruption, most values range between 5000 and 6000 m which, roughly translated, corresponds to between 500 and 400 mbars. From the comparisons shown in Figure 46 one might suggest that both the 400mbars [upper right] and the 600mbars [bottom left] Oxford AOD product fares better with the ULB equivalent, within the expected height ranges

provided by the Oxford fast algorithm results. For the Grimsvötn eruption, the range of estimated ash plume heights is very similar yielding similar comparative directions.

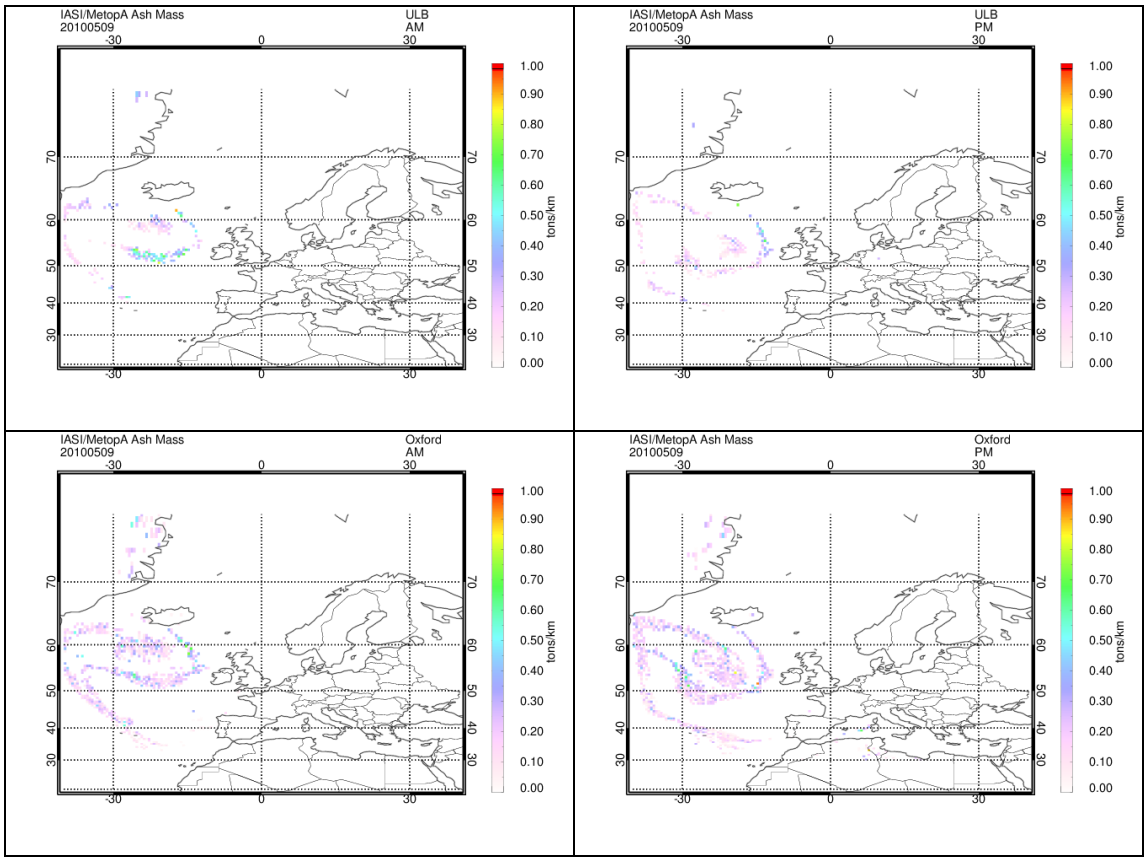

Figure 48. The ULB IASI ash mass estimates [left column] and the Oxford nominal algorithm ash mass estimates [right column] for the AM overpass [upper row] and the PM overpass [lower row] for the 9th of May 2010.

In Figure 48 and Figure 49 the ULB IASI ash mass estimates [left column] and the Oxford nominal algorithm ash mass estimates [right column] for the AM overpass [upper row] and the PM overpass [lower row] are shown for the 9th of May 2010 and for the 23rd of May 2011 respectively. The comparisons come as no surprise as the ash mass loading follows closely the ash AOD estimates as well.

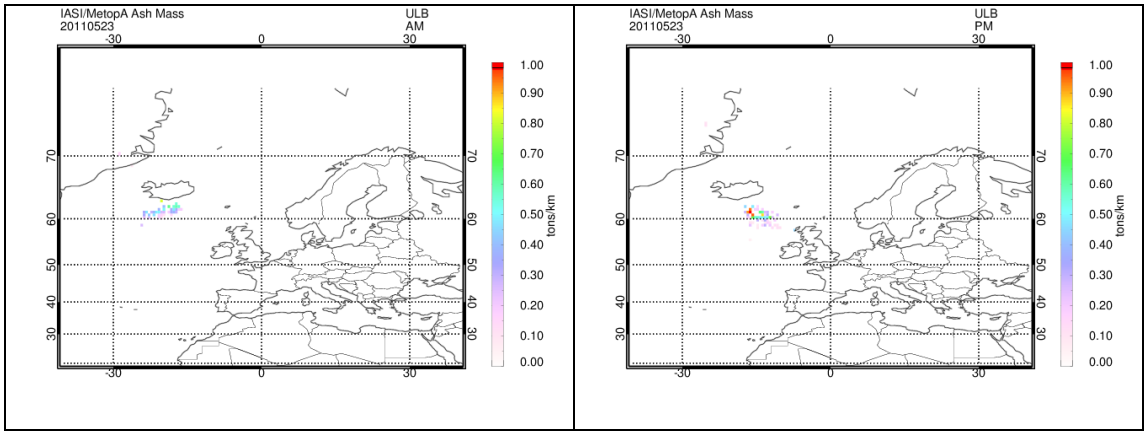

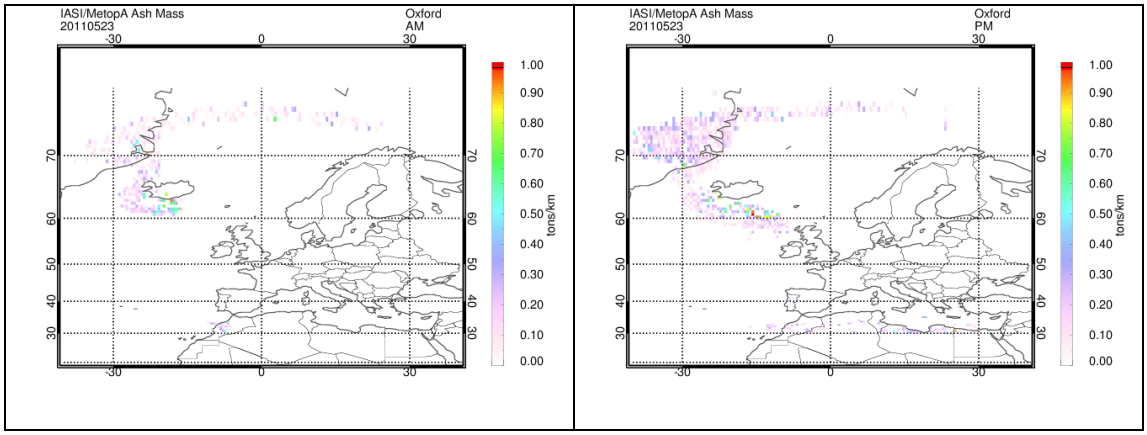

Figure 49. The ULB IASI ash mass estimates [left column] and the Oxford nominal algorithm ash mass estimates [right column] for the AM overpass [upper row] and the PM overpass [lower row] for the 23rd of May 2011.

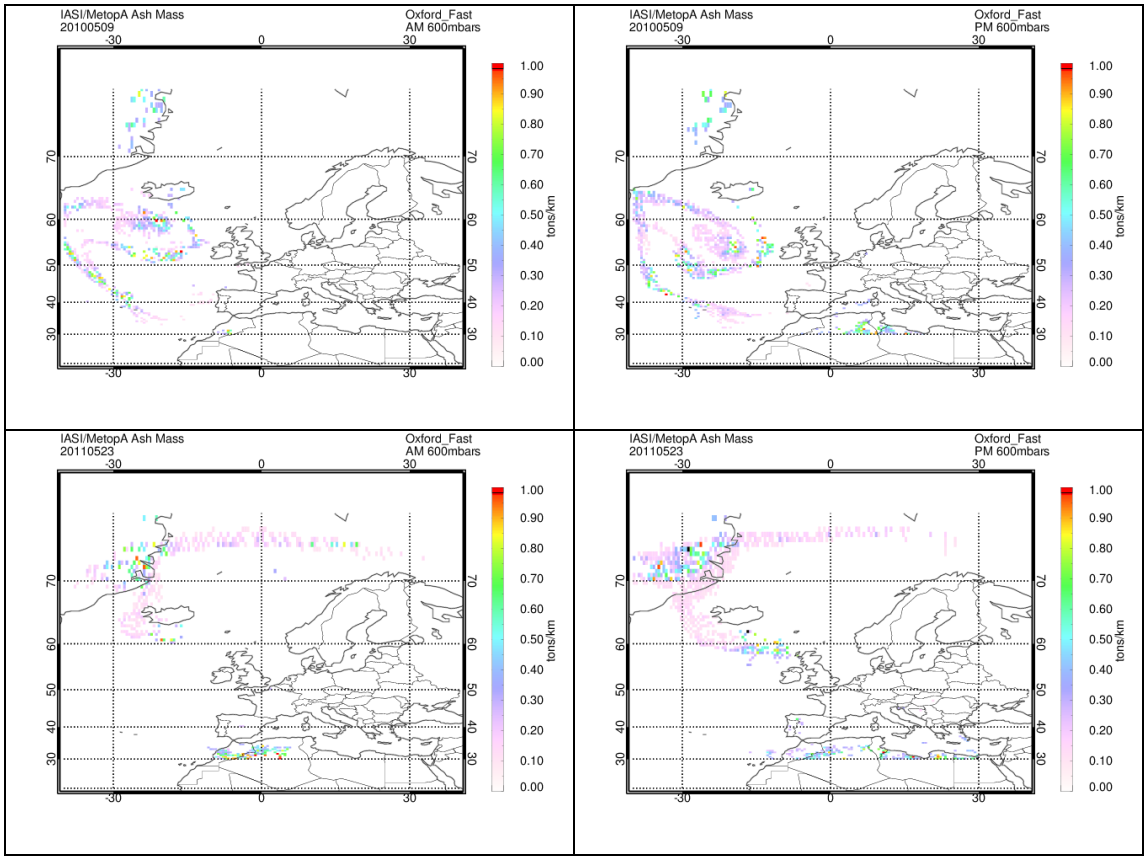

Figure 50. The Oxford fast algorithm ash mass estimates for the AM overpass [left column] and the PM overpass [right column] for the 9th of May 2010 [upper row] and the 23rd of May 2011 [lower row] for the 600mbars product.

7. CONCLUSIONS AND DISCUSSION

In the current validation report, comparisons between space-born instruments, ground-based measurements and *in situ* estimates of total sulphur dioxide [SO_2] loading and ash characteristics following major volcanic eruptions are presented. These comparisons form part of the European Space Agency's "*Satellite Monitoring of Ash and Sulphur Dioxide for the mitigation of Aviation Hazards*" (SACS-2/SMASH) projects which aim to define an optimal *End-to-End System for Volcanic Ash Plume Monitoring and Prediction* while:

1. Maintaining the existing Support to Aviation Control Service alert system.
2. Developing and characterizing improved satellite algorithms for the retrieval of ash characteristics and SO_2 concentrations.
3. Independently validating the ash and SO_2 algorithms using sources of ground-based, aircraft and auxiliary satellite measurements.

This independent validation was performed for three eruptive periods, namely, the 15th to the 26th of April 2010, over Eyjafjallajökull, Iceland; the 4th to the 20th of May 2010, also over Eyjafjallajökull, Iceland and the 21st to the 28th of May 2011, over Grimsvötn, Iceland.

As far as the comparisons of the SO_2 loading are concerned, it became rather obvious from the start that the levels over the ground-based Brewer stations for the three eruptive periods chosen was nominally low and not sufficient to permit proper quantitative comparisons. Nevertheless, some of the satellite products showed good correlations when the signal was high enough, namely: the DLR/GOME-2 total SO_2 column is promising for the 2.5km plume height, with an acceptable signal during the main eruptive period and noise levels otherwise. A moderate correlation, R^2, was found for some of the ground-based stations, with values between 0.3 and 0.5. And the ULB/IASI ULB total SO_2 columns are very promising when there is a strong signal with correlations, R^2, for some of the ground-based stations, 0.3 and 0.7.
When inter-comparing satellite algorithms [for the same space-born instrument] the BIRA and DLR GOME2/MetopA algorithms produce very similar patterns for the SO_2 loading as well as very similar absolute SO_2 column levels providing the SO_2 signal is high enough, i.e. the SO_2 loading is high enough. Similarly, the ULB and Oxford IASI/MetopA algorithms produce very similar patterns for the SO_2 plume height [where given] however the absolute SO_2 levels vary dramatically. There is an order of magnitude difference between the two Oxford algorithms, with the nominal algorithm providing absolute SO_2 columns within the same order of magnitude to the ULB findings and the GOME2 findings. The SO_2 loading patterns are the same for the three IASI algorithms pointing to a very promising future for these algorithms. The exception to the above are the INGV and RAL MODIS/Terra & /Aqua algorithms deviate quite a bit, both in the magnitude of the estimates SO_2 column but also in the geographical extend of the loading, which bares further investigation.

As far as the comparisons of the ash AOD loading are concerned: first of all, we will discuss the comparisons with the ground-based EARLINET LIDAR network. These suffered from the small number of co-locations found between satellite observations and ground-based measurements, however the Oxford nominal IASI algorithm ash AOD values show an acceptable correlation with the ground values, with coefficients ranging between 0.6 and 0.85, and, even though it provides rather low values, these are of the same order of magnitude as the LIDAR ones. The Oxford fast IASI algorithm also provides same order of magnitude AOD estimates as the ground, with the narrower spatiotemporal choice providing the most promising results, with a correlation ranging between 0.7 for the 400 mbars product to 0.8 for the 800 mbars product. The ULB Eyjafjallajökull refractive index AOD estimates are also quite promising, with correlations ranging between 0.74 and 0.94, the highest yet.
As far as the ash height is concerned, even though the correlations and co-variability are not encouraging, the mean height values and standard deviation observed are very close indeed.

As far as the comparisons with the aircraft-born LIDAR are concerned: the Oxford nominal IASI algorithm presents quite good comparisons for the AOD patterns observed during the course of

the flight shown in the Figures, a promising result which is not so for the height estimate. The Oxford fast IASI algorithm shows an excellent agreement, with the 800mbar product appearing to perform best. The ULB IASI algorithm also shows an excellent agreement, both with respect to the absolute AOD values as well as AOD features during the flight shown above. Similarly, the RAL MODIS/Aqua IR algorithm, shows an excellent agreement between 13:00 and 14:00 UTC both for the AOD, the ash height and the features observed at those hours, another promising result.

As far as the comparisons with the space-born LIDAR are concerned: in general, on days with sufficient signal, there is some agreement observed with the space-born spectrophotometers, namely over the North Atlantic, the Iberian Peninsula and Greece. The ash AOD values shared a similar range. However, the validation strategy requires redefinition in this case in order to increase the co-locations found and, as expected, the comparisons between the two types of observations.

As far as the inter-comparisons within satellite algorithms for the same space-born instrument ash characteristics are concerned: the RAL and INGV MODIS products were compared and found to be rather different, both in the range of values found as well as the spatial spread of the ash loading after the eruptions. The actual loading as well is estimated to be quite different between the two algorithms. The comparison between the ULB and Oxford algorithms for the IASI observations is found to be quite promising, with the Oxford algorithms tending to identify more pixels as affected by the ash loading than the ULB algorithm. Still, the IASI products show in this inter-comparison the same stable behaviour as in all the above comparisons to auxiliary datasets.

As a whole, we conclude that the majority of the satellite products studied within the framework of the SACS-2/SMASH project mature enough to form part of an optimal *End-to-End System for Volcanic Ash Plume Monitoring and Prediction*, while still benefiting from continuous algorithmic improvements that may still be applied.

REFERENCES

Carboni, E., Grainger, R., Walker, J., et al., (2012), A new scheme for sulphur dioxide retrieval from IASI measurements: application to the Eyjafjallajökull eruption of April and May 2010, Atmos. Chem. Phys., 12, 11417-11434, doi:10.5194/acp-12-11417-2012.

Clarisse, L., F. Prata, J.-L. Lacour, et al. (2010), A correlation method for volcanic ash detection using hyperspectral infrared measurements, Geophys. Res. Lett., 37, L19806, doi:10.1029/2010GL044828.

Clarisse, L., Coheur, P.-F., Prata, F., et al., (2013), A unified approach to infrared aerosol remote sensing and type specification, Atmos. Chem. Phys., 13, 2195-2221, doi:10.5194/acp-13-2195-2013.

Clerbaux, C., Boynard, A., Clarisse, L., et al., (2009), Monitoring of atmospheric composition using the thermal infrared IASI/MetOp sounder, Atmos. Chem. Phys., 9, 6041-6054, doi:10.5194/acp-9-6041-2009.

Marenco F., B. Johnson, K. Turnbull, et al., Airborne lidar observations of the 2010 Eyjafjallajokull volcanic ash plume, J. Geophys. Res., 116, D00U05, doi:10.1029/2011JD016396, 2011.

Munro, R., Eisinger, M., Anderson, C., et al. (2006): GOME-2 on MetOp, in: Proc. of The 2006 EUMETSAT Meteorological Satellite Conference, Helsinki, Finland, 12–16 June 2006, EUMETSAT p. 48, 2006.

Lerot, C., Van Roozendael, M., Lambert, J.-C., et al., (2010), The GODFIT algorithm: a direct fitting approach to improve the accuracy of total ozone measurements from Gome. Int. J. Remote Sensing, 31, 543-550.

Pappalardo, G., Amodeo A, Mona L, et al., (2004), Raman lidar observations of aerosol emitted during the 2002 Etna eruption, Geophysical Research Letters, 31 (5): Art. No. L05120.

Pappalardo, G. et al., Four-dimensional distribution of the 2010 Eyjafjallajokull volcanic cloud over Europe observed by EARLINET, Atmos. Chem. Phys., 13, 4429-4450, doi:10.5194/acp-13-4429-2013

Platt, U. and J. Stutz, *Differential Optical Absorption Spectroscopy: Principles and Applications,* Springer Verlag, Heidelberg, ISBN 978-3540211938, 597pp, 2008.

Rix, M., Valks, P., Hao, N., et al. (2012): Volcanic SO_2, BrO and plume height estimations using GOME-2 satellite measurements during the eruption of Eyjafjallajokull in May 2010, J. Geophys. Res., 117, D00U19, doi:10.1029/2011JD016718.

Sawamura, et al, (2012), Stratospheric AOD after the 2011 eruption of Nabro volcano measured by lidars over the Northern Hemisphere, Environ. Res. Lett., 7, 034013.

Theys, N., Campion, R., Clarisse, L., et al., (2013), Volcanic SO_2 fluxes derived from satellite data: a survey using OMI, GOME-2, IASI and MODIS, Atmos. Chem. Phys., 13, 5945-5968, doi:10.5194/acp-13-5945-2013.

Theys, N., J. van Gent, H. Brenot, et al., (2014), Algorithm Theoretical Basis Document, European Space Agency Support to Aviation Control Service-2 Project, February 2014.

Thomas, G.E., E. Carboni, A.M. Sayer, et al., (2009), Oxford-RAL Aerosol and Cloud (ORAC): aerosol retrievals from satellite radiometers in Satellite Aerosol Remote Sensing Over Land (Eds: A.A. Kokhanovsky and G. de Leeuw), Springer.

van Gent, J. Spurr, R., Theys, N., et al., (2014), Towards operational retrieval of SO_2 plume height from GOME-2 radiance measurements, manuscript in preparation for Atmos. Meas. Tech., 2014.

ACRONYMS & ABBREVIATIONS

AOD	Aerosol Optical Depth
ATBD	Algorithm Theoretical Basis Document
AUTH	Aristotle University of Thessaloniki
BIRA-IASB	Belgian Institute for Space Aeronomy
CALIOP	Cloud-Aerosol Lidar with Orthogonal Polarization
CALIPSO	Cloud-Aerosol Lidar and Infrared Pathfinder Satellite Observations
CCI	Climate Change Initiative
DLR	German Aerospace Centre
DOAS	Differential Optical Absorption Spectroscopy
EARLINET	European Aerosol Research Lidar Network
ESA	European Space Agency
ESRIN	European Space Agency Research Institute
EUMETSAT	European Organisation for the Exploitation of Meteorological Satellites
GOME-2	Global Ozone Monitoring Experiment-2
IASI	Infrared Atmospheric Sounding Interferometer
INGV	National Institute of Geophysics and Volcanology
KNMI	Royal Netherlands Meteorological Institute
LIDAR	Laser Imaging Detection and Ranging (system)
MODIS	Moderate Resolution Imaging Spectrometer
NASA	National Aeronautics and Space Administration
OE	Optimal Estimation
OMI	Ozone Monitoring Instrument
OXFORD	University of Oxford
RAL	Rutherford Appleton Laboratory
SACS	Support to Aviation Control Service
SCIAMACHY	Scanning Imaging Absorption spectroMeter for Atmospheric CHartographY
SMASH	Satellite Monitoring of Ash and Sulphur dioxide for the mitigation of aviation Haz ards
SO_2	Sulphur Dioxide
TOMS	Total Ozone Mapping Spectrometer
ULB	Université Libre de Bruxelles
UV	Ultraviolet
VCD	Vertical Column Density
WOUDC	World Ozone and Ultraviolet Radiation Data Centre

TABLE OF TABLES

TABLE OF FIGURES